CONSTANT TEMPERATURE EMBOSSING OF SUPERCOOLED POLYMER FILMS

A Thesis
Presented to
The Academic Faculty

by

Ramasubramani Kuduva Raman Thanumoorthy

In Partial Fulfillment
of the Requirements for the Degree
Doctor of Philosophy in the
School of Polymer, Textile and Fiber Engineering

Georgia Institute of Technology
MAY 2011

CONSTANT TEMPERATURE EMBOSSING OF SUPERCOOLED POLYMER FILMS

Approved by:

Dr. Donggang Yao, Advisor
School of Polymer,Textile & Fiber Engineering
Georgia Institute of Technology

Dr. Youjiang Wang
School of Polymer,Textile & Fiber Engineering
Georgia Institute of Technology

Dr. Wallace W. Carr
School of Polymer,Textile & Fiber Engineering
Georgia Institute of Technology

Dr. Kyriaki Kalaitzidou
School of Mechanical Engineering
Georgia Institute of Technology

Dr. Karl Jacob
School of Polymer,Textile & Fiber Engineering
Georgia Institute of Technology

Date Approved: [January 17, 2011]

Dedicated to my parents

ACKNOWLEDGEMENTS

The author is deeply grateful to his advisor, Dr. Donggang Yao, for his kind guidance, continuous encouragement and excellent support throughout this research.

The author would like to especially thank Dr. Wallace W. Carr, Dr. Karl Jacob, Dr. Youjiang Wang, and Dr. Kyriaki Kalaitzidou for kindly consenting to serve as thesis committee members, and providing very useful suggestions and recommendations.

The author appreciates Dr. Pratapkumar Nagarajan for the technical discussions and support throughout the course of the thesis. The author is thankful for the help and encouragement from Dr. Jasmeet Kaur during this study.

The author is thankful to Dr. Krishna Parachuru for the tensile testing experiments. The author wishes to acknowledge Sarang Deodhar, Jun Jia, Ericka Ford, Yubin Shen for the technical discussions and support. The author also acknowledges the assistance from Wei Zhang, Ian Winters, Tom Wyatt, Sudhakar Jagannathan and Ruihua Li during this Ph.D. study.

The author thanks Wenjun Xu and Zhan Liu for supplying the initial set of silicon stamps. The author also acknowledges the help from Ananda Barua and Sathyanarayanan Raghavan during the modeling studies.

The author appreciates the help from Dhaval Kulkarni, Sehoon Chang and Srikanth Singamaneni during the SEM studies. The author is also thankful to Michelle Schlea, Ji Hoon Lee and R. Bradley Johnson for help during the embossing studies on the hydraulic press.

The author also wishes to thank Ms. Angie Abbott, Ms. Hope Holly, Ms. Linda Roberson, Mr. Michael Boyett, Mr. Joseph Brooks and Mr. James Gallman for their administrative assistance during the Ph.D. study.

The author thanks all friends and colleagues in PTFE, in particular, Bilge Gurun, YoungHo Choi, Mihir Oka, Shamal Mhetre and Kishor Gupta for their help and support.

The author is grateful to National Science Foundation for the financial support for this research.

TABLE OF CONTENTS

LIST OF TABLES

LIST OF FIGURES

LIST OF SYMBOLS AND ABBREVIATIONS

T	Embossing temperature
P	Embossing pressure
t	Embossing time
η	Viscosity
η^*	Complex viscosity
$\dot{\gamma}$	Strain rate
ρ	Density
S_{ij}	Second Piola-Kirchhoff stress tensor
E_{ij}	Green Lagrange deformation tensor
θ	Degree of crystallinity
φ	Suspension concentration
G^*	Shear storage modulus with particles
ξ	Reduced time for the non-isothermal crystallization kinetics
T_r	Reference temperature
$K(T)$	Non-isothermal rate constant as a function of temperature
a_T	Shift factor for the non-isothermal crystallization kinetics
γ	Hencky Strain
A_0	Initial cross-sectional area before stretching
A_t	Instantaneous cross-sectional area
$F(t)$	Tensile force
$\sigma(t)$	Tensile stress
n	Avrami index
m	Ozawa exponent

Z_t	Composite rate constant
λ_c	Time constant
N	Number of nuclei per unit volume
$\dot{\gamma}_n$	Characteristic shear rate
ϕ_m	Maximum volume concentration of spheres
η_a	Newtonian fluid viscosity
ν	Poisson ratio of matrix
ν_c	Poisson ratio of crystalline phase
G_c^*	Shear modulus of crystalline phase
G^*	Shear modulus of matrix
ϕ_0	Shape-dependent maximum packing concentration
CTE	Constant Temperature Embossing
PET	Poly (ethylene terephthalate)
PEEK	Poly (ether ether ketone)
T_g	Glass transition temperature

SUMMARY

In this dissertation work, a constant temperature embossing process was developed and investigated. By softening and crystallizing a supercooled polymer at the same temperature, the embossing and solidification stages can be carried out isothermally without thermal cycling. The new process was demonstrated for replicating rectangular trenches with different aspect ratio for two different polymers: PET and PEEK.

The raw materials were characterized for their thermal and rheological properties to determine the processing parameters. The polymers were also characterized by a modified tensile testing apparatus to determine the tensile properties of the film during embossing. The processing parameters including embossing temperature, embossing pressure and embossing time were varied based on the material properties and optimized.

A semi-empirical model was established to correlate the crystallizing kinetics of the materials to the change in rheological properties during embossing. The model was used as a tool to predict the rheological properties of the polymer at conditions where experimental determination is difficult.

Finally, embossing simulations with the semi-empirical rheological model were conducted to study the unique process dynamics of constant-temperature embossing and verify some experimental findings. Different cases of constant-temperature embossing involving low to high rates of crystallization were simulated and compared with the conventional embossing process. Based on the experimental and simulation results, processing strategies for constant-temperature embossing were devised.

CHAPTER 1

INTRODUCTION

Hot embossing is an important micromolding process with a relatively simple tooling and process setup. Recent studies have demonstrated that hot embossing, as a versatile microfabrication technique, is capable of producing complex microstructures cost-effectively for automotive, biomedical and microelectronics applications[1-3]. Hot embossing has been used for the production of micro-optical benches and optical waveguides[4], valve-less diffuser micropumps[5] and integrated optical sensors[6], to name a few. Advantages of the hot embossing process compared to other micromolding techniques include low residual stress in the molded parts and ease of modification of the process setup. In particular, the hot embossing process has benefits such as reduced mass flow and low tooling cost over the most used micro-injection molding. The low tooling cost is due to the low pressure experienced during the hot embossing process and the need to fabricate only the required features. During the process, the material flow is limited to only the regions where the microstructures are to be replicated. The key process variables in the hot embossing process are the embossing pressure, the embossing temperature, the holding time and the cooling time. In hot embossing, the thermal and stress fields are induced into the polymer film, effecting morphological changes. Extensive research has been conducted to understand the complex process dynamics of hot embossing and develop useful process control schemes for highly demanding applications[7-17].

Although hot embossing largely benefits from its relatively simple tooling and process setup compared with other micromolding techniques such as micro-injection

molding, its long cycle time has been a major limitation for volume production. A total cycle time of 10 minutes or longer is not uncommon in hot embossing. In the standard hot embossing setup, the embossing mold needs to be heated before embossing and cooled after embossing. The large thermal mass of the embossing mold results in long thermal cycling and hence the observed long cycle times.

Different variations of the hot embossing process have been developed to make the process more suitable for mass production. Most of these variations center on modification of tools used in the embossing in order to increase the rate of thermal cycling. However, such tooling modifications typically result in a substantially more expensive setup and increased costs. Some other studies have attempted to soften the materials by chemical treatment in order to facilitate a room temperature embossing process. In this case, a vapor of a good solvent including supercritical CO_2 is used to plasticize the polymer film prior to embossing[18]. Rather than to involve solvents, the current work attempts to develop a constant temperature thermoplastic embossing process which allows the feature transfer to be complete at a same temperature. The new process utilizes the unique crystallizing kinetics of supercooled amorphous films to achieving softening and re-solidification at a single processing temperature.

The constant temperature embossing process was studied by developing a correlation between deformation and crystallization occurring during processing. The crystallization occurring during the embossing process manifests itself as a change in mechanical properties. A semi-empirical model was established to link the increase in crystal content to the change in rheological properties. Analyses and simulations with this semi-empirical rheological model were conducted to predict the phase change occurring at

temperatures where there is a high rate of crystallization and it is hard to measure the change in rheological properties.

CHAPTER 2

CONSTANT TEMPERATURE EMBOSSING (CTE) PROCESS DEVELOPMENT

2.1 Abstract

This chapter reports the development of the constant temperature embossing process and explains the physical phenomena occurring during the process. The conventional hot embossing process is evaluated for its merits and limitations. The chapter also lists different variations of the conventional hot embossing process and presents the current stage in its development. The CTE process mechanism is described in terms of the phase change occurring during the process along with the key process parameters.

2.2 Introduction

2.2.1 Hot Embossing

Hot embossing is predominantly done as a batch process during which the polymer film is softened, then pressed against a patterned mold, cooled and finally demolded. A schematic of conventional hot embossing process is shown in Figure 1. Hot embossing process can be isothermal and non-isothermal. In isothermal embossing, the entire setup with the polymer film is heated to the required embossing temperature and the pressure is applied, while in non-isothermal embossing the polymer film is not pre-heated.

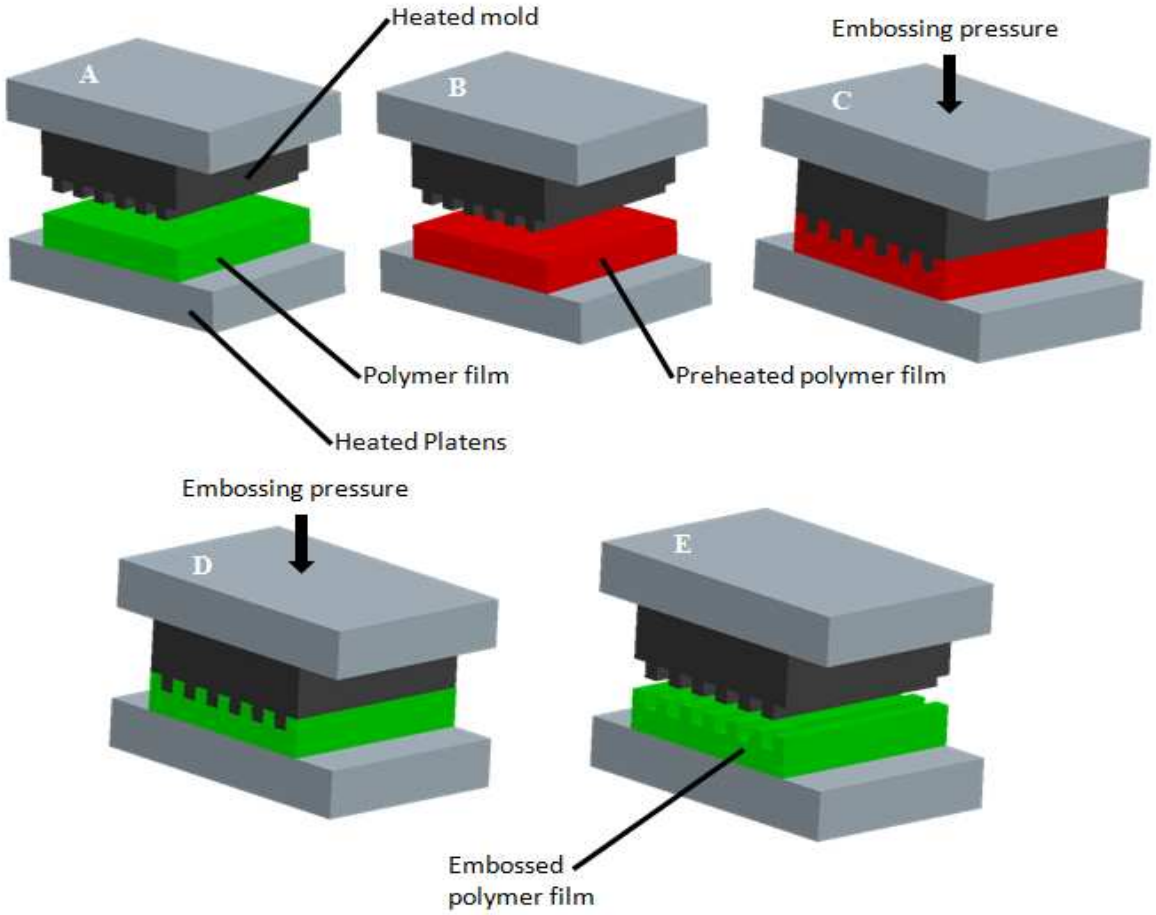

Figure 1 Steps in conventional hot embossing: A – Mold preheating (non-isothermal embossing); B – Mold and polymer preheating (isothermal embossing); C – Embossing and holding stage; D – Cooling stage; E – Demolding stage

The isothermal embossing has a long cycle time due to the need to heat and cool the complete embossing setup. Hot embossing is often carried out on thick polymer substrates as required for many applications. In such applications, the cycle time considerably increases as the thick polymer substrate is heated above its glass transition temperature (T_g) and then cooled after the process is complete. On the contrary in non-isothermal embossing, only the mold setup is heated to the embossing temperature and pressed against a room temperature polymer film. The process involves localized heating of the cold polymer film by pressing the heated mold. Embossing of thick polymer sheets is quicker when non-isothermal embossing is employed. Non-isothermal embossing requires stringent optimization of the process parameters such as embossing temperature and pressure than the isothermal embossing process. The temperature and pressure profiles in the polymer during isothermal hot embossing are shown in Figure 2.

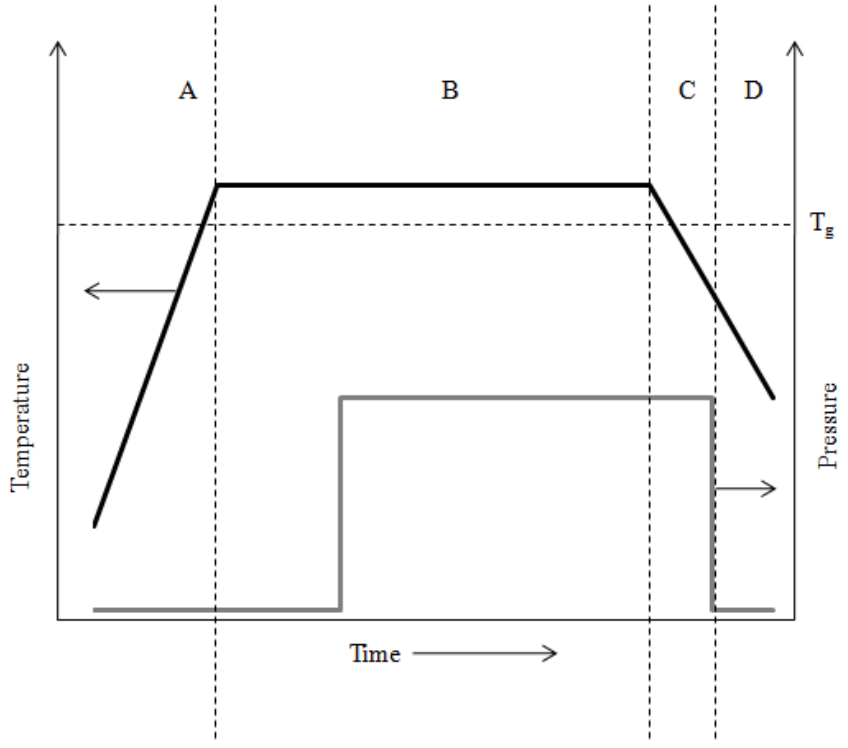

Figure 2 Temperature and pressure profiles during isothermal hot embossing: A-Preheating Zone; B-Embossing Zone; C-Cooling Zone; D-Demolding Zone

2.2.2 Thermal cycling and its effects on hot embossing

Thermal cycling is a technique where the temperature of the tool used in processing is alternatively increased and decreased to enable successful completion of the process. Thermal cycling is very useful in micromolding processes such as microinjection molding and micro embossing where the polymer has to fill extremely narrow cavities. As compared to a conventional injection molding where the mold is cold when the polymer fills the cavity, when using thermal cycling technique the mold is alternatively heated and cooled during the process. This enables the flow of polymers into narrow cavities due to reduction of its viscosity and faster solidification of the part after completion of filling. In the case of micro hot embossing for both isothermal and non-isothermal cases, the mold is initially heated and then cooled after the embossing is completed.

Though thermal cycling leads to an increase in cycle time in the microinjection molding process as a large amount of thermal mass is involved, it is essential for very large aspect ratio parts or for high performance polymers where the viscosity is high at the required processing temperatures. In the case of hot embossing, thermal cycling of the mold is required as the polymer is in film form which forms the shape of the cavity from the heat supplied from the embossing tool, In conventional hot embossing, the thermal cycling can be minimized by pre-heating the polymer film separately from the embossing set-up before the embossing stage. In the current study, thermal cycling is minimized by eliminating the cooling cycle as the embossing, holding and demolding steps are carried out at the same isothermal temperature.

2.2.3 Advantages and limitations of hot embossing as a microreplication technique

The hot embossing process has advantages as a micromolding technique. A successful micromolding technique depends on a combination of factors such as ability to replicate different variety of features with low to very high-aspect-ratio, time required for embossing, and capital and operating cost involved and scale-up capabilities. Taking into consideration these criteria, some advantages of the hot embossing process are:

- *Simple setup enabling quick changes in tooling in-between experiments:* Hot embossing involves very simple setup. In microinjection molding, complex tooling removal and replacement have to be performed for shifting the production to completely different types of features. In hot embossing a simple mold replacements can vary the type of features replicated.
- *Low residual stresses due to smaller flow path of polymers:* In hot embossing the polymers are used as films that can be softened and the features are replicated. In microinjection molding, the polymers are melted and follow a complex flow path through runners and gate into the mold insert. This flow generates a large amount of flow induced shear which results in a large amount of residual stress in the part if proper methods to relieve the accumulated stresses are not followed. The smaller feature sizes magnify the amount of stress remaining in the polymer after injection molding.
- *Low thermal cycling range leading to reduced shrinkage in finer features:* The hot embossing process requires the complete mold setup to be heated and cooled. Due to simpler setup, the amount of thermal mass generated is less compared to microinjection molding process where larger molds are to be heated and cooled. In

conventional injection molding processes, the molds are maintained at low temperatures. In microinjection molding process where the size requirements are much less, the mold temperatures are raised to avoid premature freezing of the polymer. This leads to the large amount of thermal mass in the mold which also leads to longer cycle times.

The hot embossing process has certain limitations which must be addressed to use it as a mass production process. The major factors are a result of the longer embossing time and ability to produce complex features. Some limitations of the hot embossing process when compared to other micromolding process are:

- *Large amount of thermal mass involved since heating and cooling of the entire setup is required:* Hot embossing involves large thermal mass compared to micro injection molding. Lithography based replication processes does not involve any thermal mass. The large thermal mass during the process leads to longer cycle time. The hot embossing process involves less thermal mass than the microinjection molding process. However, the thermal mass involved is significant when compared to lithography based replication processes. This thermal mass leads to a longer cooling time.
- *Difficulty for use in continuous production:* The hot embossing process requires special setup to enable continuous production of replicated films. This setup reduces the cost advantage hot embossing has against injection molding processes. The higher cooling time in the hot embossing process also leads to difficulties for use in continuous production.

- *Difficulty in producing parts with undercuts or in general three-dimensional products:* The versatility of the hot embossing process in producing 2.5D geometry is known. However, when three dimensional parts with complex geometry are required, hot embossing does not have sufficient tooling capabilities. These parts can be made with microinjection molding with suitable tooling modifications, albeit with some difficulties. In hot embossing, with increases in complexity in the replicated geometry, the challenges to design a suitable tool for the process rise rather steeply.

2.3 Literature Review

2.3.1 Hot Embossing

The hot embossing process has also been studied extensively to understand the underlying physics and the effect of the key process parameters such as embossing temperature, embossing pressure and embossing time [19-27]. A steady state model[21] to predict the replicated height during microlens embossing was derived based on an analogy from Arrhenius type relationship. The effect of temperature, pressure and surface tension on the radius of curvature and height of the microlenses was modeled and verified through experiments. The flow behavior[28] of polymer filling in nanometer sized cavities was numerically derived and compared with available data of PMMA embossing to verify the applicability of continuum theory in these dimensions. The study observed the significance of capillary forces and the actual width of the flow channel. Detailed analysis[29] of the hot embossing process with various polymers as substrate materials showed marked differences in the filling behavior of isothermal and non-isothermal cases. The study observed that replication fidelity was more dependent on the processing conditions in the case of isothermal embossing than in non-isothermal embossing. It was

reported that in isothermal embossing, time and temperature optimization was necessary to obtain good replicated parts with less residual stresses. On the contrary, in non-isothermal embossing, the good part quality was achieved as the mold heats and deforms the room temperature polymer film only at regions of contact. Such behavior led to different flow patterns in both cases – isothermal embossing exhibiting a tendency for biaxial extensional flow and non-isothermal embossing exhibiting a wall climbing flow.

Dynamic characterization and subsequent process analysis to elucidate the flow patterns in the isothermal and non-isothermal embossing processes [19] were also performed by the authors. The study was able to simulate a comparable filling pattern for the experimental results in the case of isothermal embossing process. The effects of temperature on key rheological properties such as shear and extensional viscosity were predicted and correlated with the collected experimental data. Hot embossing is often a batch process and attempts have been made to modify the process to be suitable for mass production. In continuous roll embossing[30], a continuous film passes on a roll with the desired microfeatures and is pressurized with another roll. The embossed film with the features is then sent for cooling and post-processing. The continuous roll embossing process was analyzed[30] to determine the effect of various processing parameters on the final replication quality. It was observed that the temperatures to which the film is subjected during preheating and embossing are significant factors, agreeing with mathematical modeling results.

2.3.2 Variations in Hot Embossing

Studies have been extensively conducted to reduce the cycle time of the hot embossing process. A number of attempts have been made towards tool modification facilitating rapid heating and cooling[31-36].

High frequency heating[31] was utilized to heat the mold to the required embossing temperature rapidly. Through selective high frequency heating of the surface and subsequent cooling using compressed air, total cycle times about 20 s were achieved. The surface thermal response of the mold insert and the embossing setup used are shown in Figure 3. The tool was used to replicate features onto thick polymer substrates with good replication. Thermal fatigue tests conducted on the modified tool established that the tool is stable till 10,000 cycles, indicating potential applications in continuous production of microstructured polymer films.

(a)

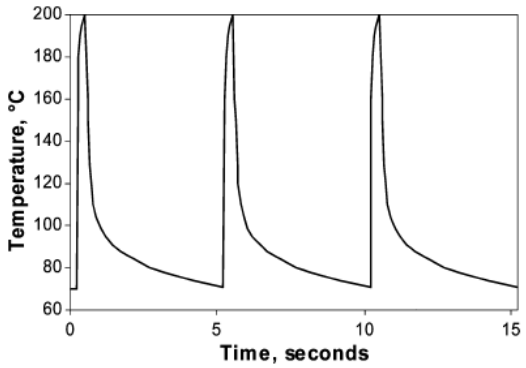

(b)

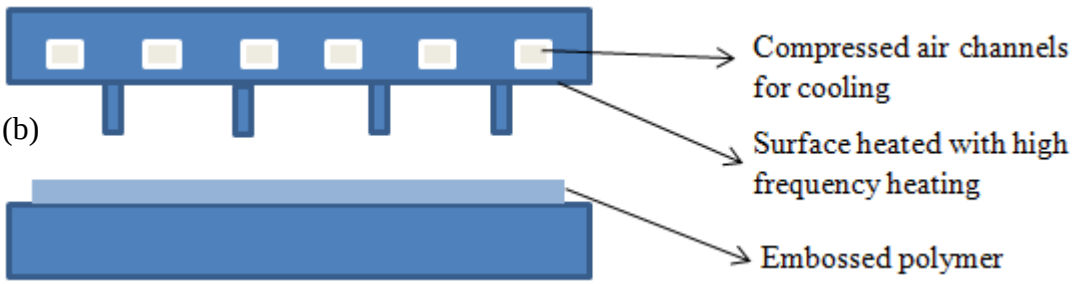

Figure 3[31] (a) Thermal response of the surface (b) Embossing setup schematic redrawn from Reference 31 Ref

Infrared heating[32, 33] were employed to transfer patterns from silicon molds to different polymer substrates to nanometer levels. The IR pulse laser was used to provide the necessary thermal energy to transfer the patterns. The study utilized the advantages of using a silicon mold for nanometer size pattern transfer. Since the process included heat transfer from the laser impulse to the silicon mold and then to the substrate, limitations were observed regarding the type of substrates that can be used in this process. The schematic of the process setup used in the IR/laser-assisted imprinting is shown in Figure 4.

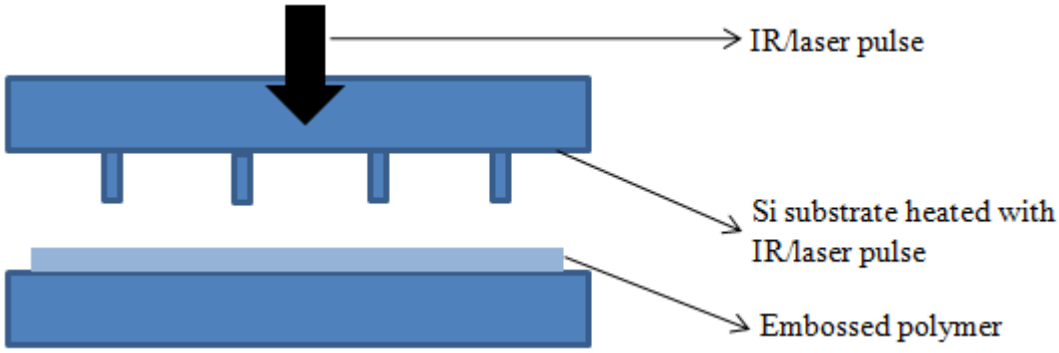

Figure 4[32] Schematic of IR/Laser Assisted Imprinting redrawn from Reference 32

Hot air heating[34] was used to minimize the embossing cycle time to less than 3 s with a hot air gun. Precise control of the temperature is difficult and it was observed sharp features were not replicated well in this method. Also, the hot gas embossing was not able to impart the required heat to completely melt the substrate and hence resulted in poor surface properties. Hot fluid heating[37] was attempted to compare three different heating methods – steam, IR and oil, and study the process thereof. It was found that though IR heating induced the shortest heating time, the temperature distribution was not

very precise. In the case of oil heating where the temperature could be controlled very accurately, the heating time is less compared to IR heating and the conventional platen-based heating methods. Schematics of the process using steam and oil as the heating medium are shown in Figure 5.

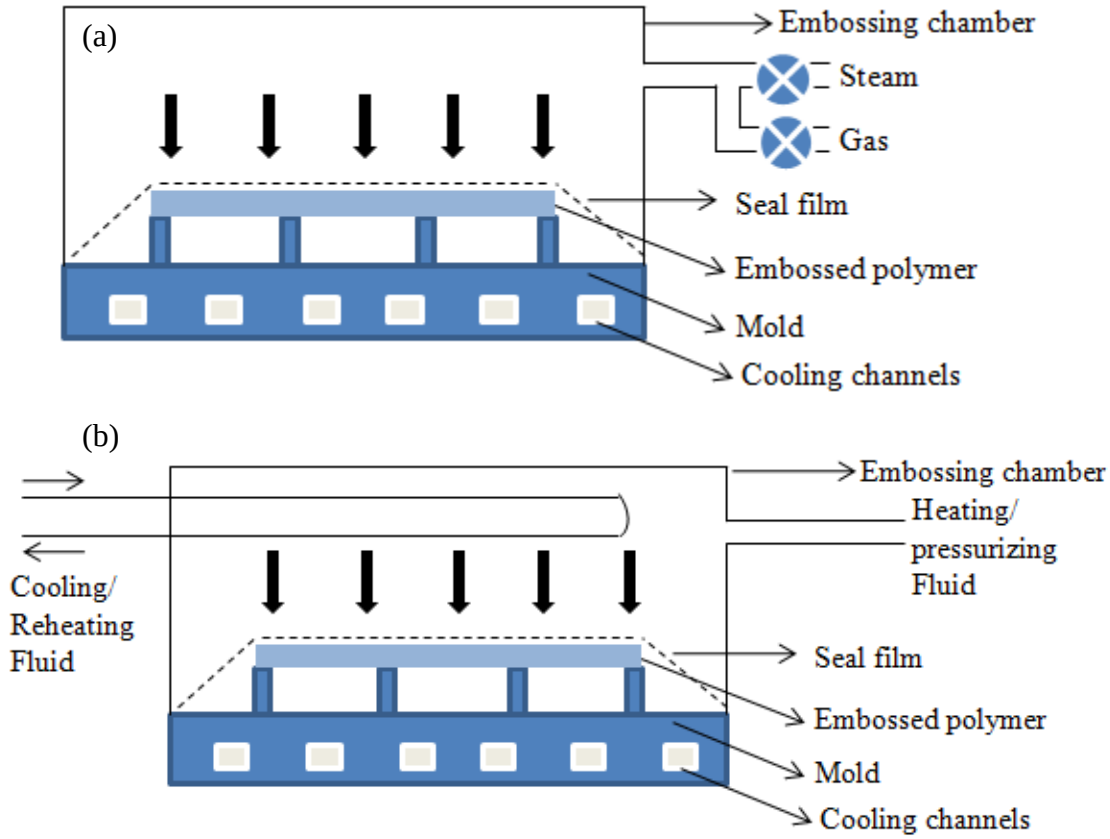

Figure 5[37] Fluid-based embossing system redrawn from Reference 37: (a) Steam Heating (b) Oil Heating

Ultrasonic heating[35, 36, 38] was another technique used for decreasing the cycle time in hot embossing to achieve cycle times less than in platen-based or fluid-based heating. As observed in the few other techniques above, the temperature control was difficult though the cycle time was in the range of few seconds. Ultrasonic vibration was used to generate the heat required for the embossing process. The study was done to

understand the effect of various ultrasonic vibration parameters on the replication accuracy of the part and to compare the application of the technique to amorphous and semi-crystalline materials. The replication of the features was better in the case of amorphous polymers compared to semi-crystalline polymers as the former have higher stiffness and vibrate in phase with the ultrasonic horn[38]. The schematic setup of this ultrasonic embossing process is shown in Figure 6.

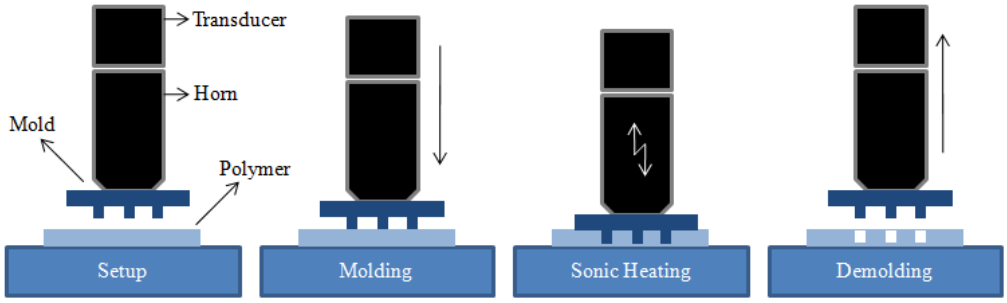

Figure 6[38] Schematic of ultrasonic hot embossing redrawn from Reference 38

The additional tooling modifications are quite expensive and may diminish the inherent cost advantage of the process. As these studies have focused on suitable design modifications to reduce the heating time, very little have been done to reduce the cooling time after the pattern transfer is completed. There has been some research conducted on modification of polymer film surface by means other than thermal influences such as solvent assisted embossing.

Solvent-vapor treatment[39] and compressed-CO_2 assisted patterning[18] have been tried as room temperature embossing variants. These processes, however, may be limited by the interaction effects and availability of suitable solvents. The solvent/CO_2 gas plasticizes the polymer surface which is pressed against the mold surface to replicate the patterns. The solvent assisted technique dilutes the polymer concentration and reduces the

T_g by plasticization leading to a room temperature imprint process to transfer features as small as 60 nm. The solvent assisted method is based on reducing the viscosity of the polymer on the polymer surface by controlling the amount of solvent to which the polymer is exposed. However, controlling the amount of solvent absorbed into the polymer is difficult and if more than required solvent is absorbed, the polymer becomes unnecessarily fluidic. Additionally, complete removal of the solvent from the polymer has to be monitored to avoid later complications. In the case of CO_2 assisted embossing, the compressed gas is used to reduce the T_g and viscosity of polymers and hence demonstrate a room temperature embossing process to transfer features as low as 100 nm. As noted in the earlier study, the exact control of the amount of the CO_2 absorbed onto the polymer layer is difficult. Also, the interaction effects of various polymers with the compressed gas have to be taken into account. A schematic of the solvent assisted and compressed-CO_2 assisted embossing process is shown in Figure 7.

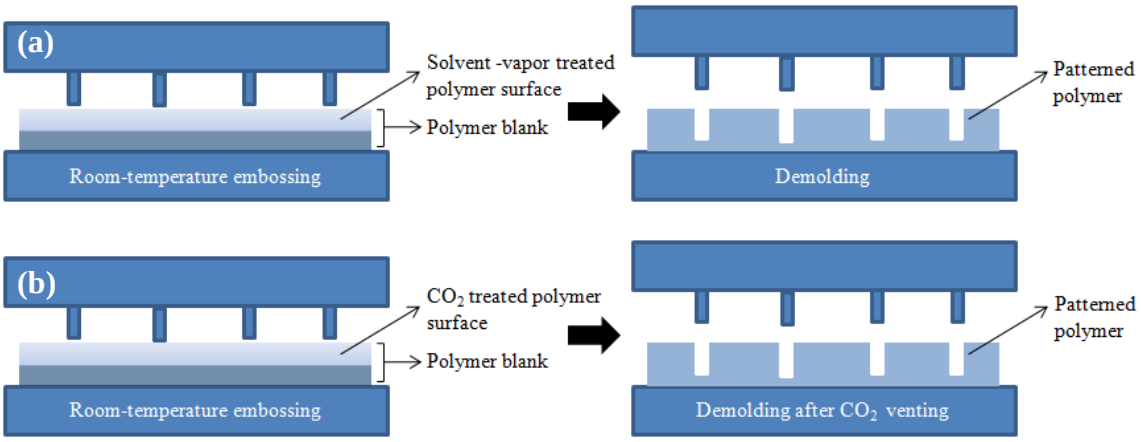

Figure 7 Schematic of (a)[39] Solvent-assisted Embossing redrawn from Reference 39 and (b)[18] Conpressed-CO_2 assisted Embossing redrawn from Reference 18

Studies[40] have also been done to emboss amorphous poly (ethylene terephthalate) (PET) films at low and high temperatures with focus on optical properties. The work

studied the embossing of PET at temperatures lower and significantly higher than T_g of around 85°C. The embossing temperatures used accordingly were 75°C and 150°C. The authors reported that at temperature higher than T_g, significant crystallization occurs in the polymer and the film becomes opaque with less replication accuracy. In comparison, the embossing performed at temperatures few degrees less than T_g gave good replication up to sub-100 nm resolution but with longer cycle time.

Additionally, a water-soluble polymer mold has been used as sacrificial template to produce high-aspect-ratio microstructures to avoid cooling period[41]. A water-soluble mold made from poly-vinylpyrrolidone (PVP) by soft lithography was used to emboss PMMA avoiding demolding. The process was aimed at reducing the cooling time as well as eliminating the demolding process which frequently results in damage of parts. IR/laser assisted heating was employed to enable fast heating of the films. Though the process can be used to produce good quality features, the total cycle time including the soft-lithography steps to produce the PVP mold, the embossing time and the time required to dissolve the sacrificial mold is over 60 min.

2.3.3 Crystallization of PET

Infrared absorption and X-ray diffraction was used to study the crystallization phenomena in PET at temperatures well above the T_g of the polymer[42]. At temperatures near 190 °C, the minimum half-time of crystallization was observed and inverse parabolic behavior in the total temperature range. Based on a modified Avrami equation, the polymer was observed to undergo a plate-like growth at crystallites in the temperature range of 120 °C to 180 °C. Temperature-dependent development of crystallinity was measured using an infrared spectrometer. It was observed that the optical densities

reached varying levels of maxima during crystallization indicating that the polymer was crystallizing at different rates. The half-time for crystallization at different temperature with a broad minimum is shown in Figure 8. As the crystallization process constituting formation of nuclei and their growth is highly temperature sensitive, the induction time and the half-time of crystallization show different values during isothermal crystallization.

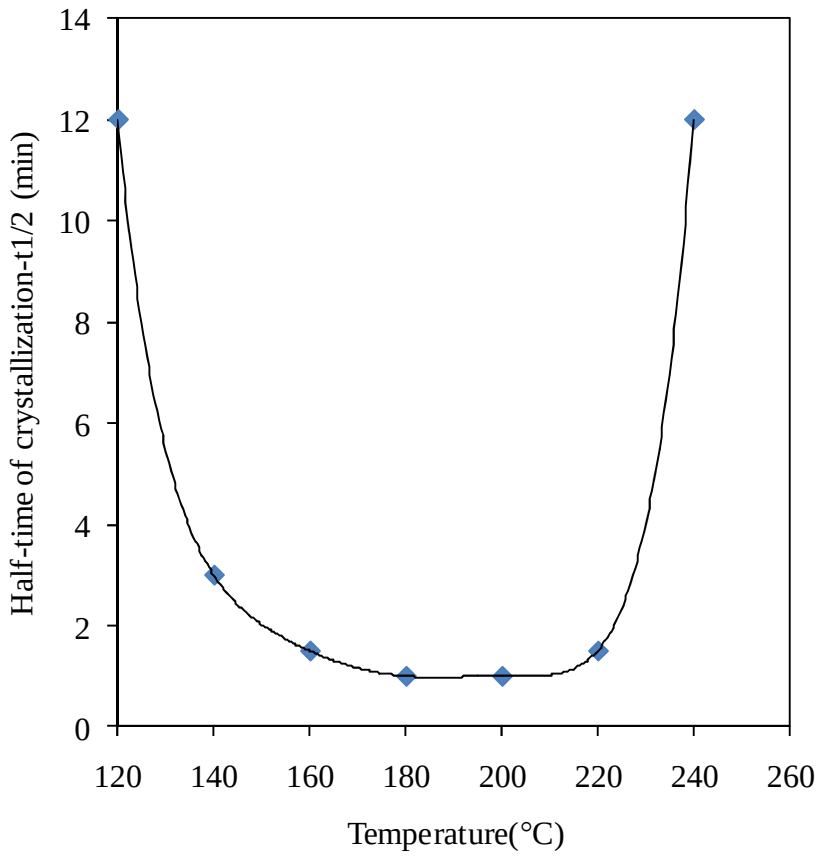

Figure 8[42] Half-time of crystallization of PET as a function of temperature: redrawn from Reference 42

Crystallization kinetics of amorphous PET films heated in silicone oil was measured with a spectrophotometer[43]. The spectrophotometer was modified to measure the transmission of light with time. It was observed that crystallization occurred at temperatures about 30

°C above T_g and at temperatures above 125 °C, but the crystallization was so rapid that it was difficult to obtain accurate measurements. The authors concluded that at initial stages of crystallization, linear growth of the crystals occurred. Isothermal crystallization kinetics[44] showed that at low crystallization temperatures, highly branched lamellae with small lateral dimensions are formed and at high crystallization temperatures, lamellae bundles with radial orientation appear.

Several other studies[45-47] have been done to understand the thermodynamic relaxation phenomena occurring at the early stages of crystallization and the morphology development during isothermal crystallization at different temperatures. It was observed that PET on heating above its Tg initially undergoes a relaxation stage leading to an isotropic material and subsequently reorients itself with time[47]. It was also observed that only long-range density fluctuations leading to ordering occur during the induction period[46].

2.3.4 Structure of amorphous PET

PET film shows high modulus and toughness even in their amorphous state and becomes increasingly brittle when crystallized under non-restrained conditions. Since the thermal conductivity of polymers is less, it is not practical to assume that the crystallization is completely obstructed even when PET is quenched from melt. In the case of slowly crystallizing polymers such as PET, variations in cooling rate are experienced at different layers of the structure. The varying degree of cooling experienced by the polymer affects the final amorphous structure formed and results in certain type of low level ordering in the polymer[48]. The low level ordering has been related to physical links rather than entanglements. Spontaneous nematic transition[46] has

been reported in amorphous PET with a change from the gauche to trans[47, 49] structures near its T_g. The stress hardening which occurs at high strain levels results in chain orientation and high crystalline content depending on the strain rate applied[50]. There are two types of crystallization in the polymer – thermally induced crystallization and stress induced crystallization. At low temperatures below or near the T_g, the thermally induced crystallization is very slow and the stress induced crystallization which results in orientation of the molecular chains can be more effective. When the amorphous PET samples are heated greatly above their T_g, the orientation and stress induced crystallization take place very rapidly through formation of local physical links.

In the amorphous PET film quenched from melt, a low level of order in the microscopic scale exists in the form of a nodular structure as shown by different studies[51, 52]. The nodular structure has molecular chains with one-dimensional ordering and with chain folds. These studies have shown that nodules measuring about 75 A are present in the amorphous PET and any annealing process even at temperatures lower than T_g results in an increase of the structural ordering although they may not result in significant increases in crystalline regions. The nodular structure formed in the amorphous PET results in a three dimensional network once the sufficient thermal energy has been supplied. Some other small angle x-ray scattering studies have reported heterogeneous structures in the amorphous PET even in the size range of 100 - 2000 A[53]. Annealing of the samples below T_g results in close packing of crystallites to a small degree. Annealing the samples below T_g under strain increased the crystallinity at the crystallization temperature but resulted in lower orientation. The crystallization studies conducted at higher temperatures

eliminated any structural changes associated with the pretreatment but resulted in additional stress during the stress-hardening step.

The relation between shrinkage and orientation has been studied to understand the effects of the starting morphology[54, 55]. It has been found that annealing the amorphous PET films leads to disorientation in the amorphous chains and subsequently results in more shrinkage. The orientation of the chains during various levels of extension and its relation to crystallization have been studied in detail for PET films and it was shown that at low levels of extension, thermally induced crystallization is dominant[56, 57].

The crystal structure of PET has been reported to be planar and fully extended based on the x-ray diffraction analysis[58] and it has been shown that the high melting point of the PET molecules is due to the rigid aromatic rings. The x-ray analysis also showed that the unit cell is triclinic with a = 4.56 A, b = 5.94 A, c = 10.75 A, $\alpha = 98.5°$, $\beta = 118°$ and $\gamma = 112°$. X-ray scattering studies conducted on PET samples crystallized unconstrained from their glassy state indicate formation of spherrulites[59, 60] which deform to platelet type structures when subjected to high strains at higher temperatures[45].

2.4 Constant Temperature Embossing Process

2.4.1 Process Definition

The Constant Temperature Embossing (CTE) process is a variant of the conventional hot embossing process wherein some inherent property of the embossing polymer is used to eliminate the cooling step. Supercooled amorphous films from crystallizable polymers such as PET, poly (ether ether ketone) (PEEK) and poly (ethylene naphthalate) (PEN) crystallize when heated above their T_g's. The polymer after

crystallization achieves the required dimensional stability for demolding without any damage and retains the structure without any recovery.

The steps involved in the CTE process are shown in Figure 9. As seen in Figure 9, the CTE process follows a slightly different route than the conventional isothermal hot embossing process as only the mold and cover plates are heated. The initial step is similar to the case of the non-isothermal embossing process. Then the polymer film is introduced between the mold and platens and the required embossing pressure is instantaneously applied. However, after the embossing stage, the CTE process differs from the conventional non-isothermal embossing process. In the non-isothermal embossing process, the embossed polymer film is cooled below its T_g before demolding from the mold. In the case of CTE, the embossing and holding stages are conducted isothermally and are directly followed by the demolding stage.

In the current study, a new CTE process by utilizing the crystallizing nature of amorphous films from slowly crystallizing polymers such as PET and PEEK is developed and investigated. Successful replication by this unique CTE process depends on the inherent nature of the polymer used for the process. The material properties can be controlled by appropriate variation of the process parameters such as the embossing temperature, embossing pressure and embossing time. As the success of the process completely depends on selecting suitable materials and controlling their properties during the process, the CTE process is a material specific process. Any material with a glass transition temperature higher than room temperature and the ability to crystallize when reheated above its T_g may be embossed using the CTE process.

The polymer film is embossed for the required amount of embossing time and then demolded at the same temperature. The major difference between the CTE process and conventional hot embossing is that in the conventional process, the polymer film after embossing is cooled down to temperatures below T_g, irrespective of whether the process is isothermal or non-isothermal. In the case of CTE, the polymer film is demolded at the embossing temperature thereby eliminating the cooling time completely. The temperature and pressure profiles during constant temperature embossing are shown in Figure 10.

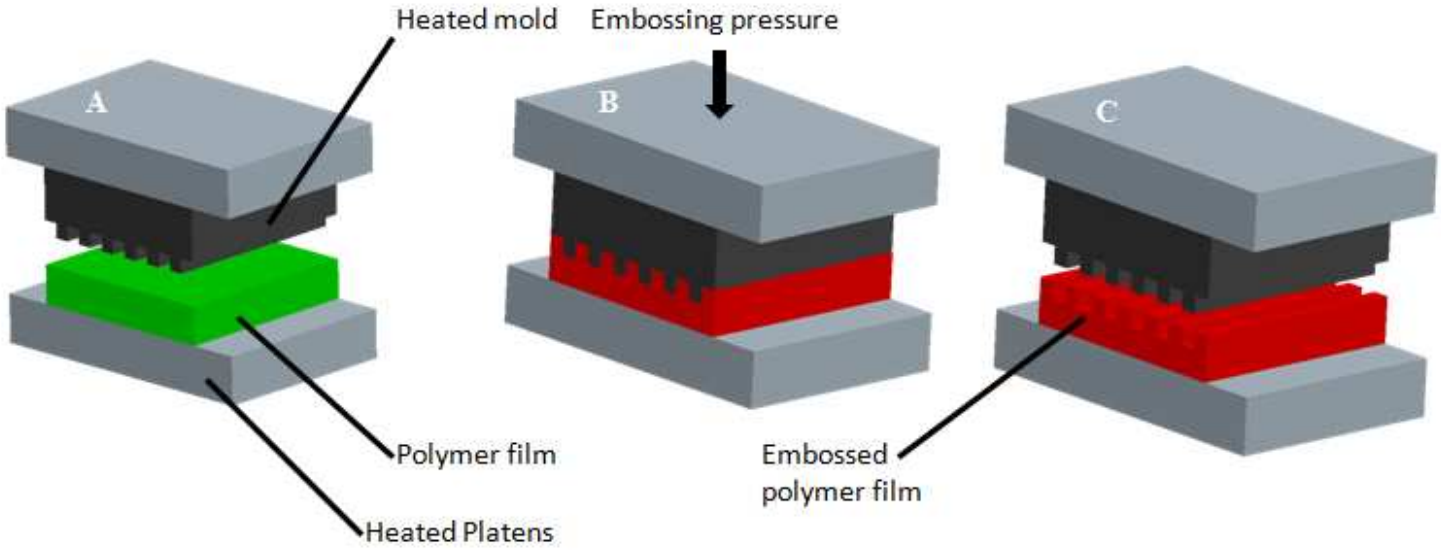

Figure 9 Steps in constant temperature hot embossing: A – Mold preheating (non-isothermal embossing); B – Embossing and holding stage; C – Cooling stage

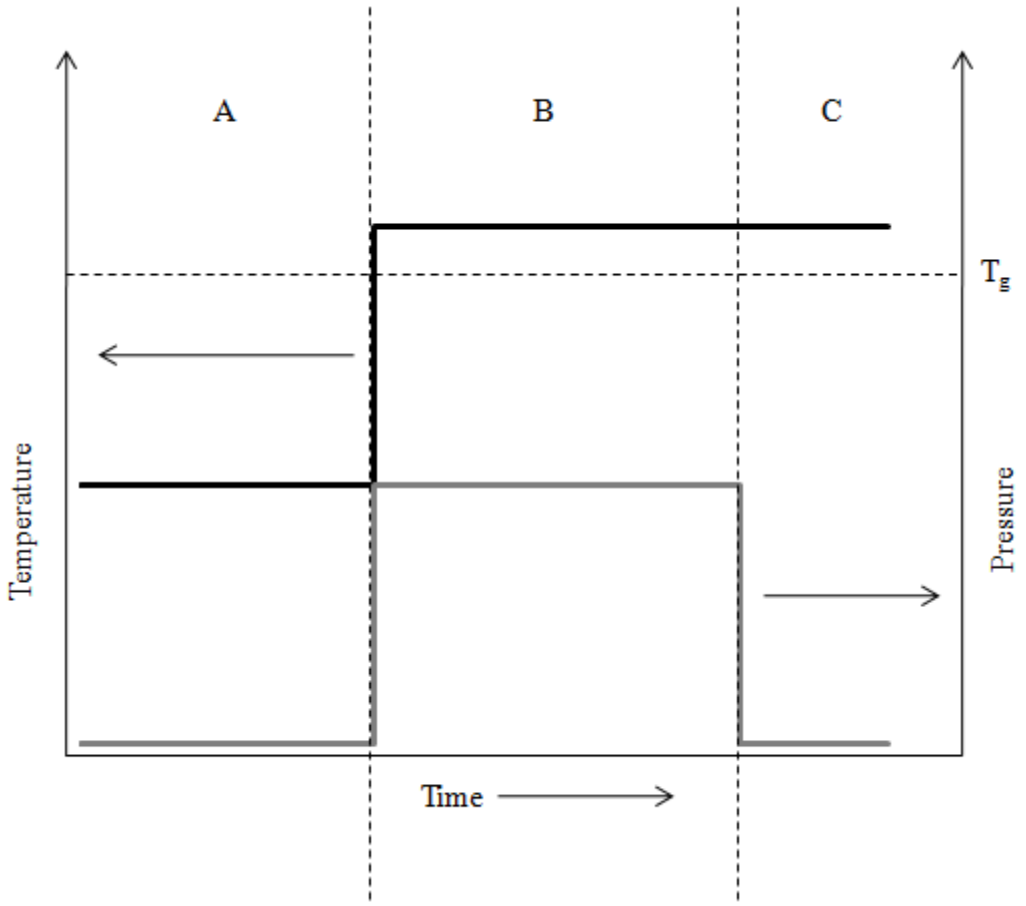

Figure 10 Temperature and pressure profiles during hot embossing: A – Mold preheating zone; B – Embossing zone; C - Demolding zone

2.4.2 Process Mechanism

The key points of the constant temperature embossing process are:

- Slowly crystallizing polymers such as PET, PEEK and PEN can be produced in amorphous states by rapid quenching.
- These supercooled films when heated above their Tg crystallize with a temperature-dependent rate.

These crystallizing polymers are produced in a nearly amorphous state (<5%

crystallinity) by quenching rapidly at the end of film melt processing. The property that these films develop crystallinity while heated above their Tg is utilized in the constant-temperature embossing process. Since the film crystallizes and solidifies during the embossing stage itself, a separate cooling stage can be avoided. The process utilizing this material property can have a total cycle time on the order of the half time of crystallization of the substrate material.

The cold crystallization peak observed in Figure 11 between the temperature range 140-180 °C in the Differential Scanning Calorimetry (DSC) thermogram of amorphous PET films has been utilized for the process. The temperature zone for constant-temperature embossing is selected in accordance with the region where the amorphous film crystallize when heated above its T_g. The key steps describing the mechanism of the CTE process are:

- *Liquefaction of the film due to rubber softening of amorphous film:* The amorphous film softens when heated above its glass transition temperature, and flow can occur when the rubber plateau termination temperature is reached.
- *Subsequent solidification due to crystallization:* When heated sufficiently above its T_g, the amorphous film obtains sufficient energy to initiate crystallization.

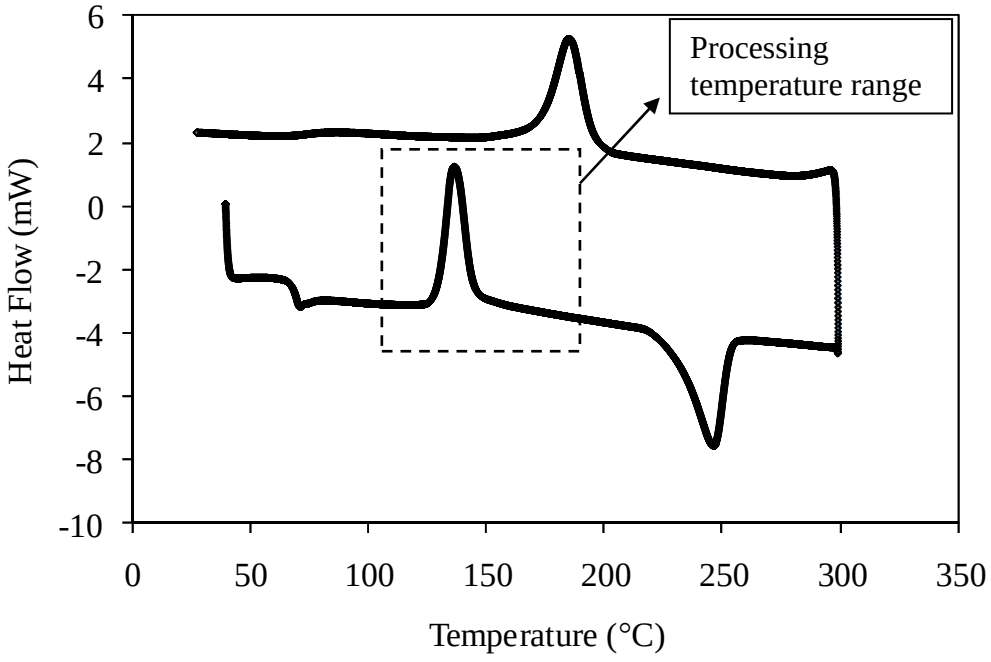

Figure 11 DSC temperature sweep of amorphous PET film

The two steps are contradictory with the material softening and hardening simultaneously, the rate of which depends on temperature. As shown in Figure 12 the rate of crystallization of the polymer is lowest at certain temperatures and increases on either side of the curve. The optimum process window can be established in the temperature region where the fill time is less than that of the crystallization induction time. The fill time is the time available for the polymer to completely fill the cavity before the crystallization starts. The softening time decreases as the temperature increases in the intermediate zone between the T_g and the melting temperature (T_m) whereas the crystallization induction starts at any temperature above the T_g.

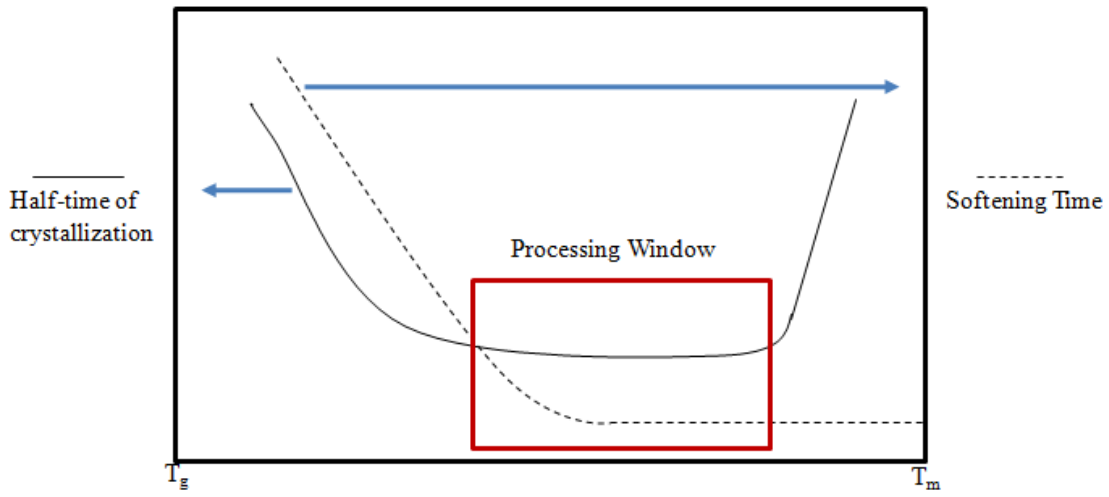

Figure 12 CTE Processing Window

2.4.3 Advantages of CTE process

The advantages of the CTE process over the conventional hot embossing process are:

- The CTE process eliminates the large thermal cycling involved in conventional hot embossing process.
- As structure formation occurs during processing, the embossed film can be demolded without cooling with less damage to the structures.
- Applicability in roll based embossing processes as the polymer can be continuously embossed and demolded without the need of cooling time.
- Through appropriate selection of polymers and optimization of processing conditions short cycle times can be achieved.

2.5 Conclusions

The proposed CTE process is one variant of the conventional embossing process where the inherent property of the embossing material is utilized. The CTE process can be employed to emboss polymers such as PET, PEEK or PEN which can be produced as amorphous film by quenching. The raw material requires the property of crystallizing when heated above its T_g. The CTE process is advantageous over the conventional embossing in completely eliminating the cooling time.

CHAPTER 3

RHEOLOGICAL AND THERMAL CHARACTERIZATION

3.1 Abstract

This chapter reports the different characterization techniques used to understand the rheological and thermal properties of the raw materials used for the CTE process. In this study, supercooled amorphous PET film was used as the model material. The material was initially characterized with techniques using conventional instruments. The conventional techniques failed to capture the change in the mechanical properties of the PET film during phase transition. An attempt to develop a tensile testing apparatus retro-fitted with an oil bath to determine the tensile properties of the PET film during the phase transition without time lag is reported. The thermal properties of the polymer film were characterized using isothermal and non-isothermal crystallization kinetics.

3.2 Introduction

Supercooled amorphous PET films may be characterized using conventional rheological and thermal techniques. Thermal characterization using DSC was used to understand the thermal properties such as the cold crystallization temperature range with its direct correlation with the temperatures used for the embossing process. The thermal characterization was also used to determine the crystallization kinetics of the polymer at different temperatures. Rheological characterization was used to understand the change in mechanical properties of the polymer during the phase transition. These changes in the mechanical properties during the embossing process happen when the material crystallizes during the holding stage. The determination of the mechanical properties

assists in optimizing the process parameters as it is essential for the embossing stage to be completed before the crystallization starts. However, tensile testing using conventional techniques failed to predict the transition properties of supercooled amorphous polymer films due to multiple parameters affecting the behavior. Different custom-designed instruments have been developed by various research groups[61-65] to conduct tensile testing of thin polymer films. These rheometers have been used to characterize extensional behavior of polymers during processing operations such as film blowing, blow molding, fiber spinning and other processes involving significant extensional flows. Most of these instruments employ oil based heating medium to facilitate rapid heating of the films as compared to the environmental chambers found in conventional tensile testing instruments. The conventional tensile testing instruments with an environmental chamber is not suited for materials undergoing phase change as there is insufficient time available for the material temperature to equilibrate before stable readings can be obtained.

The amorphous PET film is particularly challenging to characterize as the thickness of the film is around 250 µm and most conventional rheometers are designed to characterize films with thickness upward from at least 500 µm. Moreover, the rheometers are designed to measure rheological properties of materials in the melt state. The amorphous PET film in the required temperature zone undergoes softening briefly before the starting to crystallize. The material characterization technique needs to be able to conduct experiments at temperatures far lower than the melt temperature requiring specialized instruments to capture the properties accurately.

3.3 Literature Review

3.3.1 Thermal Characterization

Thermal analysis is a common technique used to determine the crystallization kinetics of polymers. Isothermal crystallization studies are well established as a means to understand crystallization phenomena in polymers[66]. The Avrami equation is the most widely used form for describing the rate of crystallization in polymers[67-69]. Crystallization is usually measured in quiescent and isothermal conditions. In actual processing conditions, there is a very narrow temperature range in which the crystallization can be measured. The difficulty arises due to the fact that the crystallization is very fast at certain temperatures which are hard to practically measure during experiments. In most polymer processing operations, non-isothermal crystallization is more prominent[70-76]. The other reason measuring crystallization kinetics is hard is that the thermal characterization equipments have limitations in terms of the rate of cooling and heating.

In order to measure the isothermal crystallization kinetics at higher supercooling and at temperatures much lower than the melting temperature, rapid cooling of the polymer melt to the required temperature is needed. Differential scanning calorimeters have limitations in terms of the rate at which the sample can be cooled and partly because polymers have very low thermal conductivity. Any rapid heating or cooling of the polymer samples would be associated with a huge temperature lag between the set temperatures and actual temperature in the sample. As mentioned above, there is a second temperature lag from the instrument itself due to the temperature lag between the set temperature and the temperature observed in the sample pans. These temperature lags can be rectified by using suitable correction factors[77] which take into account the difference

in the conductivity of the mediums. Many studies have attempted to use isothermal kinetics data to apply to non-isothermal polymer processing operations, but this has been observed to be less than accurate in describing the phenomena[76]. The basic Avrami isothermal kinetic equation has been modified to be suitable for describing non-isothermal kinetics data. These studies have taken into consideration the theory associated with the crystallization phenomena and derived equations in an integral or differential form.

3.3.1.1 Ozawa Model

The Ozawa model[78-85] is based on describing the crystallinity in terms of the cooling rate as shown in Equation 1:

$$X_T = 1 - \exp\left(-\left(\frac{K_{(T)}}{\varphi^m}\right)\right) \quad (1)$$

where $K_{(T)}$ and m are the Ozawa crystallization rate and exponent.

The Ozawa equation has been used to study the crystallization kinetics of nylon 6, PET, PP, and other materials. The integer m is similar to the exponent n in the Avrami equation describing the type of nucleation and dimensions during growth. Relative crystallinity data at a particular temperature is required at different cooling rates to use the equation given above. For the current study, where the process is to be modeled, the Ozawa analysis is not appropriate as the equation does not render any useful way to analyze the crystallization phenomena.

3.3.1.2 Nakamura Model

The Nakamura model is widely used to describe non-isothermal crystallization kinetics by assuming isokinetic conditions, independence of final crystallinity on the

cooling process, and constant number of activated nuclei. The Nakamura model is shown in Equation 2.

$$\theta(t) = 1 - \exp\left[-\left(\int_0^t K(T)dt \right)^n \right] \quad (2)$$

where $\theta(t)$ is the relative crystallinity and $K(T)$ is the non-isothermal crystallization constant. The differential form of the equation can also be used to describe the non-isothermal crystallization as shown in Equation 3:

$$\frac{d\theta}{dt} = nK(T)(1-\theta)[-\ln(1-n)]^{(n-1)/n} \quad (3)$$

For n>1 in the differential form of the Nakamura equation the relative crystallinity has to be non-zero. Khanna and Taylor[86] also suggested a similar model by modifying the isothermal Avrami equation. Both of these equations reduce to Avrami equation for isothermal conditions.

Another model very similar to the Nakamura model was independently described by Kamal[87] et al., using the integral form of the Avrami model for non-isothermal crystallization. The Kamal model is shown in Equation 4

$$\frac{X(T)}{X_\infty} = 1 - \exp\left[-\int_{T_0}^{T} k(T) n \left(\frac{T_0 - T}{R} \right)^{n-1} \frac{dT}{R} \right] \quad (4)$$

This model uses the isothermal crystallization rate constant $k(T)$ from the Avrami equation, but suitably modifies the equation to describe the non-isothermal process.

It has to be noted that these equations do not consider the secondary crystallization which has been addressed by Dietz[88], who modified the equation to account for the secondary crystallization. The current study does not consider the secondary crystallization phenomena to be occurring during the processing.

It was observed that the integral Nakamura model gave better predictions than the Kamal model as the accuracy of the Kamal model depends on the temperature at which the residence time is measured. Also, there is no specific guideline on when to start considering the residence time. The model's dependence on the residence time along with the temperature and crystallinity poses further problems. In the case of the Nakamura model, the rate of crystallization depends only on the temperature and crystallinity. Also, any form of time is excluded from the Nakamura model giving it an inherent advantage over other models. Hence, the Nakamura model is very suitable describing the crystallization in process modeling. Since the Nakamura model does not take into account the initial induction time for the crystals, there is certain extent of overprediction of the results compared to the actual observed values. Though this might be considered in order to get an accurate prediction of results, in the current study it is ignored as data is collected for a wide range of temperatures over different cooling/heating rates.

The master curve approach[70] for the non-isothermal crystallization kinetics was developed to predict more accurately the crystallization kinetics as observed in practical conditions. The experiments were conducted by melting the polymer well above the melting temperature and then cooling them at different cooling rates. Similarly, to determine the cold crystallization kinetics, the polymer is crystallized at different heating rates and the curves shifted to one master curve using a shift factor. The study was conducted using two different methods: one is using only the experimental data and another using both the experimental data and the non-isothermal model. The study was based on the assumption that the rate of crystallization is in its basic form as shown in Equation 5:

$$\frac{d\theta}{dt} = K(T)f(\theta) \tag{5}$$

where θ is the degree of crystallinity, T is the temperature of crystallization and t is the time of crystallization.

The shift factor is calculated at a constant degree of crystallinity θ_j using Equation 6[70]:

$$\frac{(d\theta/dt)_{ij}}{(d\theta/dt)_{rj}} = \frac{K(T_{ij})f(\theta_j)}{K(T_{rj})f(\theta_j)} = \frac{K(T_{ij})}{K(T_{rj})} = a_T(T_{ij}) \tag{6}$$

where $a_T(T_{ij})$ is the shift factor at temperature T_{ij} with reference to the temperature T_{rj}. The indices i= 1,2,3,. . . ,r , . . . stand for the i-th cooling rate and j = 1,2,3,. . . denote the j-th degree of crystallinity[70]. The shift factor is determined by using the data for crystallinity and rate of crystallinity as a function of temperature. Initially, for a fixed crystallinity θ_j, the $(d\theta/dt)_{ij...rj}$ are found and the shift factor is computed. Then, the shift factor is mathematically shifted vertically to determine the universal shift factor as a function of temperature. The shift factor can be used to calculate reduced time. The reduced time is needed in constructing the master curve and can be determined from the following equation[70]:

$$\xi = \int_0^t a_T(T(t'))dt' \tag{7}$$

where ξ is the reduced time for the non-isothermal crystallization kinetics with reference to the temperature T_r. The individual curves when plotted with the reduced time will collapse into one single master curve which can be used to predict the kinetics at a wide range of temperatures independent of cooling rate.

The second method uses the Nakamura model to determine $K(T)$ which is further used to find the shift factor a_T, as shown in Equation 8 & 9:

$$K(T) = \frac{d\theta/dt}{n(1-\theta)[-\ln(1-\theta)]^{n-1/n}} \quad (8)$$

$$a_T(T) = \frac{K(T)}{K(T_r)} \quad (9)$$

The shift factors from both methods were compared[70] for consistencies and they appeared to be close in the temperature regimes probed. Though the first method gives an independent assessment of the kinetics without resorting to any particular model, it is difficult to get some results accurately. The difficulty arises from the fact that shifting the curves with respect to one particular temperature in the final step is not always smooth. Since generally the temperature at which crystallization occurs is narrow in most polymers, the curves are not smoothly stacked above each other with uniform spacing. Therefore shifting the curves becomes difficult, but the curves once obtained are more accurate representations of the kinetics than a model which may overestimate or underestimate the rate and path followed during crystallization. As mentioned above, these models, however robust they may be, have certain limitations.

3.3.2 Rheological Characterization

The rheological properties are required to understand the deformation behavior of materials during processing. Conventionally, the rheological properties are characterized using rotational or capillary rheometers. These methods are useful in understanding the materials' viscoelastic properties which can be further used to develop generalized process models. The complex flow experienced by the polymers can be understood by the models developed based on measurable data[89]. The measurement of viscoelastic properties of polymers to predict the response to forces are done by using rotational rheometers. Since the shear rates experienced by the polymer during a conventional

embossing process is very low, the characterization of material at high shear rates as in a capillary rheometer has not been required.

The rheological properties for materials which undergo phase change during processing have been an important area of study[89-98]. Researchers have been developing different ways to measure accurately the properties during the transition regime. However, standard instruments have not been developed which can accurately record any abrupt change in rheological properties. Though high sensitivity sensors and fast acquisition options have been integrated into the measurement instruments, there is always an initial time lag before which the instruments can record stable readings. Studies have been conducted attempting to use rheometers as tools to represent the property changes occurring during crystallization[91]. These studies have reported some inaccuracies due to instrument limitations. The other challenge when using rheometers as tools to measure the crystallization phenomena is to account for the shrinkage happening when the polymer crystallizes. This can be rectified by adding a correction to the equation used to convert the raw data to material properties[99, 100].

3.3.3 Elongational Characterization

Simple shear is the customary mode of deformation for the study of the rheology of viscous liquids. However, knowledge of the extensional behavior of polymer melts is extremely important due to the industrial relevance of extensional flows in common processing techniques and sequences such as blow molding, film blowing, fiber spinning, melt flow through extrusion dies and injection mold filling. Hence, its understanding is important from a process optimization point of view. However, this goal has not been easy to explore. Because experimentally achieved extensional flows, such as melt

spinning and contraction flows, only provide qualitative information about the extensional characteristics of the melts. Instruments based on the concept of Meissner[101, 102] have yielded the better results, but have been expensive dedicated devices and, therefore used less in both academic and industrial communities.

The concept of elongational viscosity was first introduced by Trouton in 1906 in a study of pitch, tar and similar substances descending under their own weight. Trouton proposed the simple relationship that viscosity under tension is three times that under simple shear[103]. A clear comparison between the simple shear and the extensional response of a polymer melt[104]and elongational tests for rubbery polystyrene to determine a constant elongational viscosity were conducted.

It is well known that the elongational viscosity can be defined as the ratio of tensile stress to strain rate. Hence, while keeping one of these quantities constant at a series of levels, measurements are made of the other. This can be achieved by two methods. In the first method, the specimen volume is kept constant and the specimen length is varied by moving the clamps at two ends of the specimen which is adapted in a general tensile testing apparatus. In the second method, the specimen length is kept constant, but the specimen volume is changed by drawing the specimen between nip rolls at fixed points in space.

In the first method, the constant strain rate is achieved by separating the ends of specimen with increasing velocity, and constant stress is achieved by deforming the sample under a load which decreases in proportion to the cross-sectional area of the extending specimen. In the second method, the constant strain rate is achieved by

drawing the sample between the rotating nips at constant velocity, and the constant stress is achieved by keeping the gauge length constant.

The constant stress system has an advantage if one is primarily concerned with the equilibrium state, whereas the constant rate of strain approach will give more information about transitional behavior. Because of the more rapid equilibrium, constant stress systems are better adapted to studies of a viscosity which decreases as the stress is increased. In practice constant stress systems suffer more from friction and this limits their usefulness at low stress. The constant stress approach is, however, more perspicuous, since strain can be read directly, whereas in constant strain rate experiments stress must be calculated. Christopher et al.[103] reviewed the issues related to measurement of elongational viscosity and defined uniaxial extension, biaxial extension and the viscosity equations for the same.

Generally during viscosity measurement the material flow is assumed to be a steady and posses a spatially uniform flow. However, in practical applications where elongational viscosity is important, the flows are never steady and spatially uniform. Hence it is known that a transient extensional viscosity is used interchangeably with the elongational viscosity

3.3.3.1 Direct methods to measure the elongational viscosity

Rheometers for measuring the rheological behavior of fluids in uniaxial elongational flows have been in use since the end of the 1960s for polymer melts[105], and since the beginning of the 1990s for polymer solutions[106]. However, for polymer melts, elongational experiments present complex problems such as the difficulty of clamping

the melt without necking, gravitational effects and difficulty in conducting large strain experiments.

The original uniaxial rheometer was designed by Meissner but due to the above limitations the extensional rheometer of Meissner[102] was modified and two variations were found in the literature. The modifications include[101] the introduction of a supporting liquid to compensate for buoyancy, horizontal placement of the sample and use of rotary clamp.

The first rheometer consists of two pairs of counter rotating rollers, each pair acting as clamps[102]; the second comprises a single pair of counter rotating rollers which clamp the sample on one side, while the other is attached to some sort of fixed clamp. The rheometer was also used to solve some problems faced during the elongation viscosity measurement of melt samples[107].

3.3.3.2 Homogeneous Uniaxial Extension with Single Pair of Rotating Rollers:

Meissener et al.[101] measured the elongational viscosity of polypropylene at various temperatures and elongational strain rates using an improved apparatus. The constant elongational strain rates were calculated by simultaneous measurement of sample diameter. A new definition of critical elongational strain (γ_c) was presented, along with the effect of temperature and the elongational strain rate on γ_c.

A modified uniaxial rheometer with a pair of rotating clamps was developed[108]. Its main components were a silicone oil bath, a rotating roll clamp, tensile testing parts and a microscope. The rotating clamp had a pair of flat gears with a small module. Rotation speed was varied giving values from 0.002 to 0.6 s^{-1}. The elongational strain is

quantified using the Hencky strain and the corresponding elongational strain rate is defined by Equations 10 and 11.

$$\gamma = \int_{t_0}^{t} \frac{dl}{dt} = \ln \frac{l}{l_0} \tag{10}$$

$$\dot{\gamma} = \frac{1}{l} \frac{dl}{dt} \tag{11}$$

With two rotary clamps in a horizontal apparatus the problem of a homogeneous uniaxial extension can be solved, at least in principle. The first version of an extensional rheometer has two rotary clamps at a constant distance from each other and is driven by synchronous motors. Hence, the rod like polymer melt sample floating on silicone oil is elongated with a constant Hencky strain rate $\varepsilon_0 = (dL/L)dt$. In this relation L is the length of an element of volume, which remains within the clamps during the whole test procedure. The important feature of the rotary clamps is that they continuously transport the polymeric material within the clamps outside the basis length L_0. Therefore no necking zone can develop in the sample near the clamps, and the sample within L_0 keeps a homogeneous cross section during the deformation, provided the temperature field is sufficiently constant in space and time. In fact, the different versions of this type of rheometer had to be developed mainly to improve the temperature constancy.

The portion of the specimen remaining between the gears was stretched at a constant elongational strain rate by a pair of gears rotating at a constant angular velocity. Meissner[105] reported that elongational viscosity-time curves were S-shaped. Elongational viscosity data for various elongational strain rates were superposed at the beginning of elongational viscosity growth and almost coincided with the linear viscoelastic curve, i.e. the curve shows elongational viscosity to be three times the shear viscosity at very low

shear strain rate. After considerable time, however, elongational viscosity rose quite markedly from the superposed curve and ultimately the specimen broke. Similar elongational viscosity behavior has been reported for other polymers[109] where it was observed that the onset of rapid elongational viscosity growth occurred at the critical value of total strain (γ_c = 0.9) which was independent of elongational strain rate. The total strains at which viscosity became 10% greater than the linear viscoelastic curve was defined as the critical elongational strain. However, the exact definition of γ_c is somewhat difficult here because elongational viscosity in the vicinity of the γ_c point deviates asymptotically from the linear superposed curve. Ide and White[110] discussed in particular the fracture behavior of polymer melts.

The extensional rheometers which use rotary clamps have the advantages of a very homogeneous deformation thereby reducing necking of the polymer and achieving very large total strain. However, there is one important disadvantage: the demand of relatively long samples. The need to simultaneously drive the rollers and measure the tension in at least one of the pairs has induced the development of the latter design, which dissociates the driving and measuring mechanisms.

Munstedt et.al[65] did a comparison between the tensile rheometer based on Meissener's design and rheometer based on a double cam creep apparatus. It was demonstrated, using a low-density polyethylene sample, that these two different experimental methods give the same results for elongational viscosity and recoverable strain in the steady state of elongational flow. Measurements at constant stretching rates were conducted using a tensile rheometer based on Meissner's[102] design while the experiments at constant tensile stresses σ were carried out by the double-cam creep

apparatus. In contrast to the devices[104] in which the specimens are stretched in a horizontal position, the samples were vertically suspended in a silicon oil bath, thus reducing friction losses that would result from additional return pulleys. The advantages of the double- cam creep apparatus are its simple mechanical construction, easy handling, and its ability to measure very small amounts of material.

The Rutherford Elongational Rheometer (RER)[111] was designed and is based upon a specimen-end-separation method, with a closed-loop system imposing and controlling a constant strain rate or constant stress, depending on the selected mode of testing. The elongational rheomter was used to determine the deformation characteristics of PET in the rubbery region. In specimens deformed in the constant stress mode, the strain rate and recoverable deformation attain their equilibrium values relatively quickly, and a steady-state condition is reached at modest levels of strain.

A linear relationship between deformation and time defines the onset of steady conditions. In contrast, the advantage of the constant strain rate mode is that it utilizes the ease of strain rate control by maintaining a test-velocity increase in proportion to the specimen deformation. A much longer test interval is usually required to reach a state of dynamic equilibrium in the case of constant strain rate mode compared to constant stress mode, and steady-state conditions are rarely achieved[112]. However, transient data derived from constant strain rate tests are often more representative of polymer deformation and flow in many commercial processes[113, 114]. This mechanism provides a convenient means of calculating the instantaneous strain rate from easily measured test parameters. By maintaining a constant strain rate, i.e. by increasing the test velocity according to the specimen extension, ‘steady uniaxial extension' is developed. The principle of servo-

control to produce a constant strain rate involves the combination of feedback signals from specimen length and separation velocity.

Several attempts have been made at modifying rotational rheometers for uniaxial extensional experiments. The most notable are [115-117] based on the fiber-windup technique and the results obtained are in general agreement with the literature, but have the basic drawback of being restricted to one rotation of the plate of the rheometer since after one full rotation the polymer starts winding.

Maia et al.[118] proposed an extensional rheometer using the driving and measuring capabilities of a commercial rotational rheometer in order to measure uniaxial extensional viscosity in the same way as that of the Meissner[61] type devices. This instrument was capable of controlling temperature through sample immersion in a silicone oil bath and sample temperature can be controlled to within $\pm$1°C of the set value.

The above experimental methods have some limitations such as extensional deformation control and uniformity. Hence, Sentmanat[64] developed the dual wind-up extensional rheometer that takes advantage of the high strain and true applied strain rate capabilities of a fiber wind-up technique and addresses the issue of non-uniform deformations associated with fixed-ended fiber stretching. They also introduced the effect of density during elongational viscosity measurement. This patented technology[63, 119] employs a dual wind-up drum technique that allows the ends of a sample to be stretched by means of two counter-rotating wind-up drums whose resistance to rotation is hindered by the material response of the stretching sample. The rheometer consists of paired master and slave wind-up drums mounted on bearings housed within a chassis and mechanically coupled via intermeshing gears. Here it is assumed that, if there is no

deviation between the nominal and actual strain rates, the instantaneous cross-sectional area, $A(t)$, of the stretched specimen changes exponentially with time, t, for a constant Hencky strain rate experiment and can be expressed as:

$$A(t) = A_0 \exp[\dot{\varepsilon}_H t] \tag{12}$$

Here, A_0 is the initial cross-sectional area before stretching.

For melt rheology experiments, however, polymer samples exhibit a decrease in density upon melting, manifested as a volumetric expansion of the specimen span while loaded on the Sentamanat Extensional Rheometer (SER). Hence the cross-sectional area of the molten polymer specimen was calculated using Equation 13:

$$A(t) = A_0 \left(\frac{\rho_s^{2/3}}{\rho_M} \right) \exp[\dot{\varepsilon}_H t] \tag{13}$$

where A_0 is the cross-sectional area of the specimen in the solid state, ρ_s the solid-state density and ρ_M the melt density of the polymer.

For a constant Hencky strain rate, the tensile stress growth function, $\eta_E^+(t)$, of the stretched sample can then be expressed as:

$$\eta_E^+(t) = \frac{F(t)}{\dot{\varepsilon}_H A(t)} \tag{14}$$

Sridhar and co-workers[106, 120] demonstrated the ability to generate a uniaxial extensional flow at a constant strain rate $\dot{\varepsilon}_0$ while measuring the viscous forces exerted on the endplate by the deforming filament of fluid. In this design, a small, cylindrical sample of fluid is held between two rigid circular plates, which are then separated at a known rate. By measuring the force on one of the endplates, one can calculate the transient extensional viscosity growth function $\eta^{-+}(\dot{\varepsilon}_0, t)$ of the fluid as the Hencky strain

$\varepsilon = \dot{\varepsilon}_0 t$ of the filament is increased. As a result of the no-slip boundary condition imposed by the rigid endplates, the deformation is spatially inhomogeneous and fluid elements near the endplates exhibit mixed shear and extensional flow. Tirtaatmadja and Sridhar[106] proposed altering the endplate axial kinematics in order to produce a radial history for fluid elements at the axial mid-plane of the column that is equivalent to that of a homogeneously elongating cylinder. A detailed study of the non-idealities of the kinematics introduced by endplates of the rheometer was presented by Spiegelberg et al[121] and the subsequent effect on the measured transient Trouton ratio Tr = $\eta^{-+}(\dot{\varepsilon}_0, t)/\eta_0$ was discussed. This work demonstrated that while the velocity compensation technique introduced by Tirtaatmadja and Sridhar[120] yields a constant strain rate $\dot{\varepsilon}_0$ at the filament midpoint for the entire test, the rest of the fluid column experiences a range of strain rates and subsequent strain histories. The endplates thus result in a spatially non-homogeneous distribution of elastic stresses throughout the column and this in homogeneity is important in calculating the 'extensional viscosity' of the fluid and in governing the stability of the elongational flow in the filament at high strains.

At very large Hencky strains, the transient extensional viscosity should approach the steady uniaxial elongational viscosity $\eta^{-}(\dot{\varepsilon}_0)$. Ooi and Sridhar[122] obtained steady-state values for several strain rates for the S1 fluid, while Tirtaatmadja and Sridhar attained steady-state values for a polyisobutylene (PIB)-based Boger fluid for a few strain rates. This plateau in the extensional viscosity, and therefore the transient tensile stress, indicates the time at which the macromolecules in solution have reached their maximum extension, and is a function of the contour length of the polymer chain. For dilute solutions of flexible high molecular weight linear polymers, simple Finitely Extensible

Non-linear Elastic (FENE) dumbbell models and more realistic bead-spring chain models both predict that high levels of strain $\varepsilon > 5$ are required to ensure that the chains reach full extension, accompanied by high levels of stress to maintain this extension. James and Sridhar[123] compared the results of Tirtaatmadja and Sridhar[120] with the predictions made by Batchelor's theory for rigid rods undergoing extensional flow, and found that the theory predicted steady-state values that were one order of magnitude higher than those found experimentally. The authors attributed this discrepancy to molecular entanglements in the fluid.

The design of the filament stretching device[121] does not allow deformations of $\varepsilon > 5$, and yet experiments conducted on new polystyrene (PS)-based Boger fluids showed the approach of a steady-state plateau in the tensile stress for strains less than $\varepsilon < 4$. The midpoint radius of the filament continued to decrease at a constant rate as required for a homogeneous uniaxial elongation; however, upon imaging of the full filament profile during the progress of deformation, it was found that at high strains the filament no longer deforms as a uniform cylinder but instead begins to detach from the endplates. The onset of this decoherence is associated with a viscoelastic flow instability that is localized near the endplates, and is characterized globally by the attainment of a constant tensile stress in the filament.

Information on elongational flow behavior of polymer melts and/or supercooled polymeric liquids is of prime importance for the evaluation of the validity of phenomenological and molecular theories of the polymeric liquid rheology. Meissner (1994) invented[61] a still better apparatus, a new elongational rheometer of a gas cushion supporting, metal conveyer-belt type, which has been commercialized as Rheometrics

Melt Elongational Rheometer (Model RME) from Rheometric Scientific (TA Instruments).

In RME the sample supporting liquid was replaced with a cushion of inert gas such as nitrogen or argon. This system removed a possibility of hazardous interaction with the melts and raised the upper temperature limit to somewhere above 350°C which is 150°C higher as compared to around 200°C attained with the previous version of the rotary-clamp, silicone oil supporting type[124].

Katayama et al[125] carried out isothermal melt spinning experiments to observe the birefringence and flow properties on a low density polyethylene (LDPE) to monitor the molecular orientation and onset of crystallization in the spun fibers. The melt spinning was essentially a constant tension elongation. On the other hand, Muller and Froelich[62] reported an extensional rheometer for simultaneous measurements of elongational viscosity and birefringence and tested the stress optical rule on some polystyrene melts. Koyama and Ishizuka[126] carried out a pioneering attempt of simultaneous measurements of tensile stress and birefringence on a LDPE melt under transient elongational flow at constant strain rate just by installing an incident-light polarizing microscope into an elongational rheometer of Meissner's liquid supporting type .

In order to look into the internal structure of polymeric liquids under elongational flow, they installed a high-precision birefringence ellipsometer into RME, taking advantage of its new features. Obviously, it was very difficult to install an optical device into the previous version of the liquid supporting type, but by using RME with an inert gas cushion support it was possible to introduce relatively easily a birefringence apparatus of a reflection-double beam path type simply by mounting a small reflecting

mirror at the center of the sample supporting system of the RME[61]. The modified version of RME is called *"elongational flow opto-rheometer* (EFOR)[124]" and was able to perform simultaneous, real-time measurements of tensile stress $\sigma(t)$ and birefringence $\Delta n(t)$ as a function of time t under constant tensile strain rate $\dot{\varepsilon}_0$, or more precisely, constant time derivative of the Hencky strain:

$$\varepsilon(t) = \dot{\varepsilon}_0 t \tag{15}$$

On the other hand, from the observed tensile force $F(t)$ the tensile stress $\sigma(t)$ and the elongational viscosity $\eta_E(t)$ were evaluated, respectively, as

$$\sigma(t) = F(t)/A(t) = [F(t)/A_0]\exp(\varepsilon_0 t) \tag{16}$$

$$\eta_E(t) = \sigma(t)/\dot{\varepsilon}_0 \tag{17}$$

In Meissner's RME one can vary "the Hencky strain rate $\dot{\varepsilon}_0$" within the range of 0.001 to 1.0 s^{-1} and attain the maximum Hencky strain ε_H of 7 (or 6, depending on the conveyer design) corresponding to the maximum stretch ratio λ_{max} (= L_f/Lo) of as much as 1100. Thus if a sample strip is stretched at the minimum rate, it takes as much as 7,000 s to complete a run, while stretching at the maximum rate completes within 7 s if the strip is not ruptured during the run of course. RME allows the measurement of tensile force $F(t)$ of 0.001 to 2 N. The software of the data processor (the black box of RME) was designed to collect some 3,600 data points during each run in a prescribed manner. The highest attainable temperature can be as high as 350°C.

3.3.3.3 Indirect methods to measure the rheological property:

Liquids with viscoelastic properties, like polymer solutions, are often rheologically characterized in terms of their shear-thinning and strain hardening behaviors. The shear viscosity can easily be determined as a function of the shear rate by means of rotational viscometers, but the measurement of the elongational viscosity is much more difficult. In these measuring devices, a liquid sample is stretched at a constant strain rate to form a thread. The rheological measurement is based on the determination of the axial force in the stretched thread. In fluids with low viscosity or weak elasticity, however, this force is very small, so that it is difficult to measure it accurately. For such fluids, alternative methods were developed, which evaluate the pressure drop in a flow of the fluid through a packed bed or work on the principle of the opposed-jet rheometer, as commercialized by Rheometrics Inc (TA Instruments)[127].

The elongational rheometer consists of two plates for producing a liquid thread, and an optical unit for measuring the thread diameter. For carrying out the measurement, a drop of the liquid is put on the lower plate. The upper plate is then lowered such that the liquid sample wets both plate surfaces completely. Then, the upper plate is pulled up rapidly by means of the solenoid, so that a liquid thread of constant length is formed. Capillary forces lead to a thinning of the thread with time, which is quantified by means of the optical measuring unit. For this measurement, the liquid thread is illuminated by means of a diode laser such that a shadow of the thread is projected onto the photo detector. This shadow reduces the optical light power received by the photo detector. The reduction in the optical power is proportional to the thread diameter. The exact relationship between thread diameter and voltage measured at the photo detector output is

determined by means of a calibration procedure. From the temporal evolution of the thread diameter, the elongational behavior of the liquid can be deduced on the basis of a rheological model of the viscoelastic fluid

In the theoretical description of the liquid flow in the thread, inertial and gravity forces are neglected. The forces acting on the thread are the driving capillary and the resisting viscous and/or elastic forces. In purely viscous fluids, elastic forces do not occur, and in viscoelastic fluids, strain hardening may lead to a strong dominance of the elastic over the viscous forces, so that the latter can be neglected. In a thread of cylindrical shape a uniaxial elongational flow is produced. The rheological model applied for the calculation is chosen according to the Newtonian or viscoelastic fluid and simplified due to the properties of the flow. The equation has been derived to calculate the elongation viscosity for the Newtonian fluids and the polymer solution.

3.4 Materials and Characterization

Based on the techniques mentioned in the literature review section, the polymer films have been characterized. Certain modifications in the existing instrumental setup have also been done to obtain the properties required to describe the proposed CTE. Supercooled amorphous PET films and semi-crystalline PET films with thickness of 250 µm and 230 µm were utilized in this study. The film used was an amorphous film with no orientations in the structure. The film was produced by quenching the film from melt state into ice water and hence has an isotropic structure with nearly no crystallinity. The properties of the amorphous PET film are given in Table 1.

Table 1 Properties of amorphous PET used for embossing

Coefficient of thermal expansion ($x10^{-06} K^{-1}$)	20-80
Thermal conductivity @23C ($Wm^{-1} K^{-1}$)	0.15-0.4
Specific heat ($JK^{-1} kg^{-1}$)	1200 - 1350
Density (gcm^{-3})	1.3-1.4
Tensile modulus (GPa)	2-4
Tensile strength (MPa)	80, for biaxially oriented film:190-260

The amorphous PET films are nearly completely amorphous due to rapid cooling/quenching after melt processing, but they can crystallize upon reheating between Tg and Tm. While processing of these films at certain temperatures, there are two phenomena occurring simultaneously. On heating the modulus of the polymer decreases with increase in temperature, and at the same time the modulus starts to increase with development of crystalline structures. In order to properly process these polymer films, it is very important to understand the rate of structure development as a function of temperature. Hence while measuring property changes during crystallization process, the measurement of the initial phase from which the crystallization is initiated is significant, but often difficult to measure. For comparison purposes, DuPont Mylar (semi-crystalline PET) films were also acquired and used in the experiment. PET pellets were also used for the isothermal crystallization studies.

3.3.1 Thermal Analysis

The polymer was characterized using differential scanning calorimetry (model TA-Q200 from TA Instruments) to determine the rate of crystallization at different temperature as shown in Figure 15. The polymer samples were isothermally crystallized directly from room temperature at high heating rate of around 100°C/min to observe the crystallization time scales at temperatures above T_g where the film starts to crystallize. The sample was

heated to different temperatures in the range of 100-220°C. The rate of crystallization of the polymers is observed to be the lowest at around 180°C.

The required heating time during processing also depends on the half time of crystallization as overheating will cause the polymer to pre-crystallize before the pattern transfer is completed. Understandably, the formability of the material is excellent when it is in the initial rubber softening phase and crystallite development has yet to begin. Depending on the processing temperature, the polymer film only has to be heated to less than its crystallization induction time before the stress field is applied. Good part replication is thus highly dependent on the heating time, embossing pressure delay and the temperature. The total cycle time of the embossing is determined based on the thermal transition behavior of the polymer as complete crystallization development is intended before demolding in order to maintain dimensional stability during ejection of the film as well as during use. As seen in Figure 13, by selection of a suitable temperature range as the process window, a total cycle time as low as 20-30 s can be achieved.

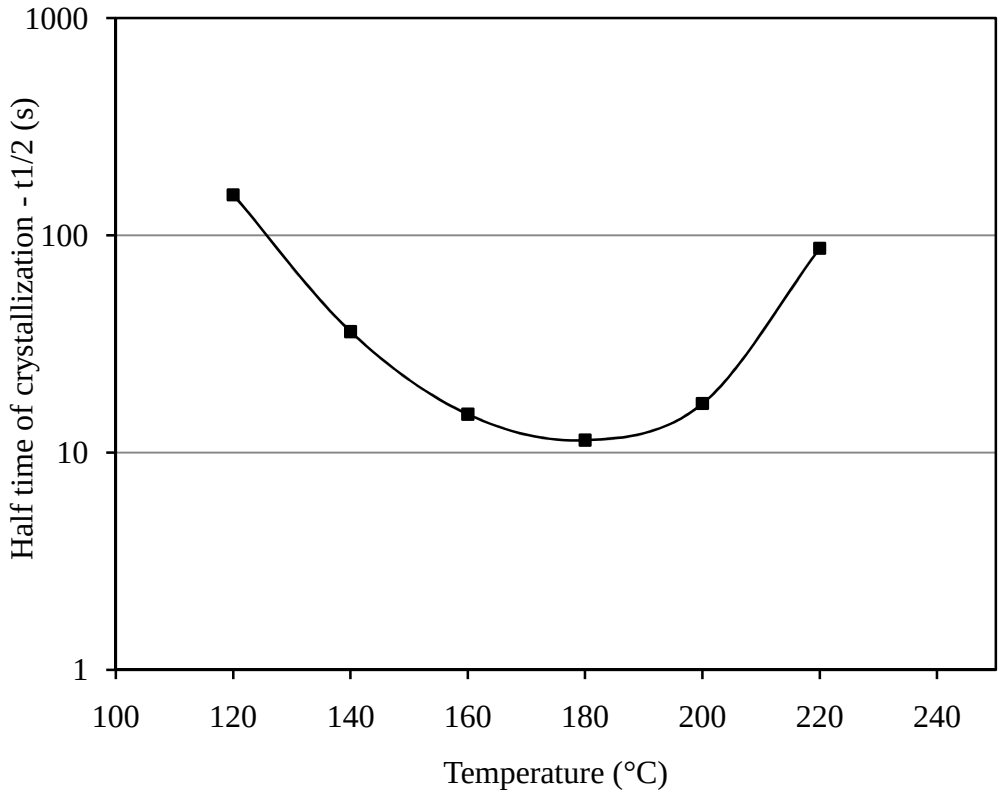

Figure 13 Half-time of crystallization of amorphous PET film as a function of temperature

Precise understanding of the crystallizing behavior is vital to determine the design and process parameters. With any processing operation where a polymer film is subjected to temperature and pressure such as in hot embossing, thermoforming and film blowing, the change in the mechanical properties (e.g., the modulus) is significant. To achieve this understanding, the raw material was characterized with different instruments such as parallel-plate shear rheometer, dynamic mechanical analyzer (DMA) and tensile tester. It has to be noted that the small thickness of the film along with sharp structural transition posed difficulties for characterization by conventional techniques as it was beyond the capability of these instruments to accurately characterize the properties. The increase in relative crystallinity has been studied for both the amorphous PET films and the semicrystalline PET pellets. For the amorphous PET films, as mentioned before, the films

were rapidly heated to the crystallization temperature and held isothermally at different temperatures. The change in relative crystallinity with time as a function of temperature is given in Figure 14.

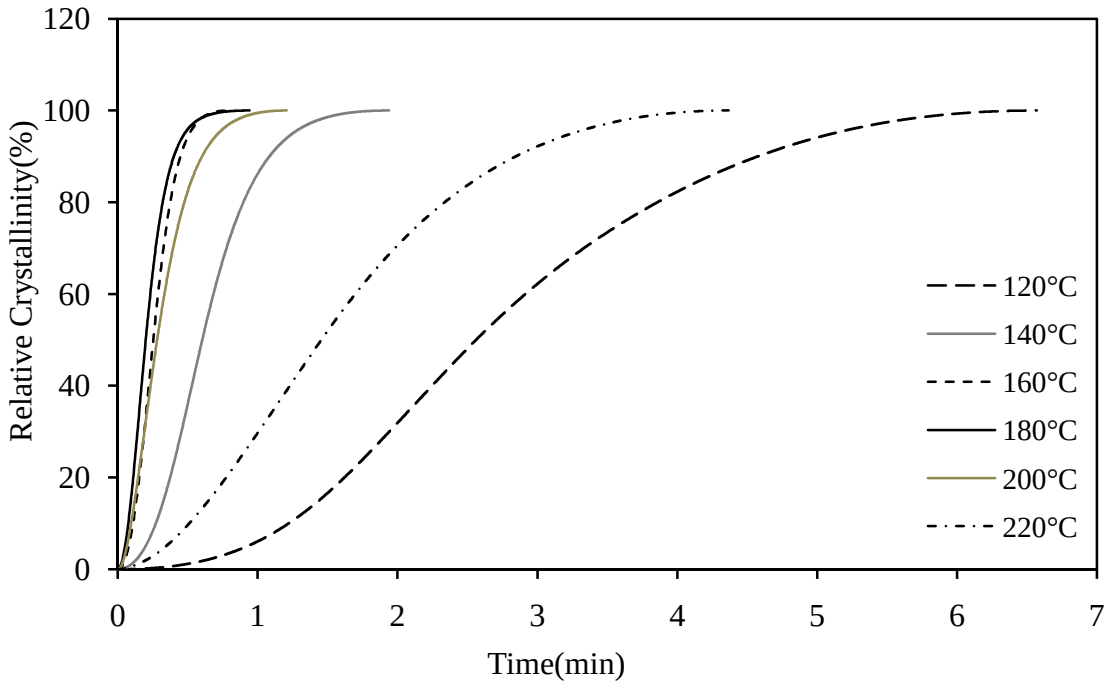

Figure 14 Relative crystallinity as a function of temperature and time for supercooled amorphous PET

The semicrystalline PET was also isothermally crystallized from melt as done conventionally. The temperatures chosen for the study were higher than the normal crystallization range in order to compare data from parallel plate rheometry.

The change in relative crystallinity with time as a function of temperature is given in Figure 15.

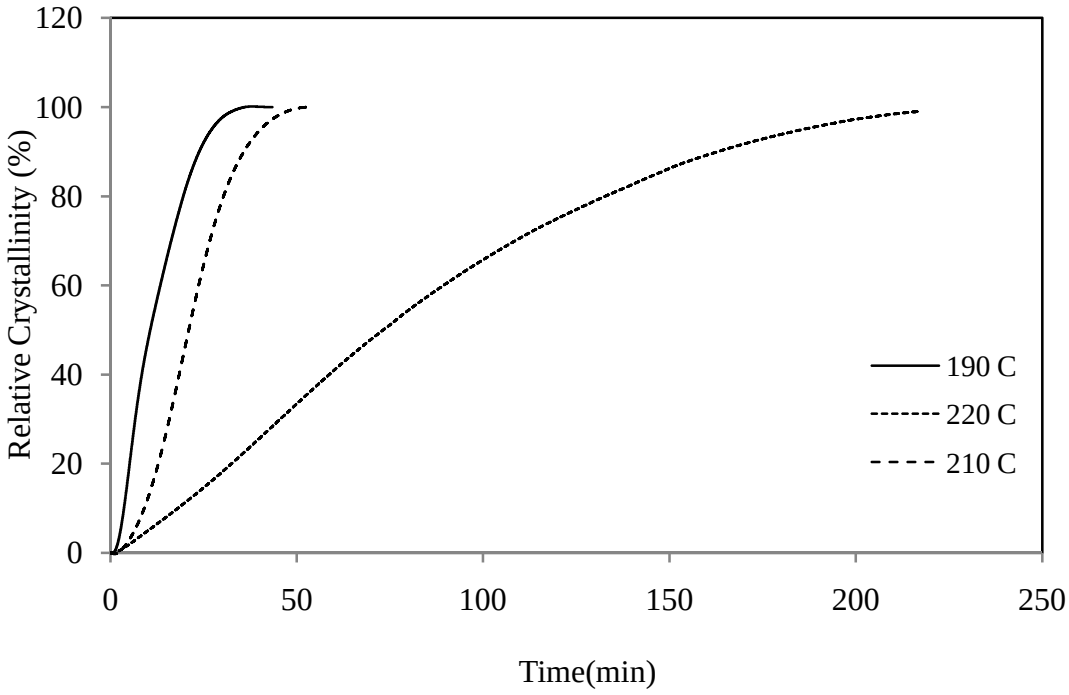

Figure 15 Relative crystallinity as a function of temperature for semicrystalline PET

3.3.2 Rheological Characterization

The rheological characterization of the polymer films were conducted in Thermo Haake and TA rheometers. As the intent was to capture the change in material properties during the embossing stage when the polymer crystallizes, the samples were not allowed to preheat in any of the temperature and time sweep experiments. The structural shrinkage in the polymer during crystallization is compensated for by setting the normal force to a minimal value so that the plates are in contact with the polymer at all times during the experiments. Figure 16 shows the parallel-plate shear rheometery data conducted at different temperatures. Oscillation temperature-sweep experiments were conducted at the frequency of 10 Hz to recognize the advent and completion of crystallization and the related dynamic property thereof.

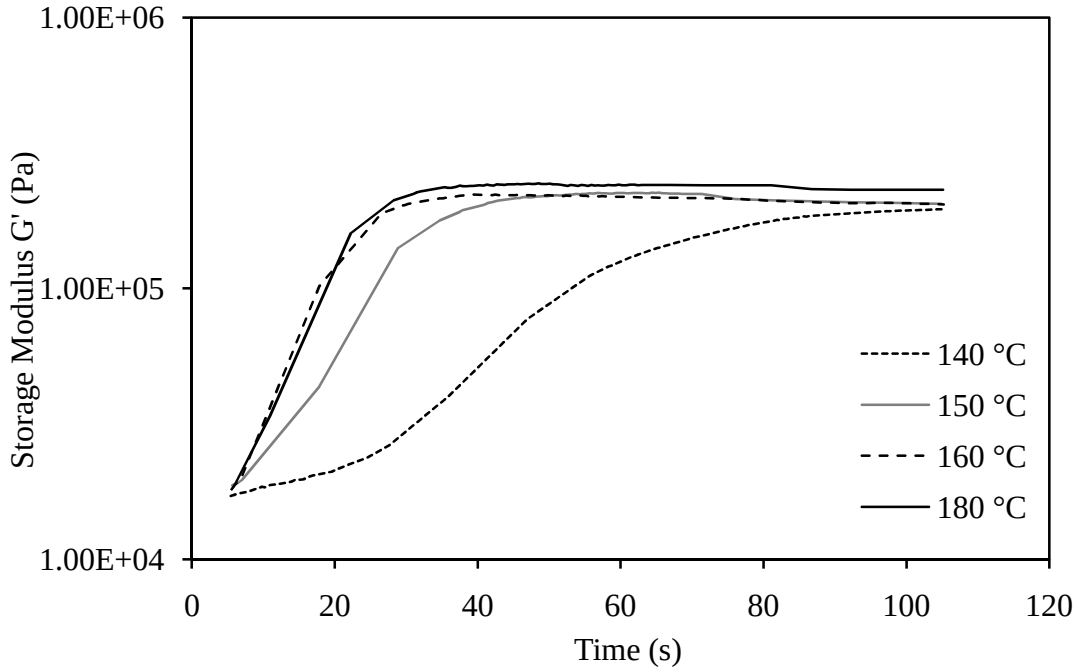

Figure 16 Shear oscillation time-sweep data at 10 Hz

The graph in Figure 17 shows the increase in storage modulus with a temperature dependent rate. But it has to be mentioned that the collection of the data has a time lag of around 10-15 s. In addition, material slippage between the plates happens once crystallinity develops and the material becomes stiffer leading to noisy data. Considering the fact that the polymer at temperatures in the range of 150-180 °C has a crystallization induction time of around 15-20 s, the data collected mostly represents the stage where the crystallinity has already started developing in the material.

The initial reduction in modulus during the embossing stage of CTE is of great importance to understand the embossing pressure required. Hence techniques which can obtain the data accurately during the initial softening zone are more useful for the current work. The dynamic mechanical analysis of the raw polymer film is shown in Figure 17.

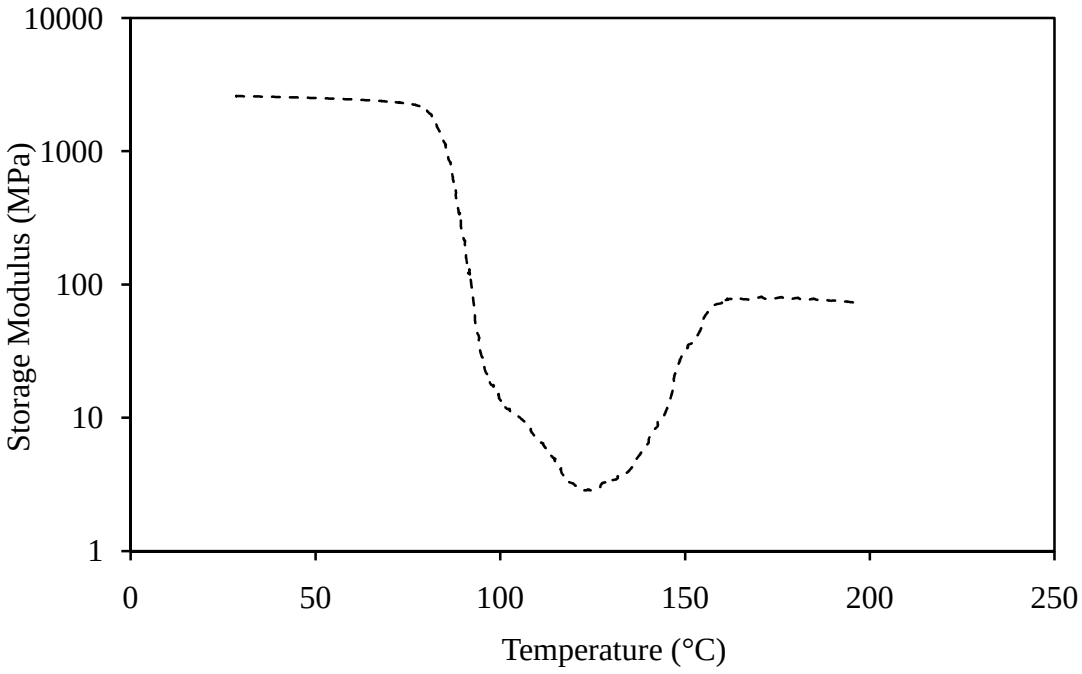

Figure 17 Elongational storage modulus at 1Hz and heating rate 3°C/min

Rheological studies to predict change in properties during crystallization at isothermal conditions were performed. The PET pellets were initially melted at 300 °C for long time to erase any memory and then quickly brought down to the crystallization temperature. The procedure followed the same route as the isothermal crystallization studies in DSC to enable reasonable comparison. The temperatures of experimentation were 190 °C, 200 °C, 210 °C, 220 °C, and 230 °C. As the rheometer did not have a quench cooling capability, approximately 6-7 min lag was seen before the temperature drops to the testing temperature. The lag had an effect on low temperatures such as 190 °C and 200 °C as the crystallization rate was relatively faster. The curves obtained for the storage modulus (G'), loss modulus (G") and complex viscosity (|η*|) are given in Figure 18.

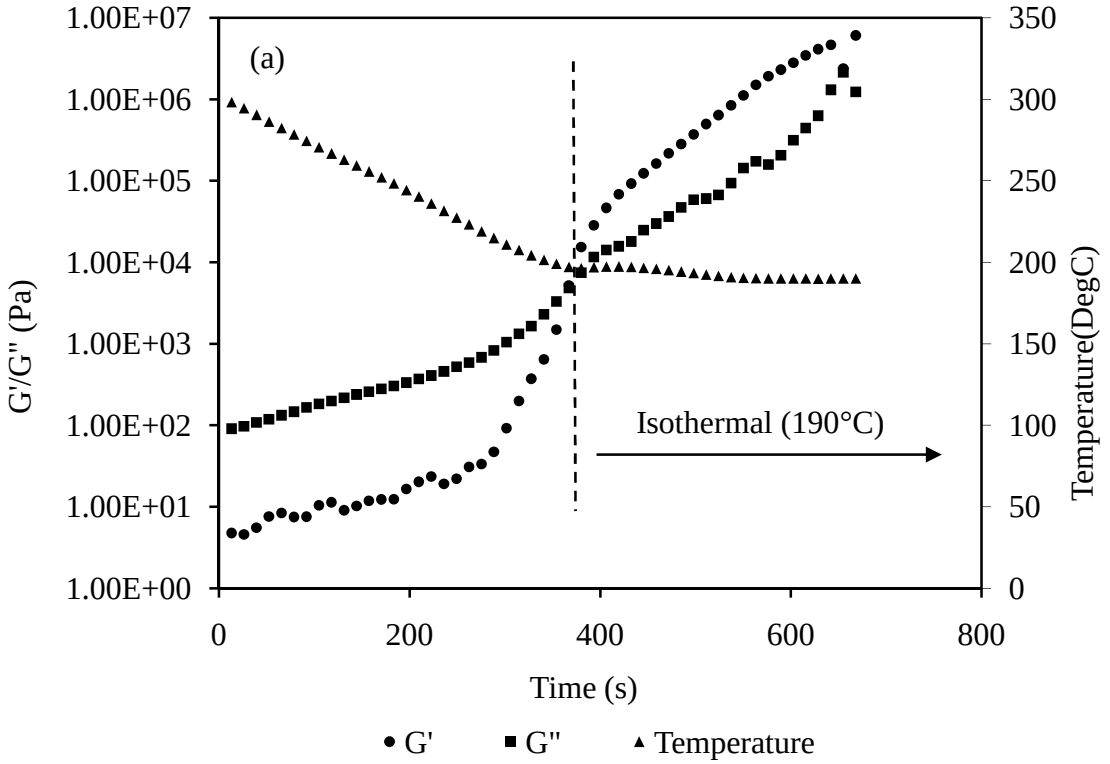
(a)
1.00E+07
1.00E+06
1.00E+05
1.00E+04
1.00E+03
1.00E+02
1.00E+01
1.00E+00
G'/G" (Pa)
350
300
250
200
150
100
50
0
Temperature(DegC)
Isothermal (190°C)
0
200
400
600
800
Time (s)
G'
G"
Temperature

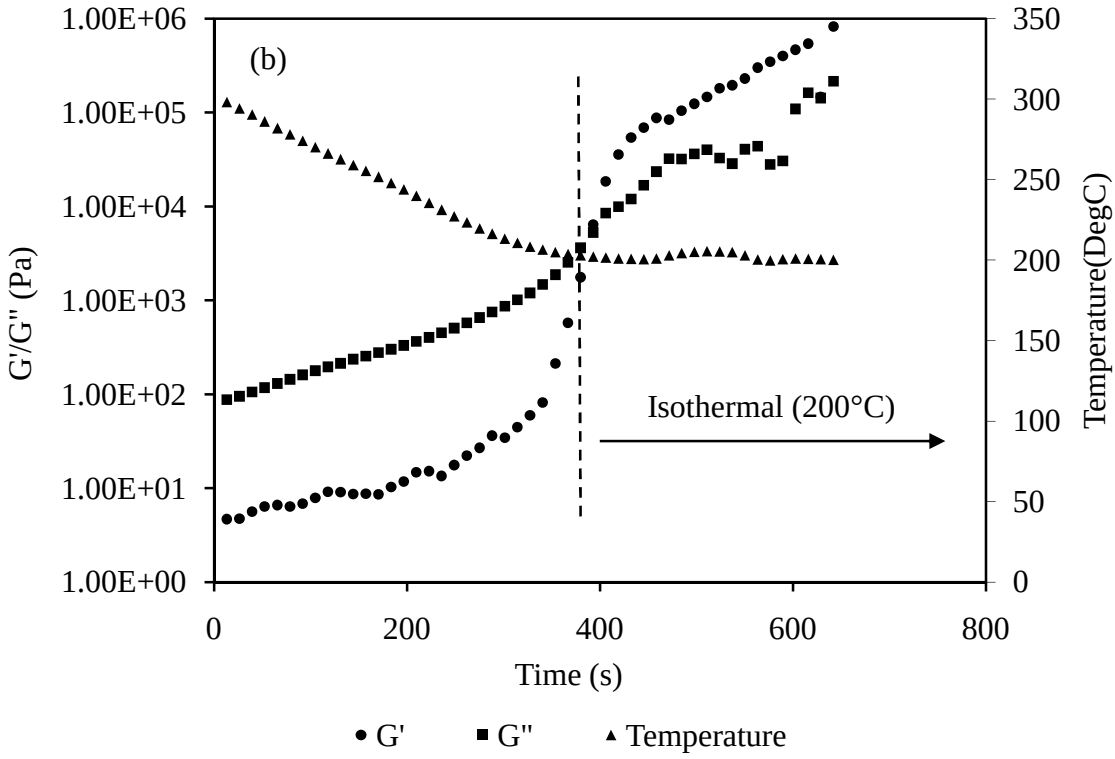
(b)
1.00E+06
1.00E+05
1.00E+04
1.00E+03
1.00E+02
1.00E+01
1.00E+00
G'/G" (Pa)
350
300
250
200
150
100
50
0
Temperature(DegC)
Isothermal (200°C)
0
200
400
600
800
Time (s)
G'
G"
Temperature

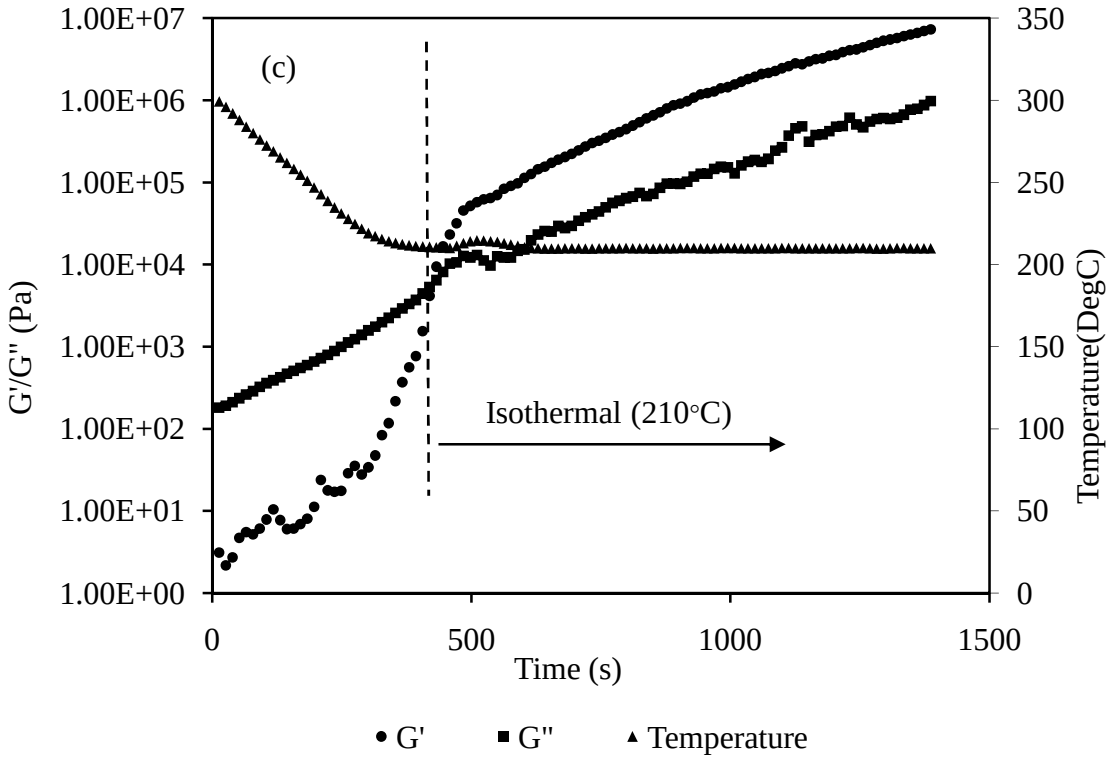
(c)
Isothermal (210°C)
G'/G" (Pa)
Temperature(DegC)
Time (s)
1.00E+07
1.00E+06
1.00E+05
1.00E+04
1.00E+03
1.00E+02
1.00E+01
1.00E+00
350
300
250
200
150
100
50
0
0
500
1000
1500
G'
G"
Temperature

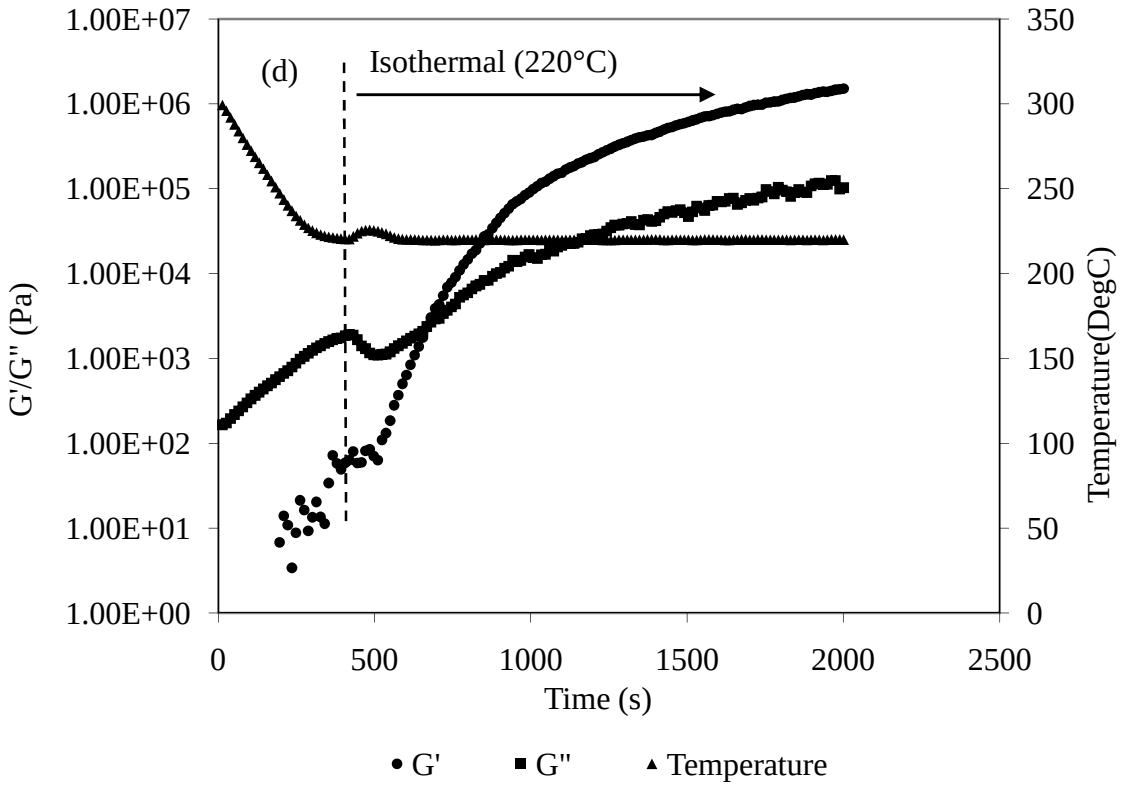
(d)
Isothermal (220°C)
G'/G" (Pa)
Temperature(DegC)
Time (s)
1.00E+07
1.00E+06
1.00E+05
1.00E+04
1.00E+03
1.00E+02
1.00E+01
1.00E+00
350
300
250
200
150
100
50
0
0
500
1000
1500
2000
2500
G'
G"
Temperature

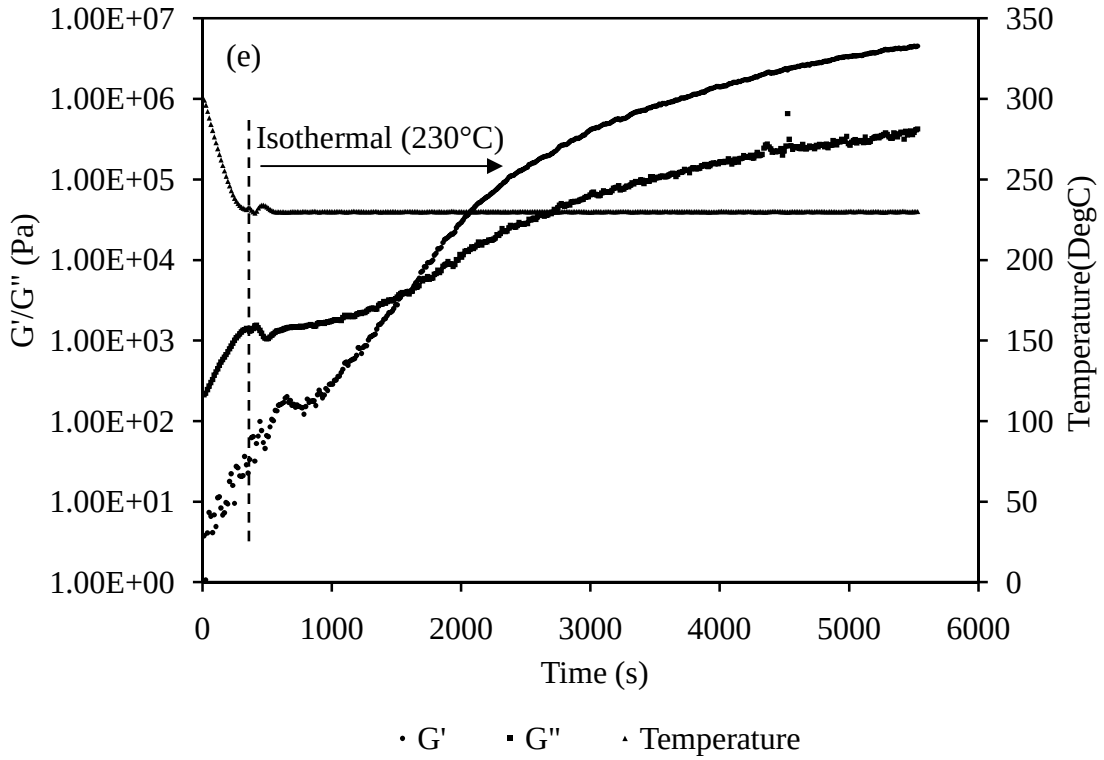

Figure 18 (a-e) Rheological data for semicrystalline PET isothermally crystallized at 190 °C to 230 °C

The increase in complex viscosity with time at different temperatures is plotted in Figure 19. The increase in viscosity is due to the crystallization occurring in the polymer, corresponding to the transformed fraction. The relation between the relative crystallinity increase with time and viscosity increase can be correlated to predict the mechanical property of the polymer at different times during processing. A model developed for the conditions at which both the relative crystallinity and rheological parameters can be used to extrapolate the properties in regimes where either testing is difficult. As mentioned before, determination of the rheological properties of the amorphous PET films at the proposed embossing temperatures is difficult and beyond the instrument's capabilities.

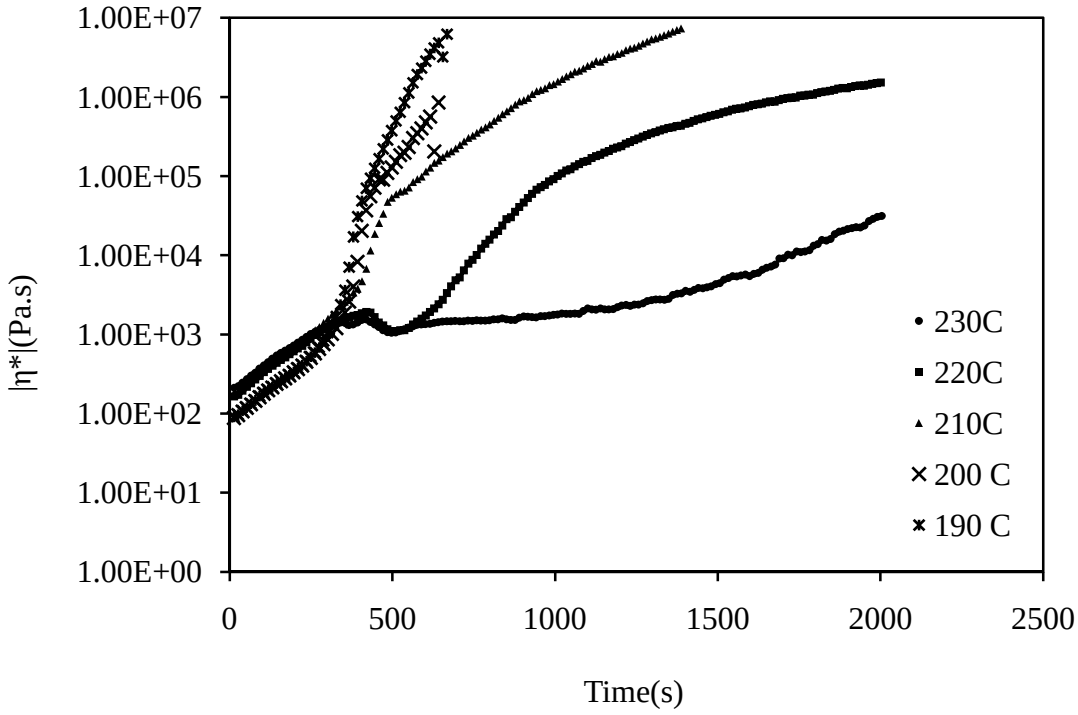

Figure 19 Change in complex viscosity with time as a function of temperature during isothermal crystallization from melt

3.3.3 Non-Isothermal Crystallization Kinetics

The non-isothermal crystallization kinetics was studied for the amorphous PET by melting the polymer and then cooling it below T_g at different cooling rates. The protocol explained by Chan et al.[70] was followed to get a master curve and also determine the shift factor as a function of temperature. The shift factor was found from the two different methods. Figure 20 shows the relative crystallinity (θ) data as a function of temperature for different cooling rates. To determine the shift factor at a particular θ, the dθ/dt value was plotted against the temperature as shown in Figure 21. From the data corresponding to a particular θ, the shift factor was calculated based on Equation 6 given earlier.

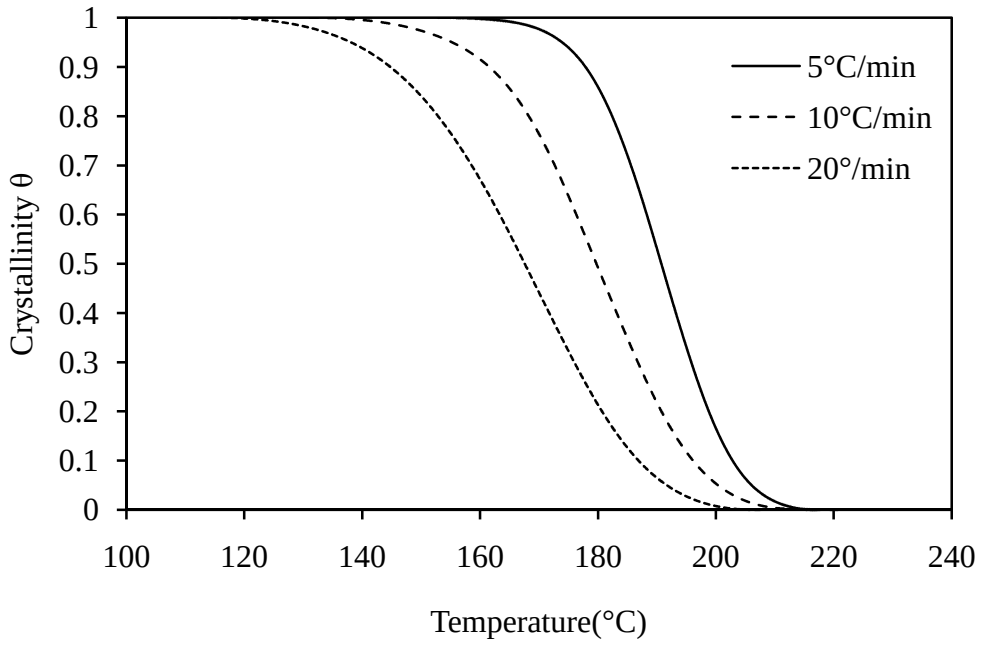

Figure 20 Crystallinity vs temperature at different cooling rates

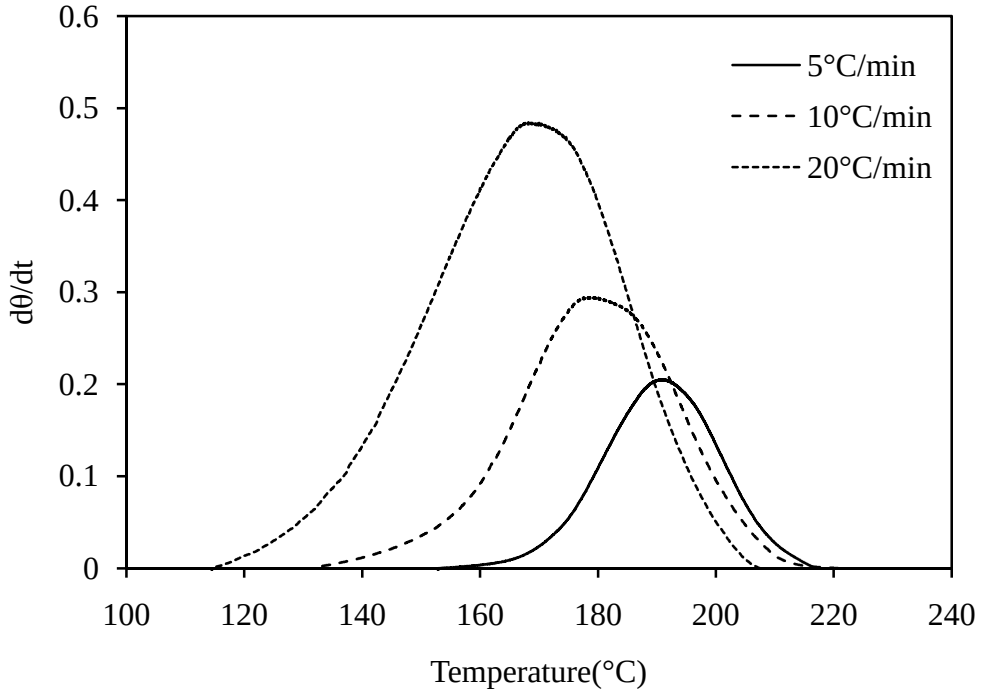

Figure 21 dθ/dt vs temperature for different crystallinity

The shift factor was then shifted again to one particular temperature which is the reference temperature by using a simple technique. The reference temperature of 176°C in this case was chosen to accommodate a broad range of data scatter, and to enable vertical shifts at all cooling rates. The plots were vertically shifted by calculating the difference between the shift factors at different θ values for a particular temperature. The shifted curve is plotted in Figure 22.

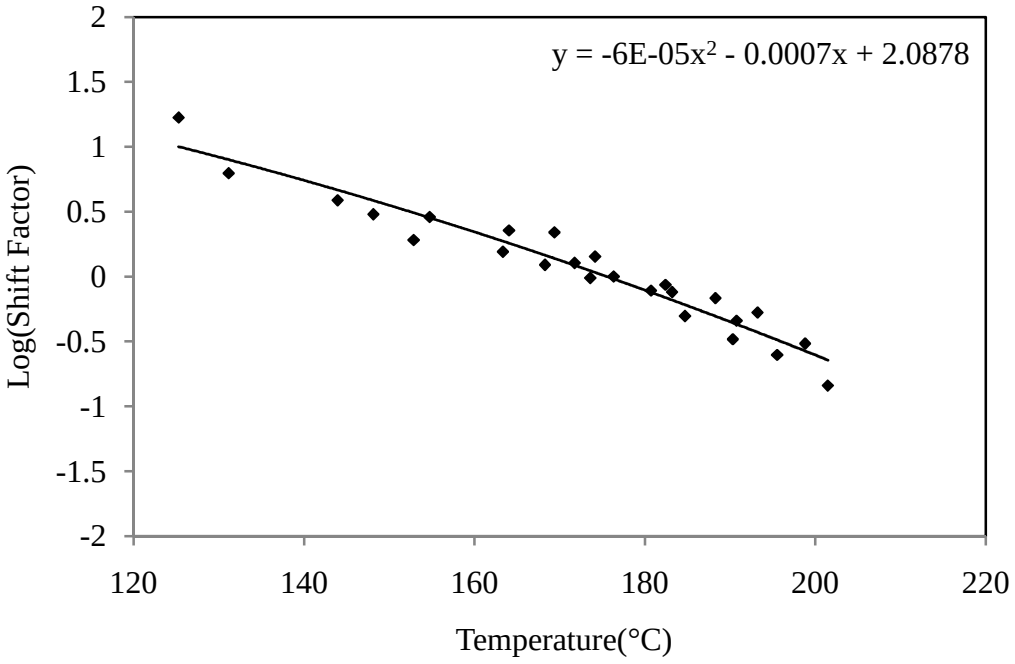

Figure 22 Shift factor as a function of temperature at Tr = 176 °C

The shift factor can hence be expressed as a function of temperature at a reference temperature of 176 °C as shown in Equation 24 and Equation 25.

$$\log a_T = -6E-05T^2 - 0.0007T + 2.0878 \quad (18)$$

$$a_T = 10^{\left(-6E-05T^2 - 0.0007T + 2.0878\right)} \quad (19)$$

To verify the applicability of the shift factor, the reduced time was calculated from the shift factor by Equation 7 given earlier. On plotting the relative crystallinity as a

function of reduced time for different cooling rates, all the curves collapsed into one single master curve, demonstrating that the shift factors calculated only by shifting the curves can be used to predict the relative crystallinity for a wide range of temperature. The figure for relative crystallinity (θ) vs reduced time (ξ) is shown in Figure 23. The current study does not require the master curve to be fitted since the shift factor is the only quantity needed to calculate $K(T)$ at different temperatures, Nonetheless fitting the master curve acts as a validation method to check if the shift factors calculated reasonbly represent the crystallization kinetics of the polymer.

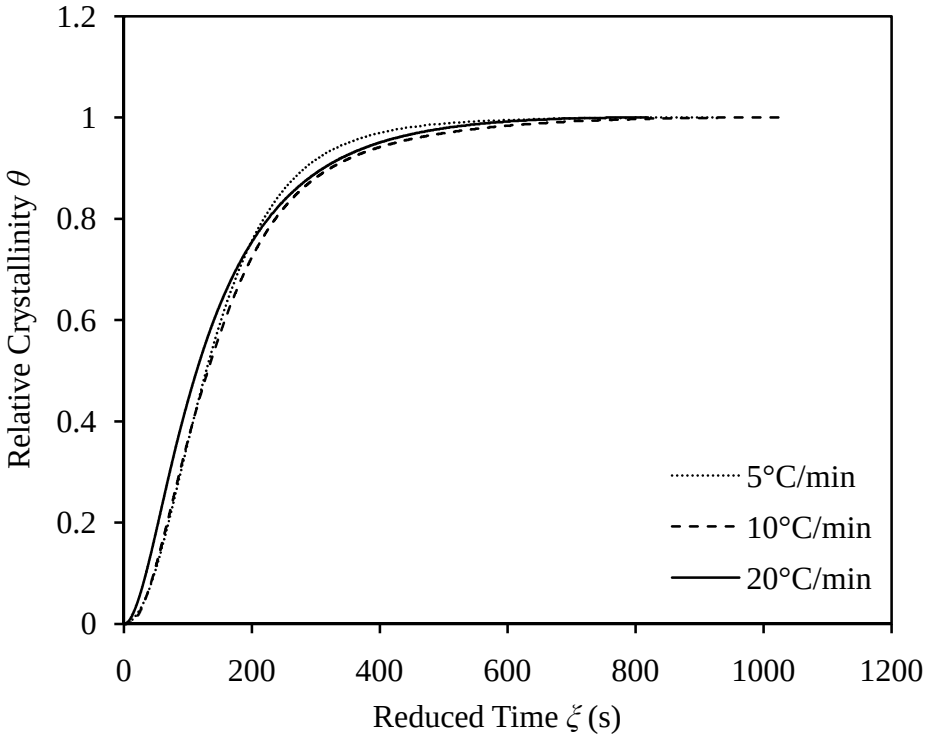

Figure 23 Relative crystallinity vs reduced time – master curve

In the second method, the Nakamura model was employed to calculate the $K(T)$ which was then used to calculate a_T at any particular reference temperature with the rate

constant as $K(T_r)$. The equation given earlier was used to directly compute the shift factor (a_T). The plot of of shift factor and temperature is shown in Figure 24. The method is a direct method which does not have a way to check if the shift factors obtained can be used to calculate $K(T)$ give a fairly accurate representation of the system. The model tends to overpredict the kinetics and is suitable for the most ideal case where there is no secondary effects.However in a real case, using only the experimental data to calculate the shift factor would give much better representation of the kinetics.

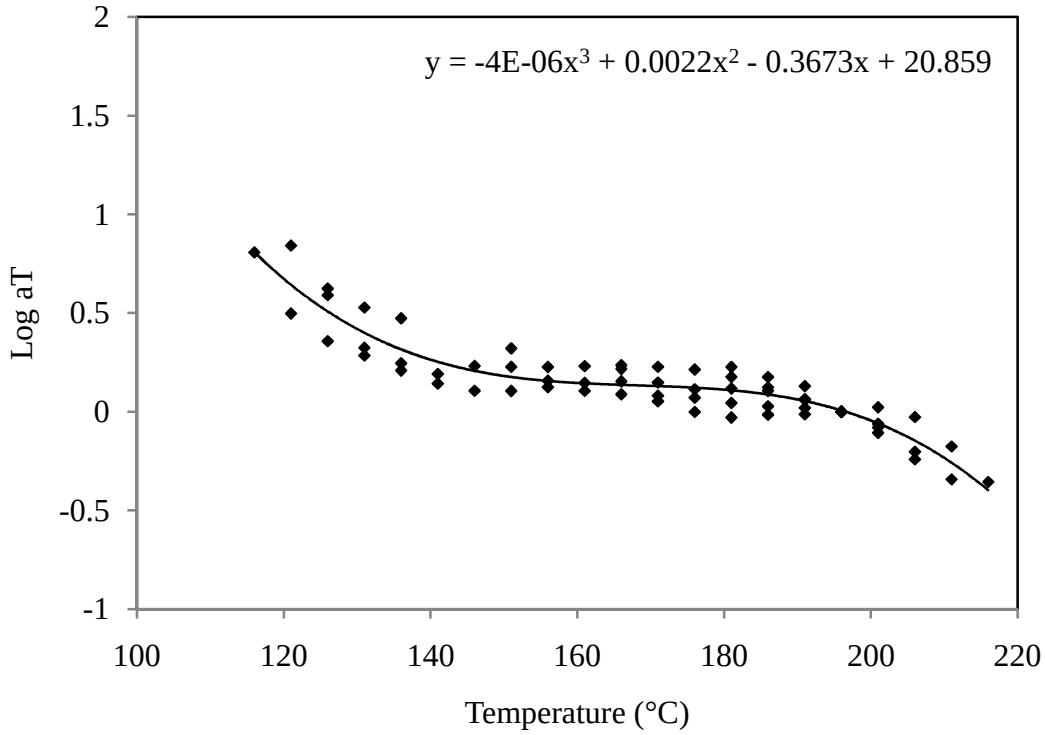

Figure 24 Shift factor vs temperature determined using the Nakamura model

3.3.4 Elongational Properties with Fluid Heating

To study the interplay between mechanical properties and in-process crystallization, rapid heating of the PET film during testing is needed. To the author's knowledge, there are no techniques available to meet such a goal. Therefore a tensile testing setup was modified to include an oil bath through which contact heating of the

polymer film can be accomplished quickly and thoroughly. The retrofitted tensile testing setup can predict the deformation behavior of the polymer film under tension accurately and with a lag of around 2-3 s. A schematic of the modification is shown in Figure 25 & Figure 26.

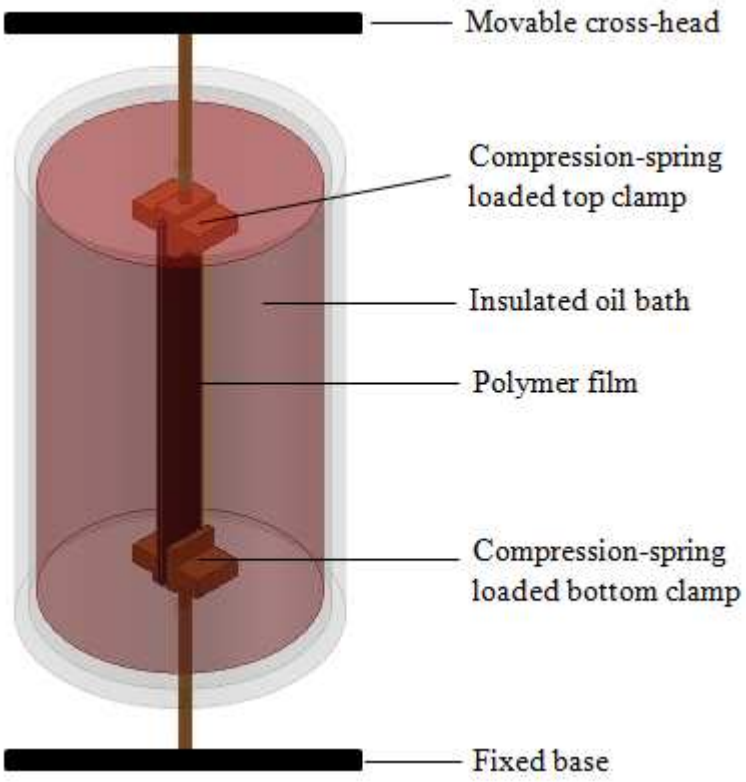

Figure 25 Retrofitted oil bath with clamping assembly for high temperature tensile testing

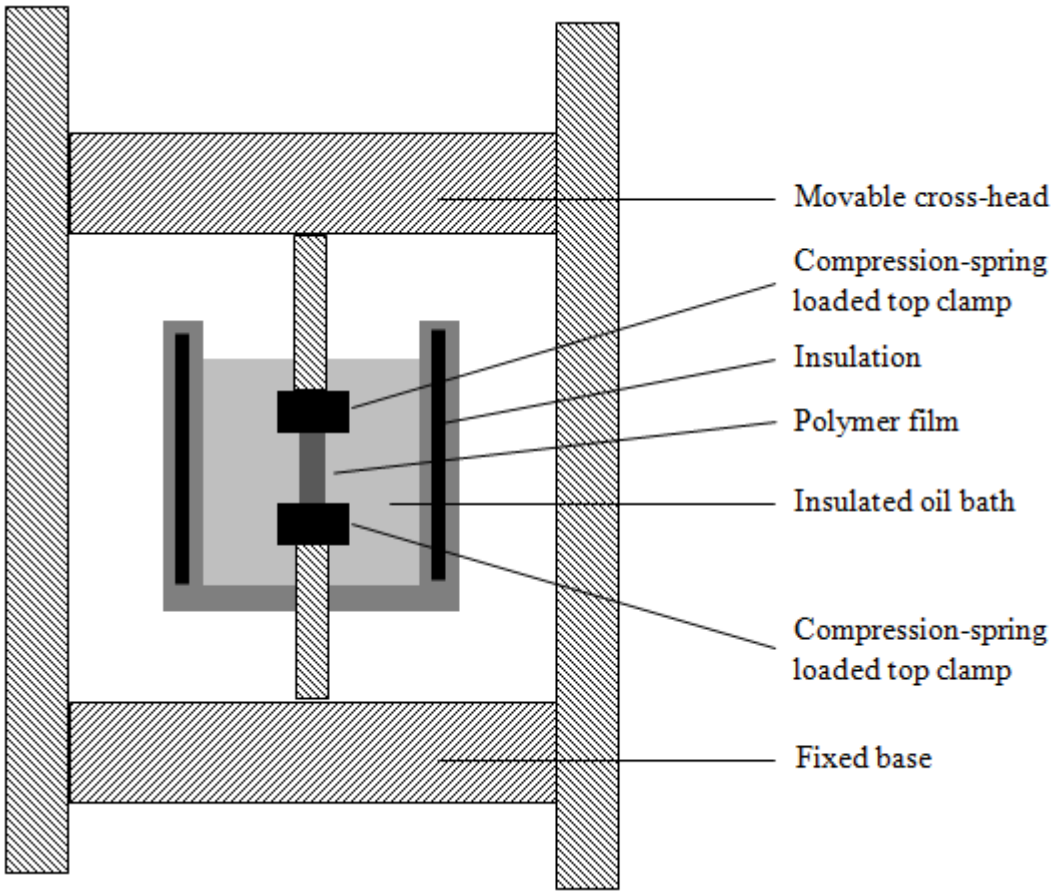

Figure 26 Retro-fitted oil bath with clamping assembly for high temperature tensile testing – 2D representation

The data from the modified tensile testing equipment is shown in Figure 27-Figure 32. The curve shows the engineering stress and strain values. The data presented here are adjusted for the initial buoyancy force experienced due to the presence of the oil medium. The buoyancy force was determined by setting up the oil bath and the compression-spring loaded clamps without the sample. This force was then subtracted from the force applied to the sample during testing. The sample was brought in contact with the high temperature oil and the test was immediately started, thereby reducing the effective lag time to 2-3 s. Upon analyzing the results, it can be seen that the test actually captures the material properties in the pre-transition zone due to the very low load values measured. There is an infinitesimal increase in the load values during the initial stage

when the material is soft, and overall the very low modulus seen is a healthy indication that the material can be used for embossing very small and high aspect ratio features. The load values at 180 °C are higher than those at 140 °C, which may be an indication that the crystallization has already been initiated as the rate of crystallization at 180 °C is higher than that at 140 °C or it may be due to measurement error as the values in this regime are too close to each other.

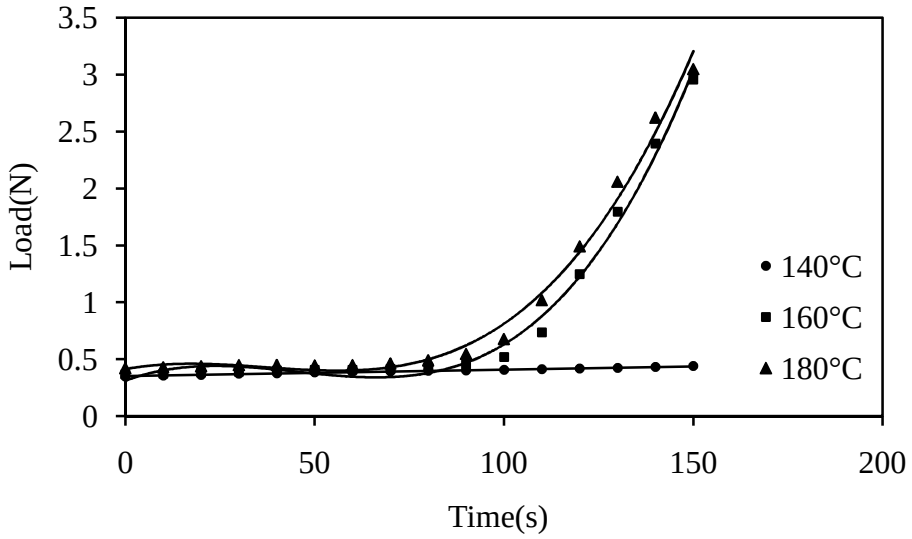

Figure 27 Load vs time data for 150 s from oil-heated tensile testing apparatus conducted with a cross-head speed of 1.5 mm/min

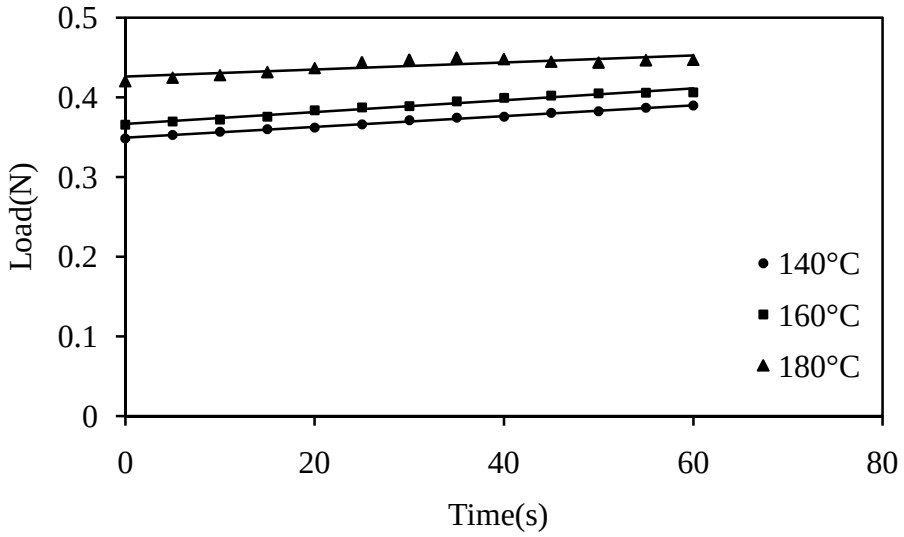

Figure 28 Load vs time data for 60 s from oil-heated tensile testing apparatus conducted with a cross-head speed of 1.5 mm/min

The tests were also conducted at high speeds in the range of 5mm/min. The plots of load versus time and stress versus strain are shown in Figure 33 - Figure 38. From the tensile testing curves at higher crosshead speeds, the measurement gives unstable values. This might be due to the various factors involved in the setup such as the presence of the oil medium and uneven clamping pressures. The testing was repeated and unstable results were obtained in the initial zone every time for speeds in the range of 5mm/min. In the later part where the polymer film has obtained certain degree of dimensional stability due to crystallization, the readings were stable. Invariably, the data showed differences in the crystallization behavior of the polymer for different temperatures, which is consistent with the data obtained at slow speed of 1.5mm/min. But in the faster case, there was a marked difference between the crystallization induction time for the temperatures 180°C and 160°C. This may again be attributed to the unstable nature of the testing at high speeds. Though the data obtained through the tensile testing using the customized setup represents the crystallization occurring in the film during the embossing without time lag,

it cannot be used quantitatively for further analysis of the process. This is due to the unstable nature of the testing at high testing speeds and the inconsistencies between the data at different speeds.

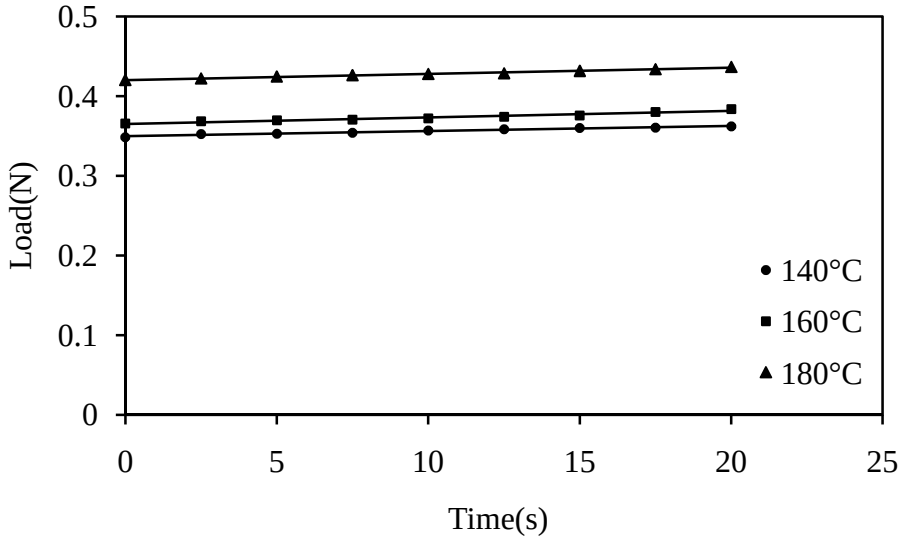

Figure 29 Load vs time data for 20 s from oil-heated tensile testing apparatus conducted with a cross-head speed of 1.5 mm/min

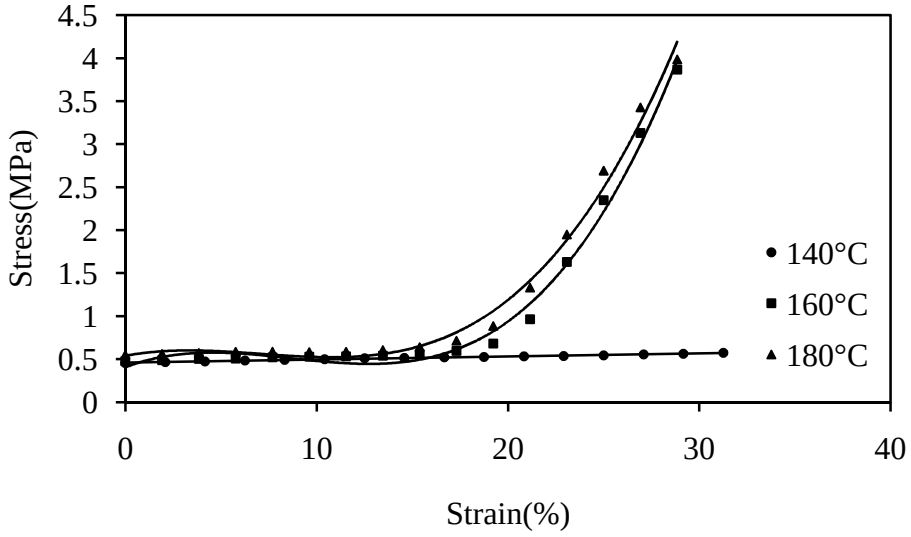

Figure 30 Stress vs strain data for 150 s from oil-heated tensile testing apparatus conducted with a cross-head speed of 1.5 mm/min

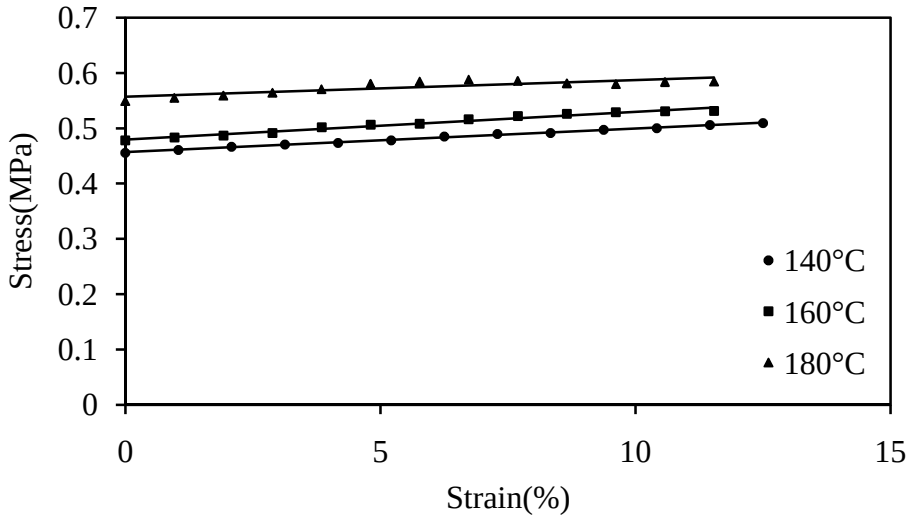

Figure 31 Stress vs strain data for 60 s from oil-heated tensile testing apparatus conducted with a cross-head speed of 1.5 mm/min

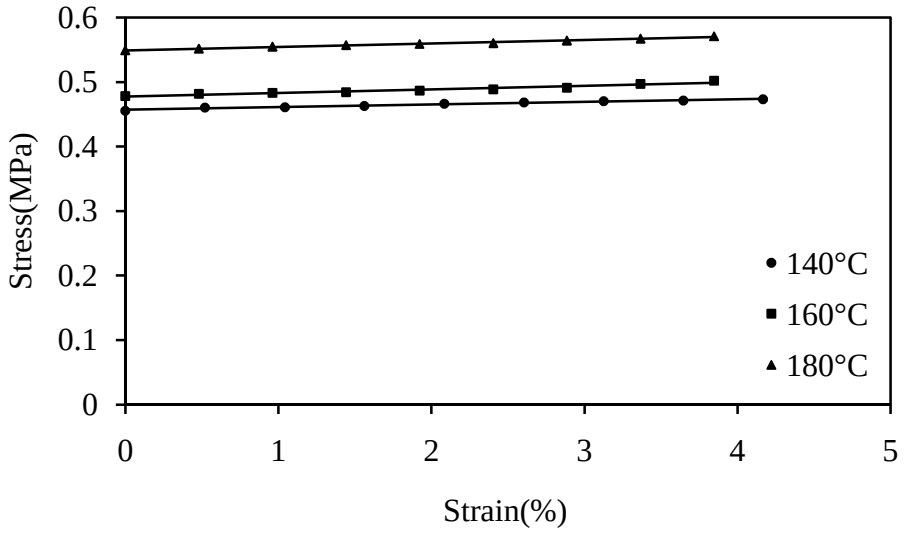

Figure 32 Stress vs strain data for 20 s from oil-heated tensile testing apparatus conducted with a cross-head speed of 1.5 mm/min

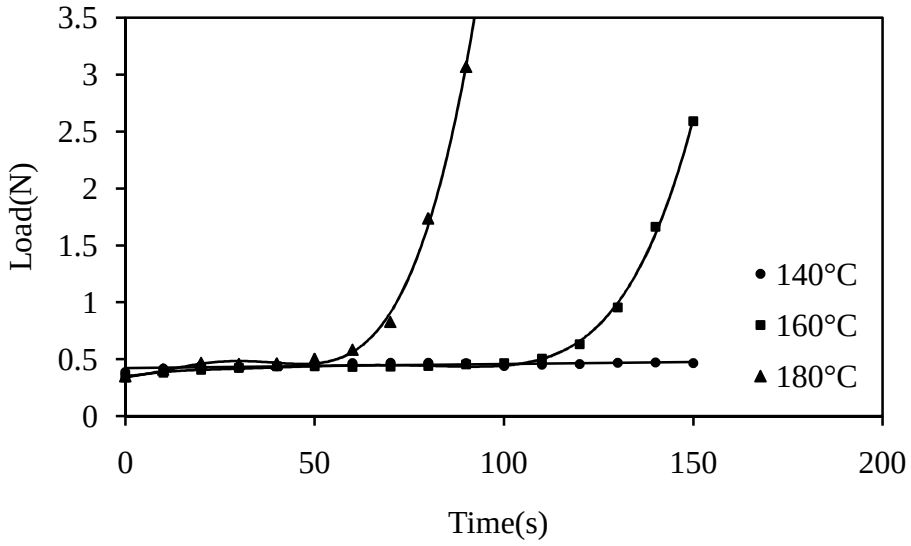

Figure 33 Load vs time data for 150 s from oil-heated tensile testing apparatus conducted with a cross-head speed of 5 mm/min

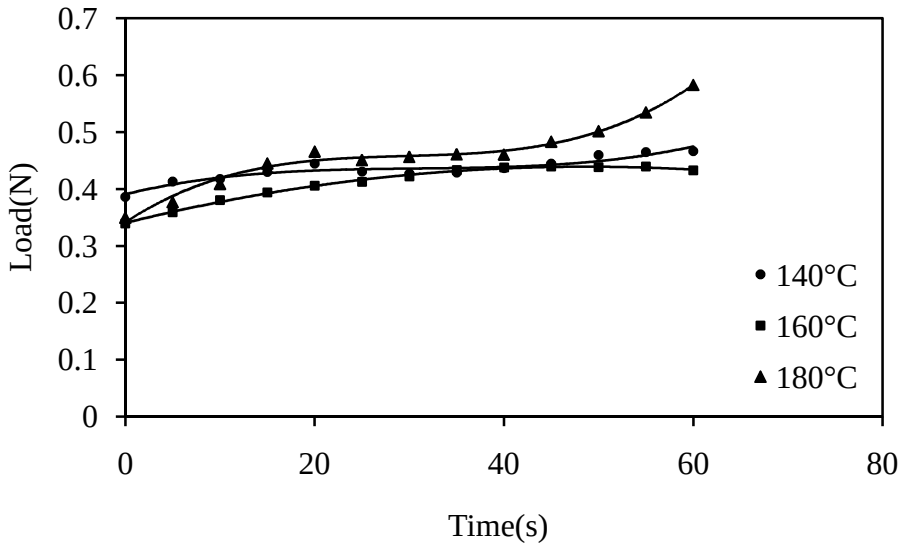

Figure 34 Load vs time data for 60 s from oil-heated tensile testing apparatus conducted with a cross-head speed of 5 mm/min

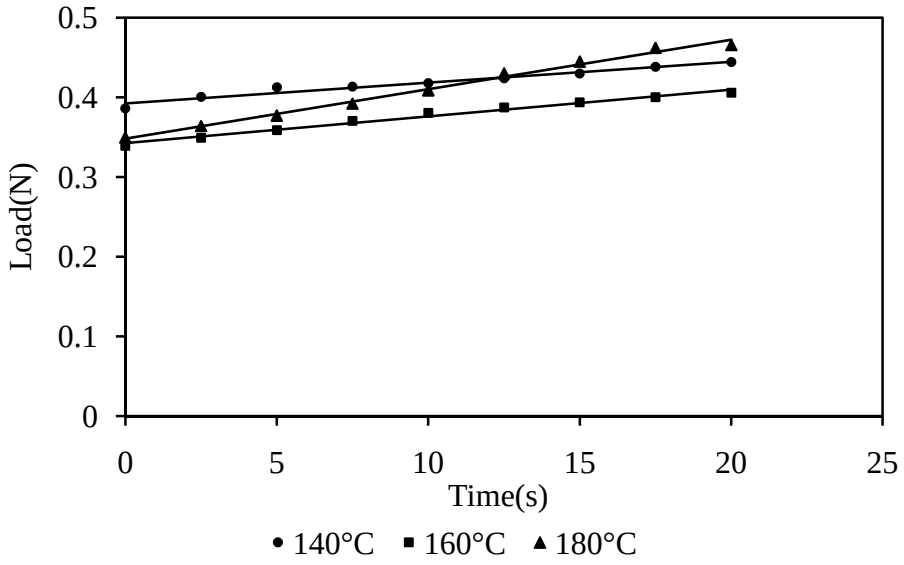

Figure 35 Load vs Time data for 20 s from oil-heated tensile testing apparatus conducted with a cross-head speed of 5 mm/min

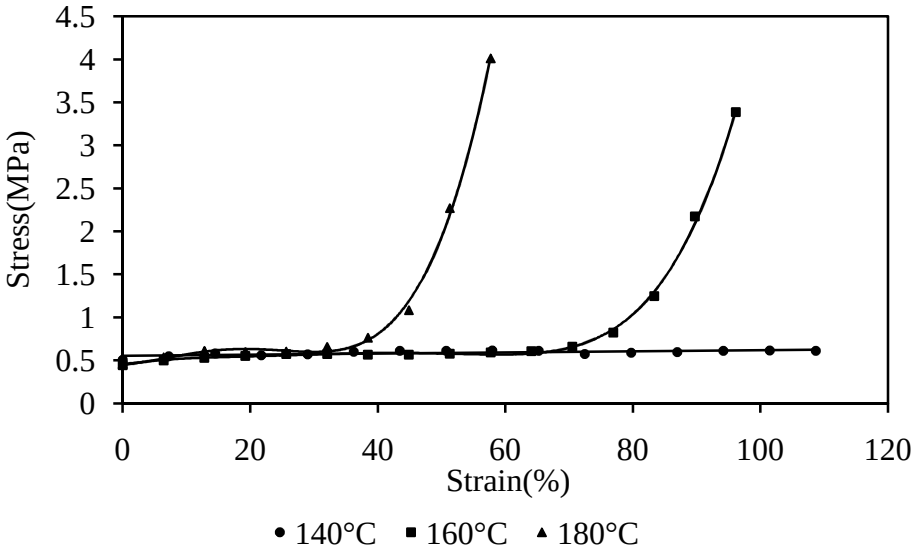

Figure 36 Stress vs strain data for 150 s from oil-heated tensile testing apparatus conducted with a cross-head speed of 5 mm/min

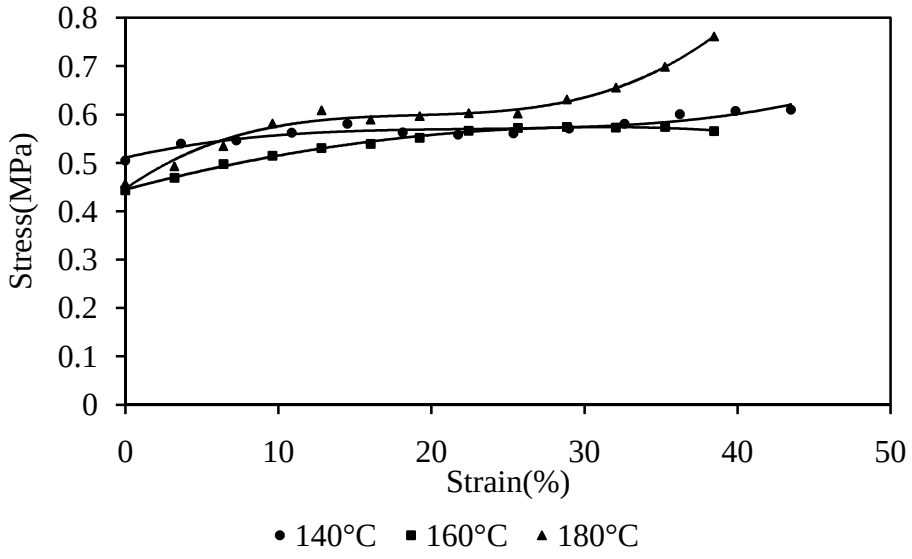

Figure 37 Stress vs strain data for 60 s from oil-heated tensile testing apparatus conducted with a cross-head speed of 5 mm/min

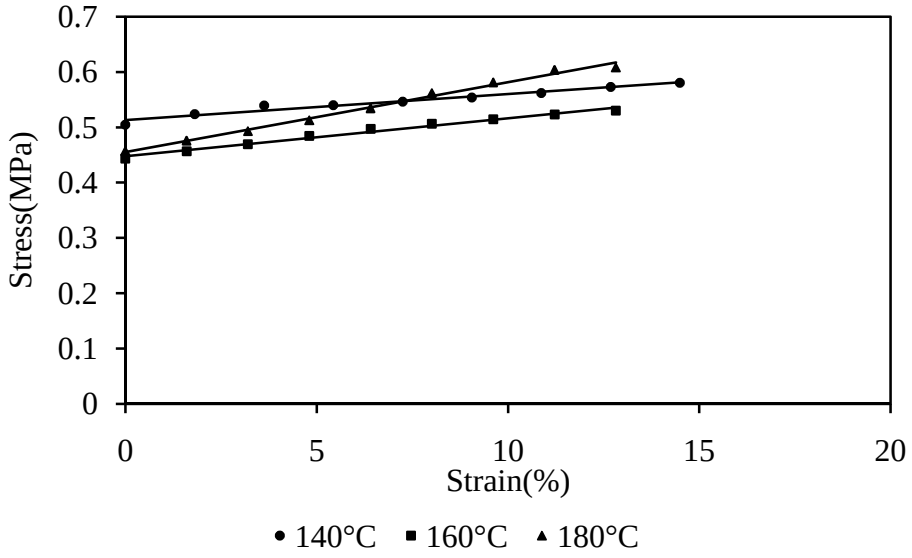

Figure 38 Stress vs strain data for 20 s from oil-heated tensile testing apparatus conducted with a cross-head speed of 5 mm/min

3.4 Conclusions

The amorphous film used for the CTE process was characterized using DSC, rheometry and tensile testing. The DSC temperature sweep of the film showed that the cold crystallization peak occurs in the temperature range of 130 - 170°C giving a fair prediction of the processing temperatures to be used for the embossing. The half-time of crystallization was observed to be lowest in the temperature zone 160 - 180°C, showing the optimum processing temperatures ranges for reducing the total holding time. Non-isothermal crystallization kinetics was predicted for the amorphous PET using the Nakamura equation. The shift factors for the rate constant were determined by mathematically shifting the shift curves with respect to different degrees of crystallinity.

The rheological studies were conducted primarily to understand the change in mechanical properties of the material with increase in crystallinity. The rheological experiments were challenging to perform due to limitations in the instruments and material. The instruments showed a time lag during collection of the rheological data. Nevertheless, the rheological data provided evidence of the change in mechanical properties during crystallization. The DMA experiments were also able to show the change in elongational modulus of the material when subjected to an oscillatory temperature sweep. Rheological experiments were further continued with semi-crystalline PET samples which were quench-cooled after pressing them into sheets. Tests were conducted to determined the correlation between the rheological data and the DSC data and hence develop a relation.

Tensile testing studies were performed in an Instron machine retro-fitted with an oil bath at temperatures 140, 160 and 180°C. The experiments reduced the time lag

associated with most conventional rheological and tensile testing instruments due to the contact heating provided by the oil medium. The tensile testing experiments were conducted at two different cross-head speeds - 1.5 mm/min and 5 mm/min - to determine the accuracy of the measuring technique. The amorphous PET was used as model material for these measurements and the data collected from the two extensional speeds were compared. The accuracy of the data was affected by the instabilities arising due to the presence of an oil medium and the buoyancy associated with it. Since the oil medium is transferred to the testing bath only when the test is started, the disturbance caused by the sudden contact of the oil medium on the clamped film was noticeable, particularly at high speeds.

CHAPTER 4

CONSTANT TEMPERATURE EMBOSSING OF PET AND PEEK

4.1 Abstract

The CTE process was conducted with amorphous PET (APET) and amorphous PEEK (APEEK) as model materials. Silicon stamps with rectangular trenches were used for the embossing. The process parameters studied were embossing temperature, embossing pressure and embossing time. The versatility of the process was demonstrated vis-à-vis a conventional hot embossing process by comparing the replication with and without cooling. The applicability of the process for features with different aspect ratio features was studied. Scanning Electron Microscopy (SEM) and Profilometry were used to determine the replication fidelity of the CTE process.

4.2 Introduction

The parametric study of CTE process is vital to understand the efficacy of the process. Unlike the conventional hot embossing process, there are material parameters which have to be considered while embossing. The amorphous films undergo crystallization during the process, and hence precise control of the processing parameters particularly the embossing temperature is significant. As described in Chapter 3, the rate of crystallization is highly dependent on temperature. The total embossing time consists of the time available for the material to fill the cavity and the holding time. In a normal hot embossing time, an additional cooling time will be included.

4.2.1 Embossing Temperature

In the conventional embossing process, the embossing temperature determines the amount of replication and the quality of the part after replication. Features replicated with improper control of temperature or under non-optimum temperature cycles tend to have multiple issues such as high-stress build-up, damage during demolding, degradation of material and partial fill. In conventional embossing, processes conducted at lower than optimum temperatures produce incomplete fill and require very high pressure. The increase in pressure leads to a large amount of stress buildup in the polymer which eventually results in failure of the parts during usage. When the embossing is conducted at temperatures higher than optimum, degradation of the material is observed in some sensitive polymers. Excessive flash of the material outside the mold cavities occurs when the viscosity of the material is too low at these high temperatures. This is particularly an issue when the embossing setup is an open mold system due to its ability to reduce the thickness of the residual film to bare minimum and subsequent difficulty during demolding.

In the case of the CTE process, the embossing temperature has much more significant effect on its replication capability than that observed for conventional embossing. In CTE, embossing temperature plays an important role during the embossing and holding stage.

4.2.1.1 Effect of Temperature during Embossing Stage of CTE

During the embossing stage, the temperature has similar effect as in the conventional hot embossing process. Lower temperature results in partial fill or post-recovery, and higher temperature in degradation of the material. The embossing

temperature also directly determines the rate of crystallization which subsequently determines the embossing time and holding time. Since the embossing, holding and demolding temperatures are the same in CTE, the main effect of the temperature is to optimize the time required at different stages of the process. Ideally, the embossing stage is essential to be completed before the crystallization induction in the material. As shown in Figure 13, the rate of crystallization of the amorphous PET films when heated above its T_g varies with temperature. At temperatures slightly above T_g, the rate of crystallization is very low and time available for the embossing stage is greater, but at these temperatures, the material is stiffer and hence requires large pressure to push the material into the cavities. The problem is magnified when high aspect ratio features are to be filled at these low temperatures.

At temperatures much higher than the T_g or closer to the melting point, the rate of crystallization is again very low as the crystallites continuously form but then immediately melt under the available high thermal energy. Though the time available for embossing is high, there are problems related to excessive flash of the material due to its low viscosity. Control of residual film thickness also becomes difficult as the material squeezes out excessively in an open mold system. The temperature range representing the lower plateau region of the inverse parabola is most ideal for the embossing temperatures. At these temperatures, the material is sufficiently softened to fill the cavity completely evenly under low pressures. The high rate of crystallization and low induction time results in less time for the embossing stage in which the material remains fluidic. The low embossing time requires that the material should not be preheated prior to the embossing process. Ideally the material should come in contact with the mold surfaces only when

the actual embossing is conducted. This ensures that there is not pre-crystallization occurring in the material before the cavities are filled. Any increase in crystalline content in the polymer results in an increase in stiffness and subsequently a partial fill or requirement of high pressure. Selection of optimum temperature ensures that there is sufficient time available for the embossing stage, thereby avoiding any pre-crystallization. One of the objectives of the study is also to keep a control on the total embossing time which can be achieved by striking a balance between the temperature used for the embossing and the crystallization induction time.

4.2.1.2 Effect of Temperature during Holding and Demolding Stage of CTE

Though the CTE process employs only one temperature in all the steps, the role of temperature in the holding and demolding stage varies from that of the embossing stage. In the holding stage, the temperature field predominantly aids in overcoming the energy barrier for crystallization. Ideally with proper control of time and temperature, the crystallization can be allowed to occur only in the holding stage. Constant temperature is maintained to enable the crystallization of the already filled material inside the cavity. At the initial stages of crystallization, the heat energy supplied provides the cavity with more material when shrinkage due to crystallization occurs. At later stages of crystallization, the stiffness of the material increases and any further material supply to the cavities is interrupted. After this stage, heat primarily ensures that the maximum attainable level of crystallization is achieved.

During the demolding stage, the embossed polymer film is removed from the stamp in the hot condition. The already crystallized film is demolded and exposed to the environment immediately. Since the temperature of the film is high, the embossed film

shows less shrinkage and hence is able to be peeled off from the stamp without much difficulty. The high temperature also results in a certain level of difference in thermal expansion between the film and the stamp. This difference in thermal expansion also aids in smooth demolding of the material.

4.2.2 Embossing Time

In conventional embossing, the total cycle time is an addition of embossing time, holding time and cooling time (neglecting the ejection time). The embossing time depends on the type of material, the feature to be embossed and the temperature and pressure fields, and usually illustrates the time required to completely fill the cavity.

4.2.2.1 Effect of Time during Embossing Stage

In the case of CTE, the embossing time depends on one more variable which is the rate of crystallization. As mentioned earlier, the crystallization of the amorphous polymer film is required to start only after the complete filling of the cavity. The embossing time is calculated based on the crystallization induction time and also the rate of crystallization which is dependent again on the temperature at which the embossing is performed. Hence, the embossing time is in direct correlation with the embossing temperature. As shown in Figure 13, the maximum embossing time available is greater at the two ends of the inverted parabola and lower at the low plateau region. This method of time control has advantages as well as some challenges. The key advantage is the total time reduction, and the challenges are the need to have a rapid embossing stage, elimination of raw film preheating to avoid any pre-crystallization.

4.2.2.2 Effect of Time during Holding Stage

The holding time in the conventional embossing is largely used to allow for the material to fill the cavity completely and pack excess material so that any thermal shrinkage occurring during the cooling stage can be compensated. The holding time in that case depends on the type of features to be produced and other processing parameters, i.e. temperature and pressure.

In the case of the CTE process, the holding time depends, similarly to the embossing time, on the rate of crystallization of the polymer film used. Assuming the ideal case where the crystallization induction occurs after the embossing is completed and the process shifts to the holding stage, the time required for the holding stage is solely dependent on the time required for the amorphous polymer to achieve the maximum possible crystallinity under given temperature. The holding time can be determined by compressing a blank polymer film between the two cover plates and collecting samples at different intervals of time. The samples collected can be tested in DSC for temperature sweeps and the crystallinity of the sample can be determined. The samples can be collected and tested in a similar fashion until the crystallinity values reach a plateau. The total time taken for crystallization collected under such practical conditions can be cross-verified with the crystallization kinetics data collected from DSC. The parametric study for this chapter utilizes the same technique to determine the holding time. Since the embossed polymer is peeled off from the stamp instantaneously, the cooling time is neglected. The total processing time is the addition of the embossing time and holding time.

4.2.3 Embossing Pressure

The embossing pressure is an important variable in the conventional embossing process as it determines the replication fidelity of the process. The embossing pressure depends on the type of features to be embossed and the temperature. The pressure used in the embossing process is relatively low compared to other micro-molding processes due to the low flow length for the polymer. Though high pressure is needed for high aspect ratio features, it is still quite smaller than that experienced in other polymer processing operations.

In the case of the CTE process, the embossing pressure along with temperature assists in complete fill of the cavities. Since, in the current study, the aspect ratio of the features is not very high, low pressures were used in the parametric study. Additionally, since amorphous polymers are used, increasing the temperature above T_g softened the material substantially such that much smaller pressures are required. Contact pressure generated by keeping the two platens of the compression molding machine in close contact with the embossing setup was sufficient for filling the cavities at certain temperatures. During the holding stage, the embossing pressure is monitored to compensate for shrinkage of the polymer film occurring due to crystallization. There is marginal shrinkage in the polymer film during the holding stage as the material crystallizes. In order to compensate for the shrinkage, a vinyl rubber support is placed between the top platen and cover plate. It has to be mentioned that the rubber sheet does not come into contact with the film surface and only compensates for reduction in film thickness. A schematic of the embossing setup with a compressible rubber sheet is given in Figure 39.

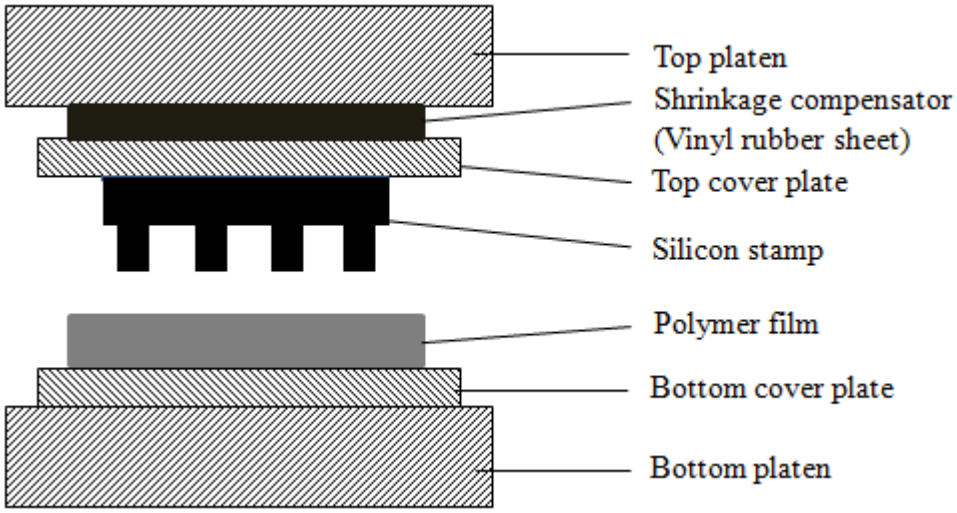

Figure 39 CTE set-up with shrinkage compensator

4.3 Constant Temperature Embossing of Amorphous PET

The amorphous PET film was embossed using silicon stamps with parallel microtrenches as a master pattern. The pitch and width of the trenches were 20 µm and depth was approximately 40µm. The embossing was carried out in a hydraulic compression molding machine as shown in Figure 40. The SEM micrograph of the embossing mold is shown in Figure 41 with the inset showing the edges. The temperatures used for embossing were based on the DSC characterization temperatures and with different rates of crystallization. The embossing was done at temperatures of 100, 120, 140, 160 and 180, 200 and 220 °C with the silicon mold sandwiched between two Teflon sheets and the polymer film of appropriate dimension.

Hydraulic compression molding machine

Pneumatic compression molding machine

Figure 40 Hot embossing equipment

4.3.1 Constant Temperature Embossing Parameters

Initially, calibration experiments were conducted without the film to determine the temperature lag at the embossing surface due to the insulating Teflon layers and the time was accounted for in the total embossing time given. A very low pressure of about 0.7-0.14 MPa (10-20 psi) was applied during the embossing and holding stage. After the holding stage the film was immediately demolded from the stamp without cooling. The parameters used in the embossing experiments are given in Table 2.

Table 2 Parametric study for CTE of amorphous PET films

Holding Time/ Temperature	100°C	120°C	140°C	160°C	180°C	200°C
10 s	X	X	X	X	X	X
30 s	X	X	X	X	X	X
60 s	X	X	X	X	X	X
90 s	X	X	X	X	X	X
120 s	X	X	X	X	X	X

Three pressures (contact pressure, 50 psi, and 100 psi) were probed for all the above conditions. It was observed that other than at temperatures of 100 and 120°C, the contact pressure was sufficient for completely replicating the features used for the experiments. The temperature on the surface of the film during embossing was measured by inserting a flat thermocouple between the preheated cover plates and amorphous PET film. The PET film initially was at room temperature when the film was introduced in-between the cover plates before applying the embossing pressure. The temperature of the film increased from room temperature to the embossing temperature in 3-5 s as measured by the thermocouple.

4.3.2 Surface Morphology Analysis of Replicated Features with SEM

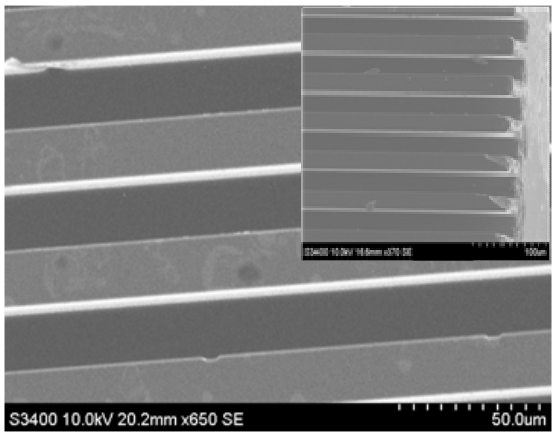

Figure 41 SEM of the silicon mold

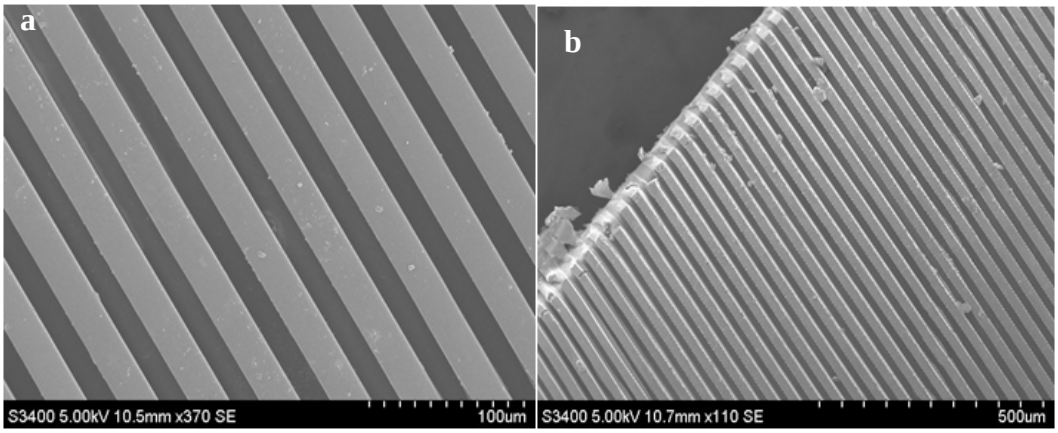

Figure 42 (a & b): Amorphous PET film embossed at 160 °C with cooling

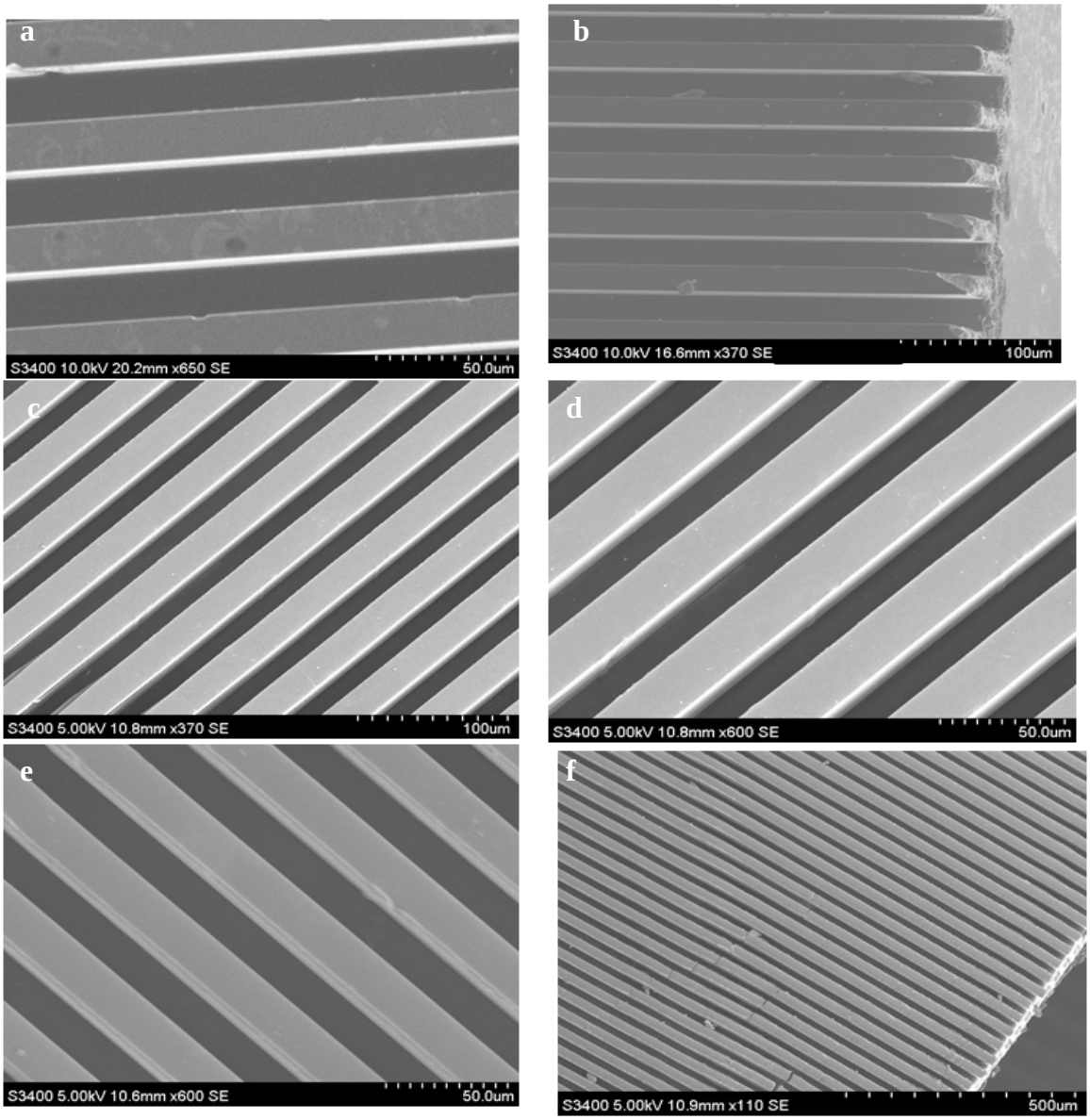

Figure 43 Amorphous PET films embossed at various embossing temperatures without cooling. 140 °C – a,b; 160 °C – c,d; 180 °C – e,f

SEM images were taken after keeping the material overnight for any structure recovery. The SEM pictures of the embossed film in Figure 43 demonstrate faithful pattern replication at different embossing temperatures and even at the edges for an aspect ratio of 2.

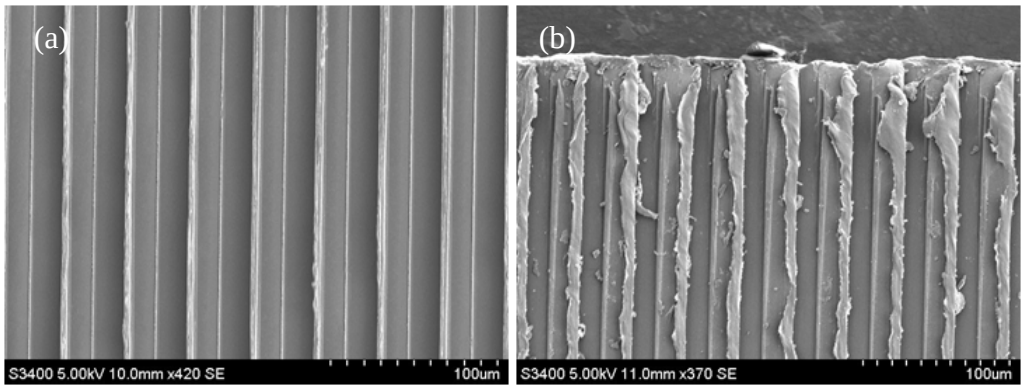

Figure 44 Semicrystalline PET embossed at 230°C and demolded with cooling (b) Semicrystalline PET embossed at 230°C and demolded without cooling

The good replication of the patterns was achieved by careful design of the experiments based on the property exhibited by the material under different thermomechanical influences. It has to be emphasized here that the embossed film was removed from the mold under the hot stage itself and no observed recovery of the shape has occurred. To confirm this aspect, embossing experiments were conducted wherein the embossed film was cooled under pressure till the temperature of the material decreases to less than its T_g and then demolded.

The SEM picture of the embossed films with sufficient cooling time is shown in Figure 42. The micrograph shown here are for the films processed at 160°C. The pictures show that there is no effect of the cooling time and that the material if demolded at hot condition does not undergo any recovery. Furthermore, the embossed films were heated at 150°C for 1 hour and characterized using SEM. There was no dimensional change in the patterns as a result of the heat exposure and features remained intact. This also shows that the films can be used for high temperature applications such as in automotive industry.

To confirm the effect of the transition behavior on the final replication quality, biaxially oriented PET films were embossed in a similar fashion with and without cooling. The semi-crystalline PET films have a T_m of around 255-260°C and are quite dimensionally stable till near its melting point requiring higher embossing pressure to form the part. The same silicon master used in the earlier study was used in the experiments. The SEM micrographs of the semicrystalline PET films embossed at 230°C with and without cooling are shown in Figure 44 (a) and (b) respectively. The patterns developed in these two cases showed a marked difference in quality as the films without cooling have damaged edges and partially recovered features. This also shows that the transition occurring in the amorphous PET film contributes to the excellent dimensional stability after the constant-temperature embossing process.

4.3.3 Replication Accuracy Analysis with Optical Interference Profilometer

The height of the features embossed was measured by using a Wyco optical profilometer. The profile scan of the silicon mold is shown in Figure 45.

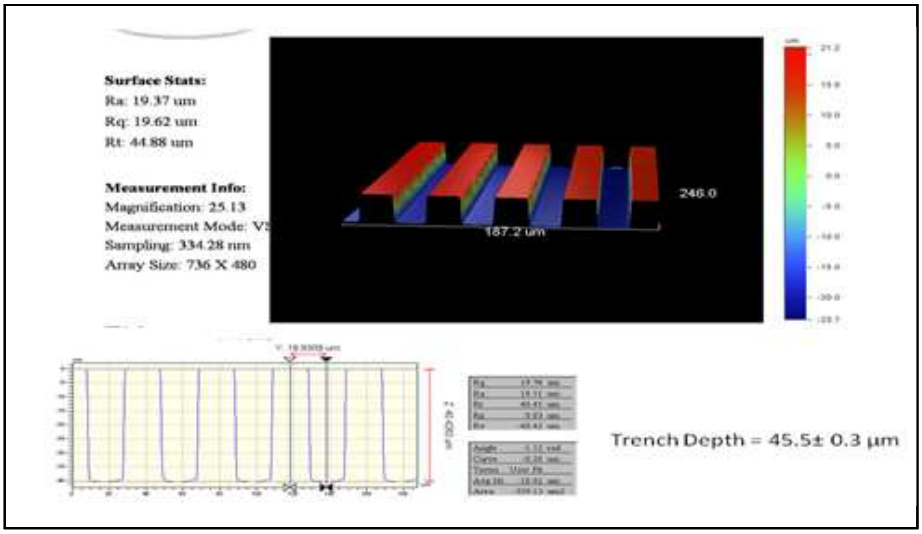

Figure 45 3D scan of the silicon mold with 20 µm width. 2D profile shows the height of the features which is measured by averaging over a large area.

46(a)

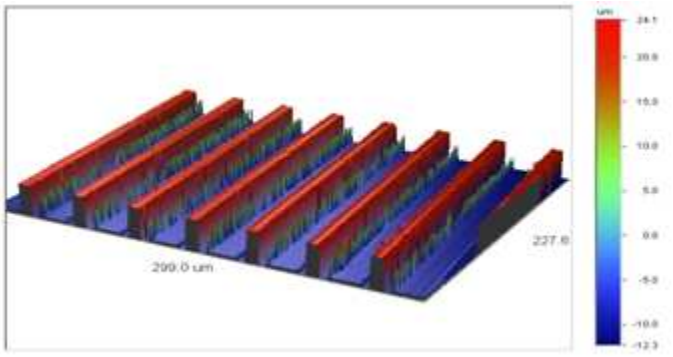

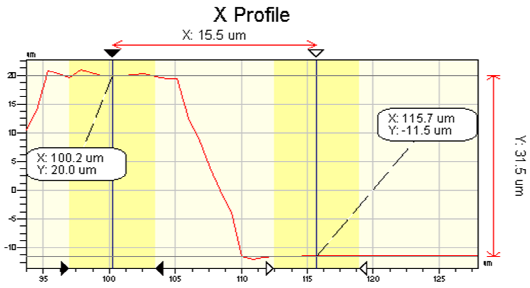

Immediate Demolding – No Cooling
Feature Height = 31.4± 0.2 µm

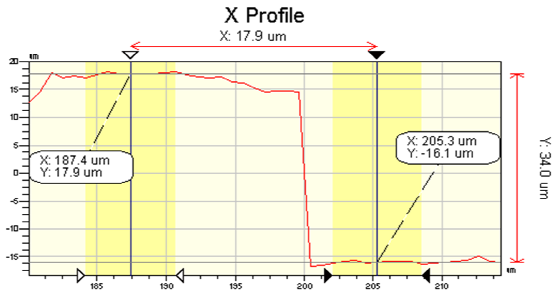

Demolding after cooling under pressure
Feature Height = 34.2± 0.3 µm

46(b)

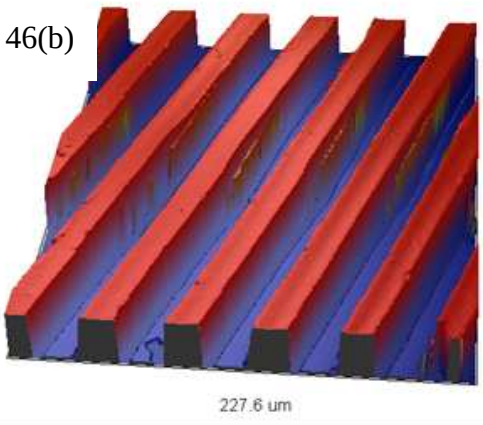

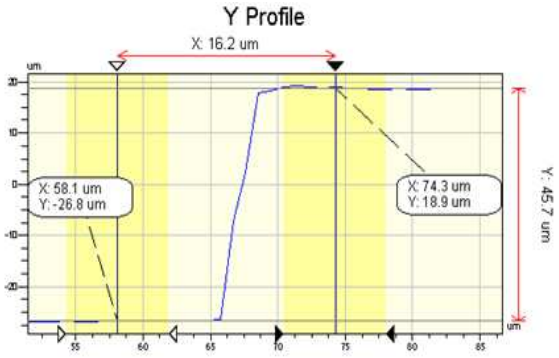

Feature Height = 45.5± 0.3 µm

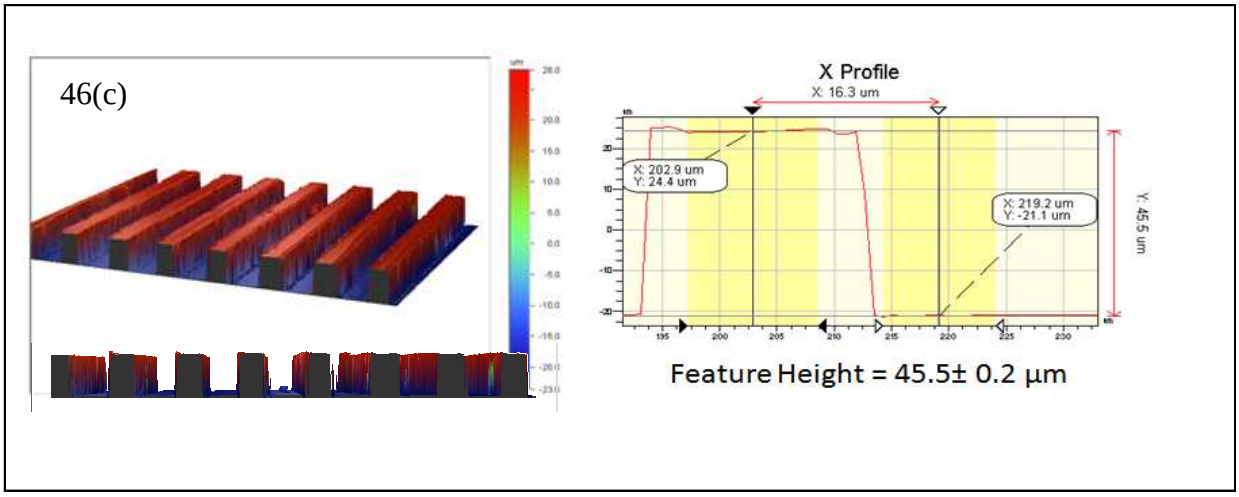

Figure 46 Profilometer 3D and 2D scans of the amorphous PET films embossed at different processing conditions (a) 100°C/120 s/50 psi (b) 160°C/120s/50 psi (c) 180°C/30 s/Contact Pressure

Profiles of samples embossed at different temperatures and time are shown in Figure 46.The results from the profilometer showed that even for a total cycle time of around 20 s, complete cavity filling was observed at temperatures in the range of 140 – 180 °C. However, at these temperatures, the rate of crystallization is the fastest. Hence, the embossing pressure was applied immediately in order to avoid any crystallization before the feature is formed. At low a temperature of 100 °C, the sample cooled under pressure always showed a taller feature than the one demolded at hot condition. This can be attributed to the high elastic entropy at temperatures close to T_g and hence on exposure to room temperature, part of the feature rebounds back to a certain extent.

The plots of the replicated height against the feature half-width are shown in Figure 47 (a-c). The profiles plotted in Figure 47(a-c) were obtained from the samples which were embossed at the respective temperatures and immediately demolded. As observed in Figure 47(a-c), the features were not completely replicated at low temperature in which the rate of crystallization is low and also the material is stiffer than at high temperatures. The filling when embossed at a temperature of 100°C is around

60% of the total height and the edges are rounded as well. This might be attributed, as mentioned earlier, to the rebound of the material after the holding pressure is released. The samples embossed at 120°C also showed around 60% filling but the edges were sharper than of samples embossed at 100°C. The samples embossed at 140°C, 160°C and 180°C showed little differences among them, but with 180°C producing more uniform and sharp-edged samples.

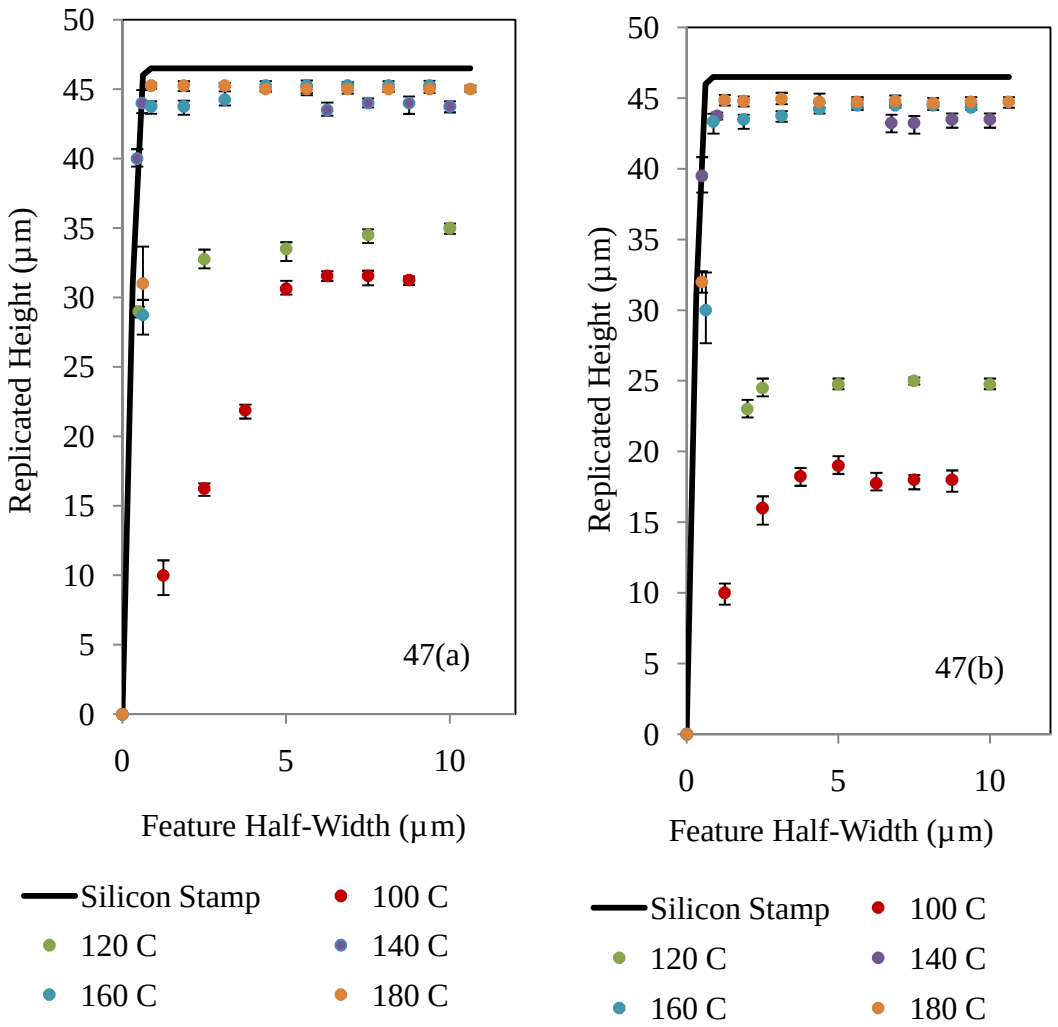

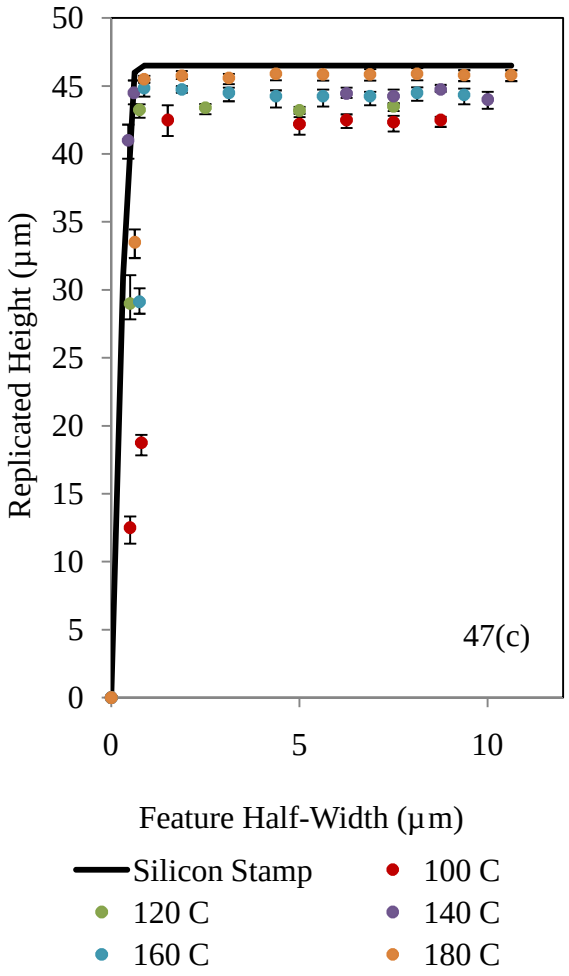

Figure 47 Replicated height of amorphous PET films embossed at different processing conditions (a) 30s/50 psi and (b) 60s/50 psi (c) 600s/50 psi

4.3.4 Versatility of Constant Temperature Embossing Process

To demonstrate the versatility of the CTE process vis-à-vis a conventional hot embossing process, samples were embossed under two different conditions:

- Samples were embossed at different isothermal temperatures and demolded immediately at that isothermal temperature and exposed to atmosphere. The sample cools down under natural air convection [No Cooling]

- Samples were embossed at different isothermal temperatures and demolded after cooling the samples in the embossing setup to temperatures less than the T_g of the polymer. Then the sample was demolded from the mold similar to conventional embossing processes [With Cooling]

Figure 48 (a-e) show the profiles of the samples demolded under the above mentioned conditions with and without cooling.

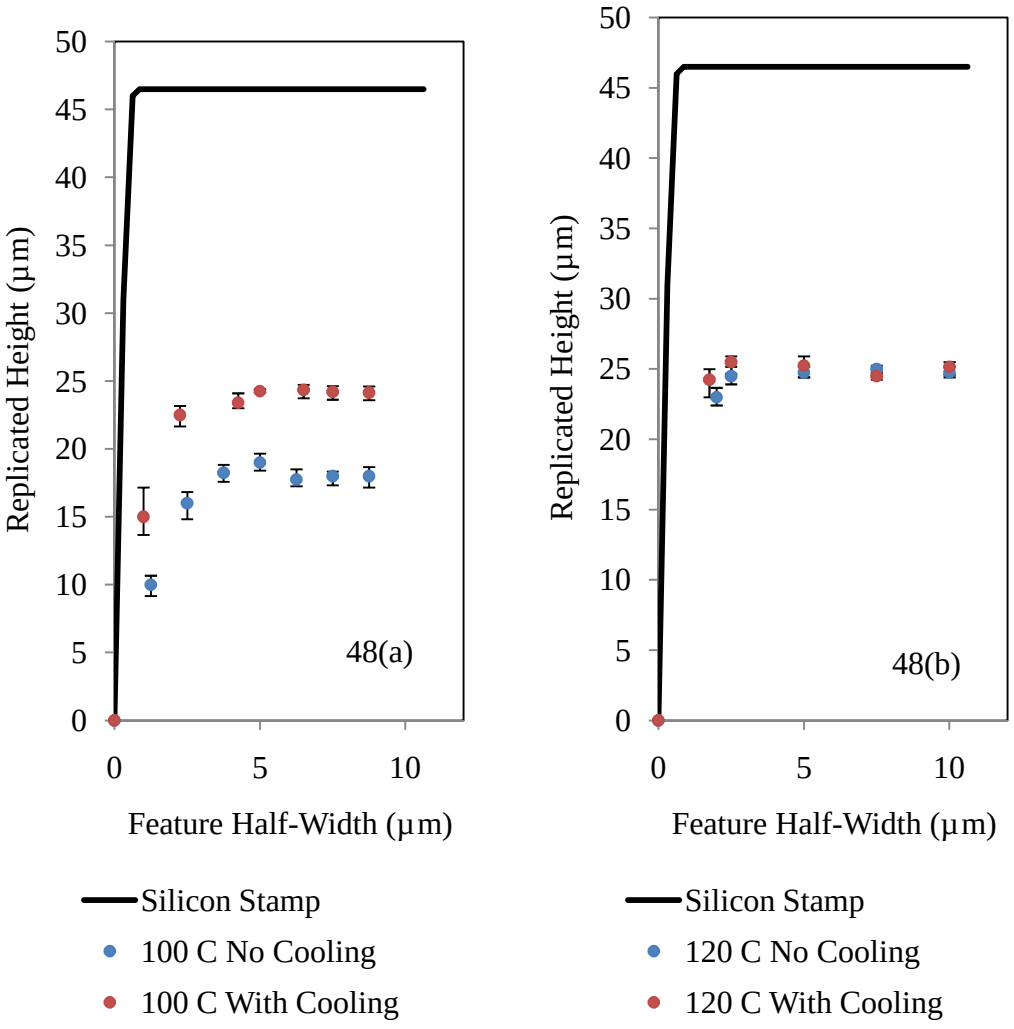

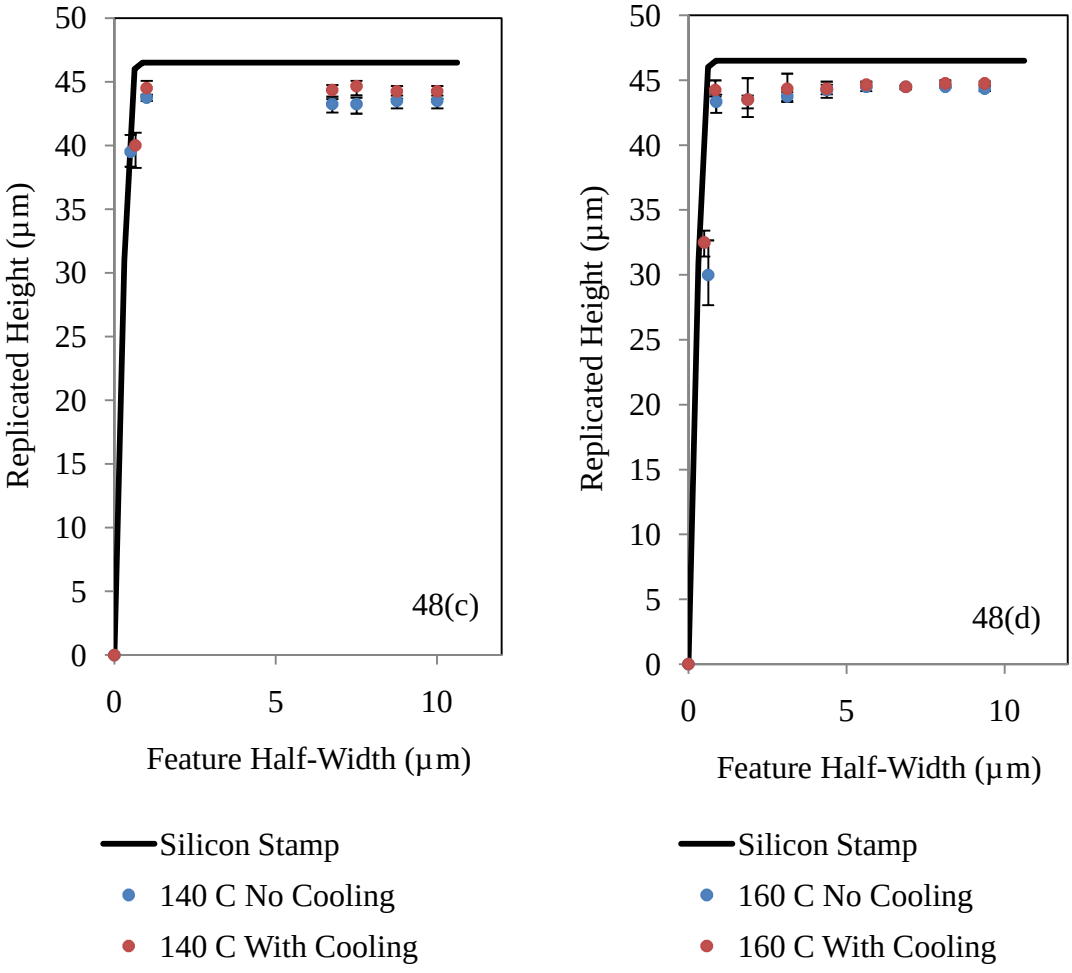
Replicated Height (µm)
Feature Half-Width (µm)
48(c)
48(d)
Silicon Stamp
140 C No Cooling
140 C With Cooling
160 C No Cooling
160 C With Cooling

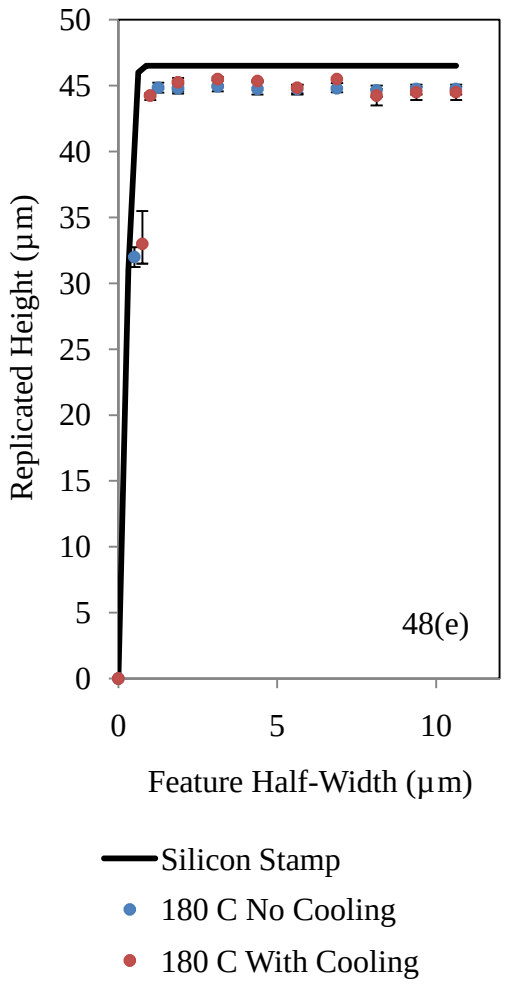

Figure 48 Replicated height of amorphous PET films embossed at different processing conditions with and without cooling (a) 100°C/30s/50psi (b) 120°C/30s/50psi (c) 140°C/30s/50 psi (d) 160°C/30s/50 psi (e) 180°C/30s/50 psi

It can be observed from Figure 48 (a) that for the samples embossed at 100°C, there is difference in height between the samples demolded after cooling and the ones demolded without cooling. The samples demolded in a manner similar to conventional embossing process (after cooling the embossed film to temperatures below T_g) show better replication compared to the case where demolding is done at constant temperature. This can be attributed, as mentioned earlier, to the recovery of the film when embossed at low temperatures. But in the case of samples embossed at 120°C, such a recovery was not

significant. Hence the partial recovery of the material cannot be the reason of the incomplete fill. For samples embossed at 140-180°C, there was little difference in replication between the samples demolded with and without cooling. This shows the versatility of the CTE Process when compared to the conventional hot embossing. The study demonstrates that the CTE process is able to produce good replication provided the optimum process parameters are selected.

4.3.5 Effect of the embossing process on the mechanical properties of the film

The amorphous polymer films used for embossing are around 250 μm thick and the rectangular trenches in the mold are of 40 μm maximum depth. Though the polymer film is heated uniformly through its entire thickness during embossing, the film comes in direct contact only with the rectangular trenches in the mold initially. The layer of the polymer film where the mold comes into contact results in deformation and filling inside the cavities. The remaining bulk of film is observed to show squeezing flow depending on the embossing pressure applied. The final film thickness can be controlled to be close to the initial thickness by only applying the minimum embossing pressure required to fill the 40 μm cavities. The mechanical properties of the film before embossing are given in Table 1. The determination of the mechanical properties of the polymer film requires testing the crystallizing film under nearly same conditions which are very difficult to simulate and hence beyond the scope of the current work. The film after embossing was opaque and appeared to be more brittle compared to the original film.

4.3.6 Constant Temperature Embossing of High Aspect Ratio Features

The amorphous PET film was embossed with a high aspect ratio stamp containing rectangular trenches as shown in Figure 49. The width of the trenches was 10 µm and the depth was around 35 µm resulting in a aspect ratio of around 3.5.

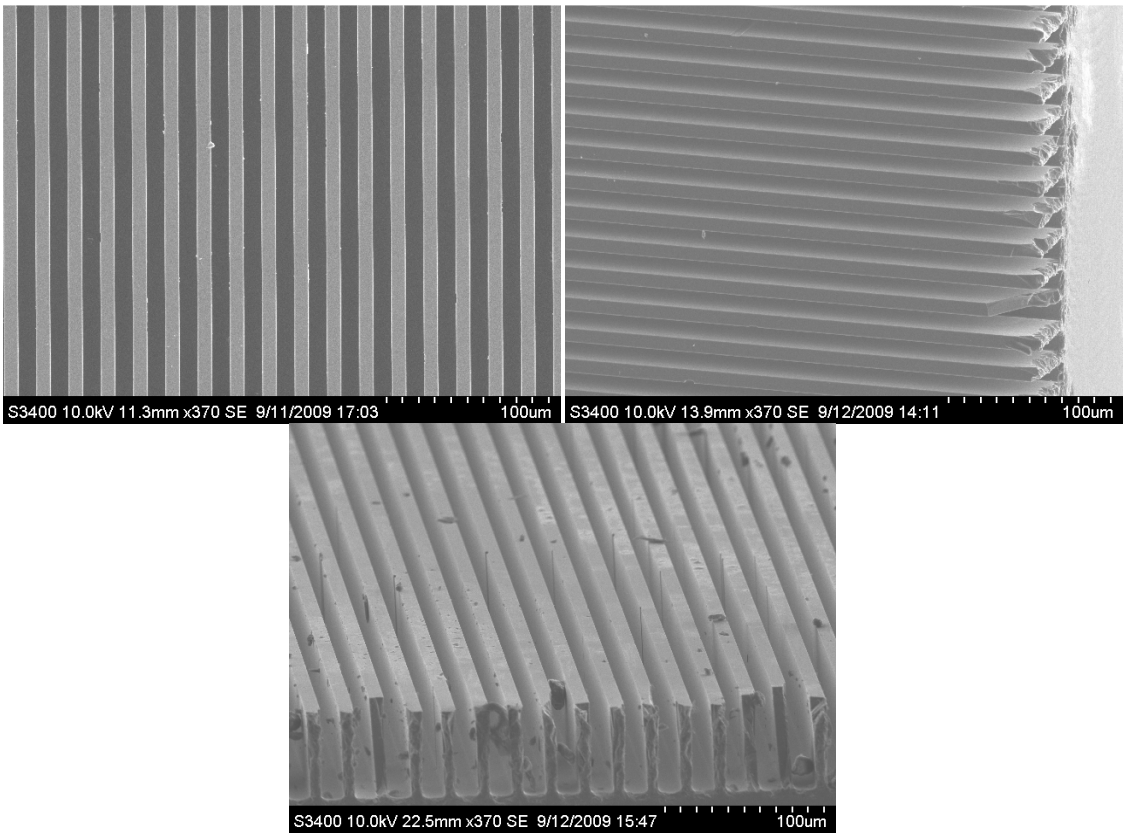

Figure 49 SEM pictures of the silicon stamp with a dimension of 10 µm width and ~35 µm depth

The constant temperature embossing was carried out at similar conditions to that for the 20 µm stamp. The samples embossed at 140°C are shown in Figure 50. The rounded surface in the SEM picture shows that the features were not completely filled as observed for the low aspect ratio stamp. Figure 51 and Figure 52 show the samples embossed at temperatures 160°C and 180°C. The samples embossed at these temperatures show sharp-edged features indicating that the cavities were completely

filled. These results are different from that of the samples embossed with the 2:1 ratio stamp. The reason that the sample did not completely fill might be the high pressure required for the polymer to fill the 10 µm cavities. At 140°C, the polymer is relatively stiffer than that at high temperatures such as 160°C and 180°C. The pictures with a red border in Figure 51 and Figure 52 show samples that were purposefully damaged immediately after demolding to see the type of damage. The damage seen in the features are more brittle in nature than a plastic yielding. This demonstrates that the samples were fully crystallized when the demolding was done. Also the high aspect ratio of the features and the smooth side walls are visible. The study demonstrates the capability of the CTE process to produce high aspect ratio features provided the suitable processing parameters are identified.

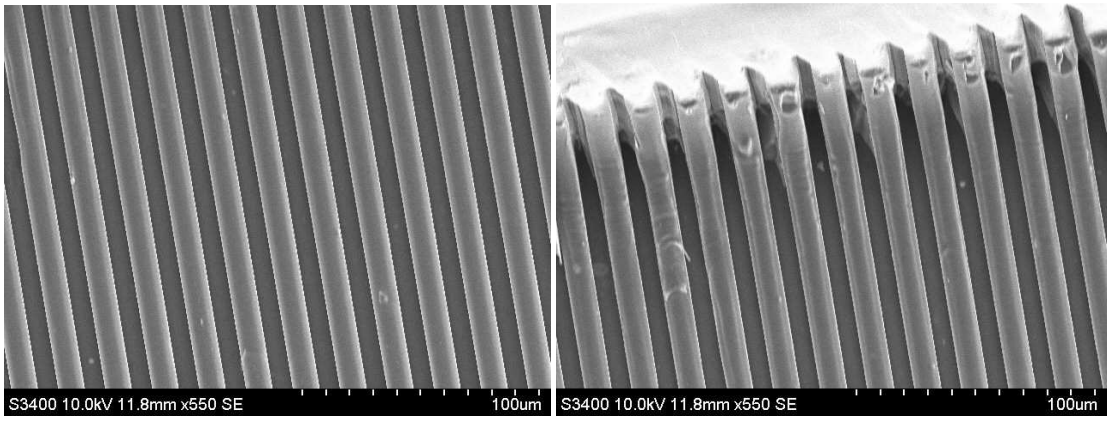

Figure 50 Amorphous PET embossed at 140°C and immediately demolded

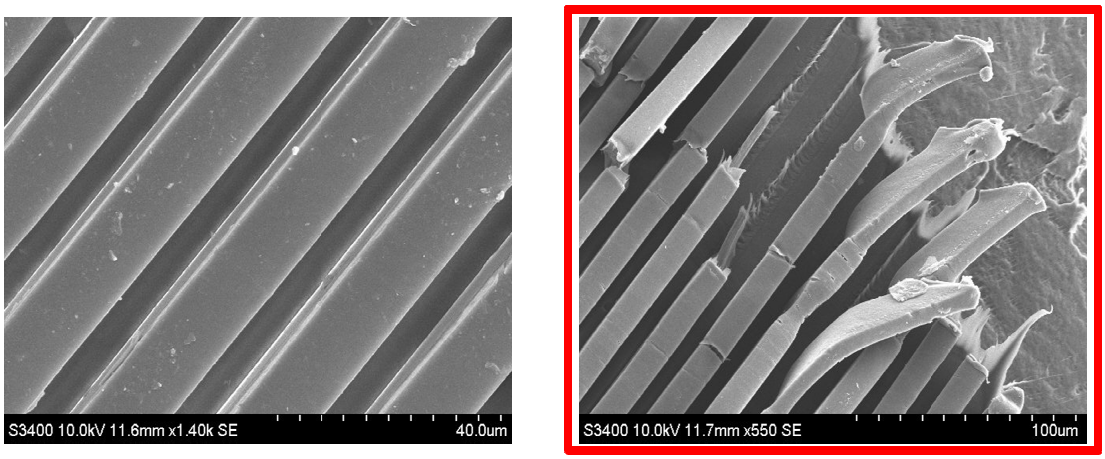

Figure 51 Amorphous PET embossed at 160°C and immediately demolded

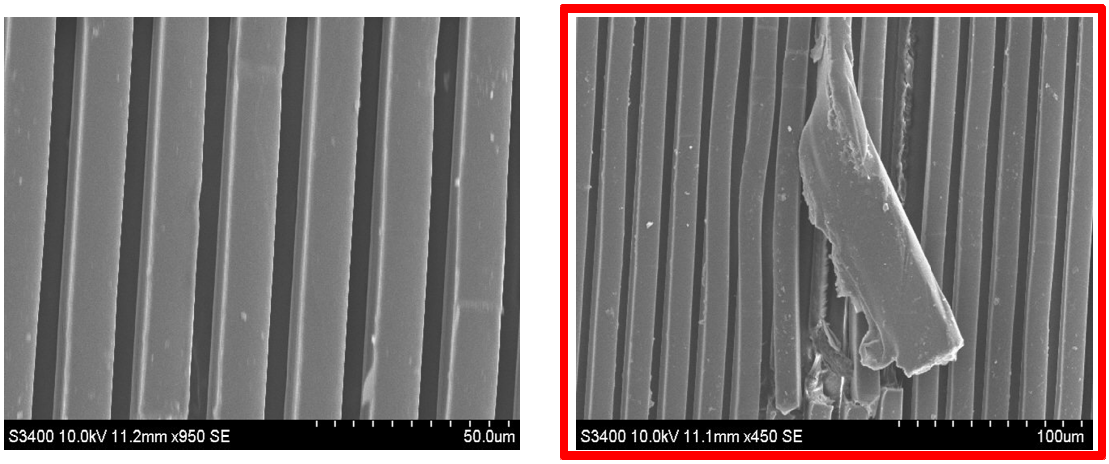

Figure 52 Amorphous PET embossed at 180°C and immediately demolded

4.4 Constant Temperature Embossing of APEEK

4.4.1 Equipment Setup and Material

The constant temperature embossing of the amorphous PEEK films were conducted in the similar way as for the APET. The embossing was conducted in the hydraulic embossing machine and the material used is a 230 µm film. The film's initial crystallinity was found to be 10-12% from DSC. The embossing mold used was also the same: ¼"x¼" Silicon mold with parallel trenches. The width and pitch of the trenches is

20 µm or 10 µm. The depth of the 20 µm molds is around 45 µm and the depth of the 10 µm molds is around 38 µm.

Since the rate of crystallization of PEEK films are quite higher than the amorphous PET films, the films initially embossed using the same mold setup did not produce well replicated features.

Also the crystallization induction time is in the order of 5-7 s in most of the operating temperature ranges, the crystallization started before the film completely filled the cavity. Hence, the replication was very poor. This may be attributed to two reasons:

- The APEEK film does not soften as much as the APET films and the viscosity of the softened film at the processing temperature ranges are much higher than that of the softened APET films. This results in extremely high pressures needed for embossing. The initial crystallinity of the films was also high compared to that for the amorphous PET films.
- The crystallization induction time is very short in the processing temperature range. Hence, during the embossing stage, before the cavity is completely filled, the crystallization starts. This resulted in the increase in stiffness of the film as the cavity is being filled. The higher the viscosity, the more the pressure required to push the film into the cavity. Since PEEK films reach a maximum crystallinity to about 30% and the initial crystallinity of the films was 10-12%, the time interval during which the films remain in the rubbery phase was short. Any crystallization occurring in the film before the embossing stage started leads to increase in viscosity. The embossing stage under these conditions resembled a solid deformation pattern in which the already solidified film was

pushed into the cavities. This required very high pressure and also partial to complete recovery after the pressure was released.

4.4.2 Modified Zero-lag Time Embossing Setup

In order to accommodate the fast rate of crystallization, the time lag between the time at which the polymer film is sandwiched between the mold and platens and the time at which the embossing pressure is applied is reduced to near-zero. This can be accomplished by using a collapsible support for the APEEK films to load the film during embossing as shown in Figure 53. The polymer film is kept on a support and the mold is strapped on to the top platen and pre-heated.

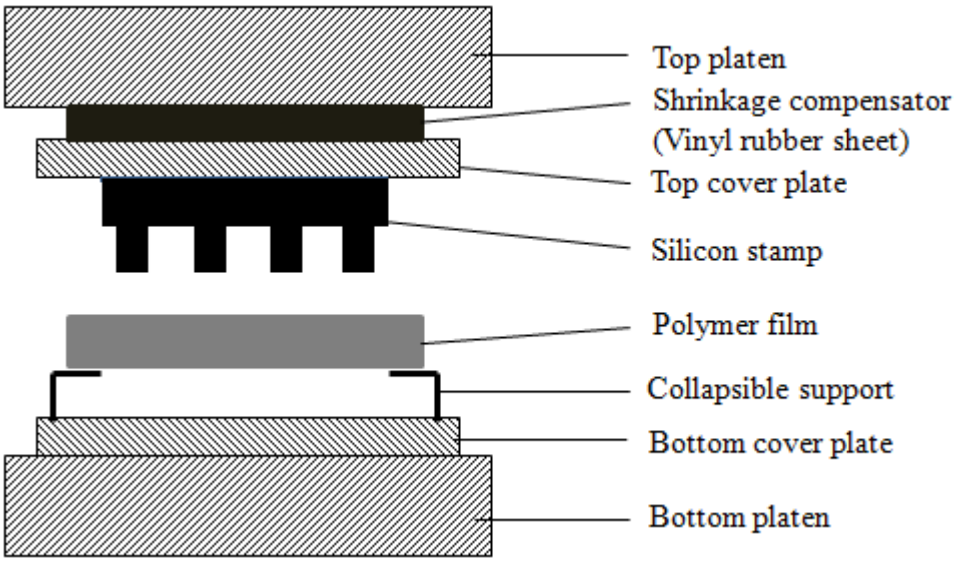

Figure 53 Embossing setup for amorphous PEEK

The pre-heated mold comes in contact with the polymer film only when the embossing pressure is applied. The support is made of a thin aluminum foil ring which is knocked of once the mold comes in contact with the polymer film. With this technique reasonable amount of replication was achieved. The replication was improved to a certain extent with increase in pressure but attaining a complete fill of the cavity was very

difficult in the processing parameter range which is understandable considering the film was highly crystalline at the beginning. The process parameters used for the APEEK embossing are given in Table 3

Table 3 Parametric study for CTE of amorphous PEEK films

Holding Time/ Embossing Temperature	200°C	220°C	240°C	260°C
5s	x	x	x	x
10s	x	x	x	x
35s	x	x	x	x
60s	x	x	x	x
120s	x	x	x	x

4.4.3 Surface Morphology Analysis of Replicated Features with SEM

Figure 54 – Figure 66 show the amorphous PEEK samples embossed at 220°C, 240°C and 260°C. From the SEM pictures of the samples it can be seen that, even though at 240 and 260°C, the replication was relatively good, complete filling of the cavity was almost impossible for the material. Amorphous PEEK is relatively stiffer than the amorphous PET in its natural form. When heated above its T_g, amorphous PET film becomes very soft and behaves like a low viscous liquid. This enables the embossing process to be carried out very easily and completely filled features are obtained. In the

case of amorphous PEEK, the material even after heating to temperatures well above T_g does not soften sufficiently to fill the cavities completely. This again is due to the high crystallinity of the films at the beginning compared to the amorphous PET films. The difficulty encountered here resembles the problems faced in the case of traditional embossing. The films due to their high crystallinity exhibit high viscosity at these processing temperatures and hence require very high embossing pressures which are impossible to achieve due to the brittleness of the silicon stamp. This problem is magnified by the rapid rate of crystallization observed in PEEK at most processing temperatures. At temperatures near 200-220°C, the half time of crystallization is in the range of 5-7 s. To counter this rapid rate of crystallization, the embossing method using collapsible support has been mentioned earlier. Even after reducing the lag time during embossing, the samples embossed at temperatures less than 200°C did not show any embossing.

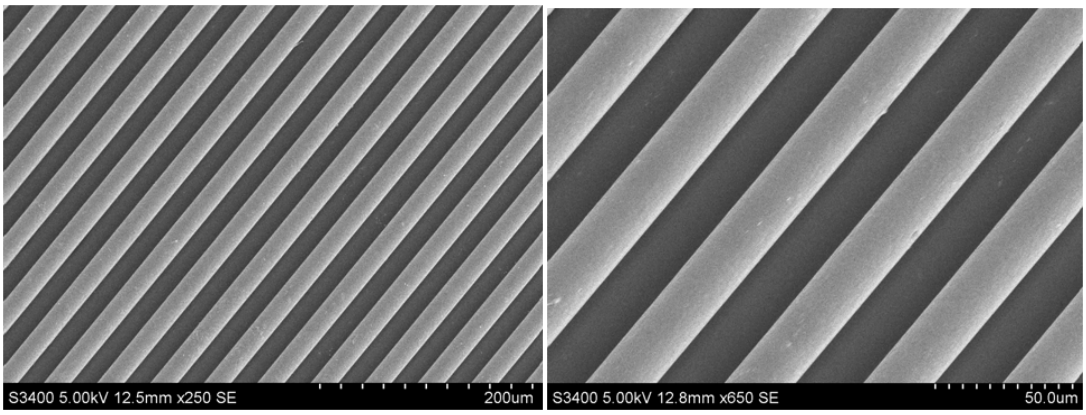

Figure 54 SEM of PEEK film embossed at 220°C/300 psi/7s with the 20 µm Si stamp

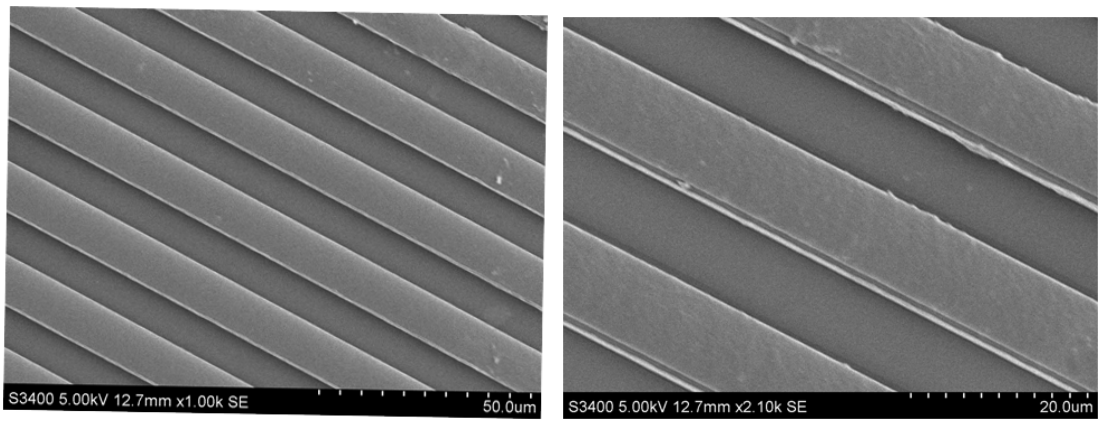

Figure 55 SEM of PEEK film embossed at 220°C/300 psi/35s with the 20 µm Si stamp

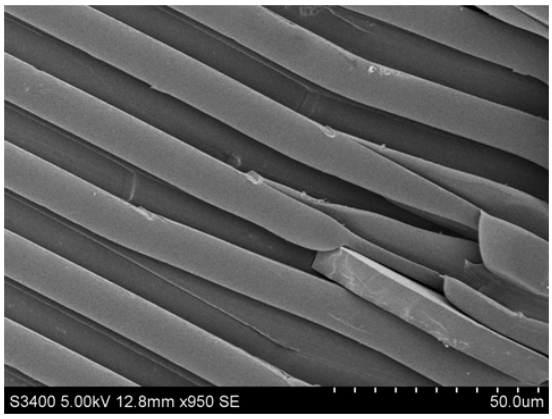

Figure 56 SEM of PEEK film embossed at 240°C/300 psi /7s with the 10 µm Si stamp

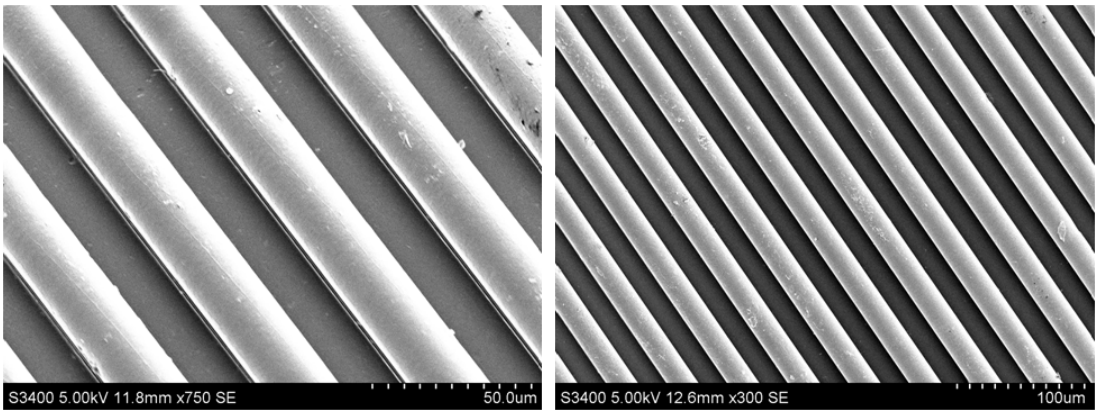

Figure 57 SEM of PEEK film embossed at 220°C/300 psi/35s with the 10 µm Si stamp

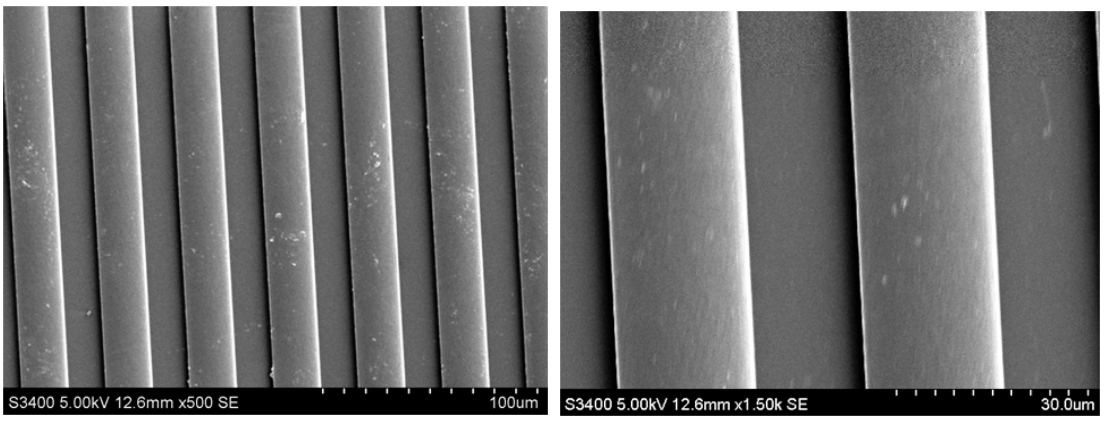

Figure 58 SEM of PEEK film embossed at 240°C/300 psi/7s – 20 µm

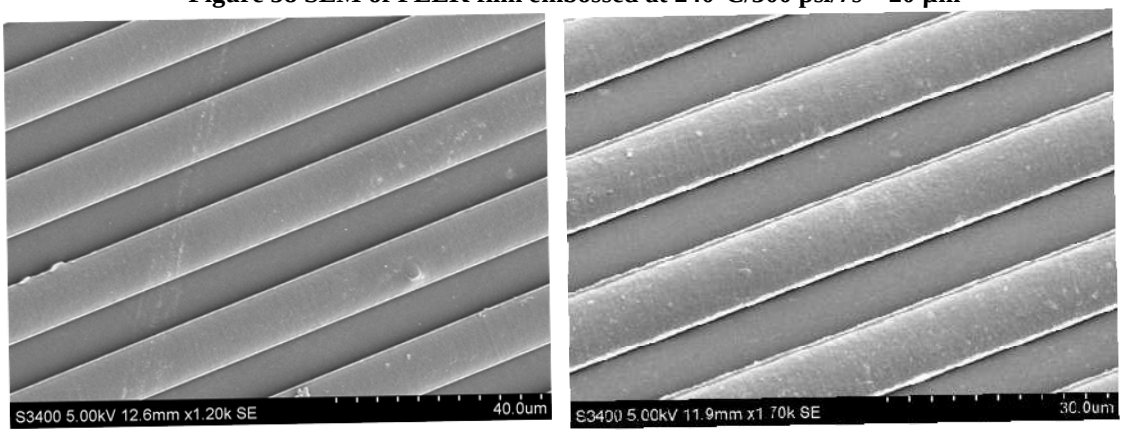

Figure 59 SEM of PEEK film embossed at 240°C/300 psi/35s with the 20 µm Si stamp

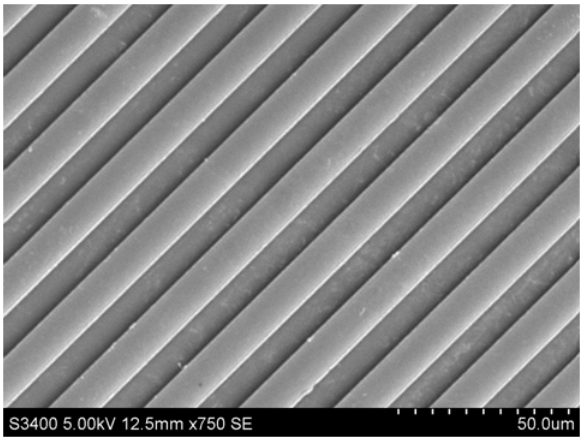

Figure 60 SEM of PEEK film embossed at 260°C/300 psi/7s with the 20µm Si stamp

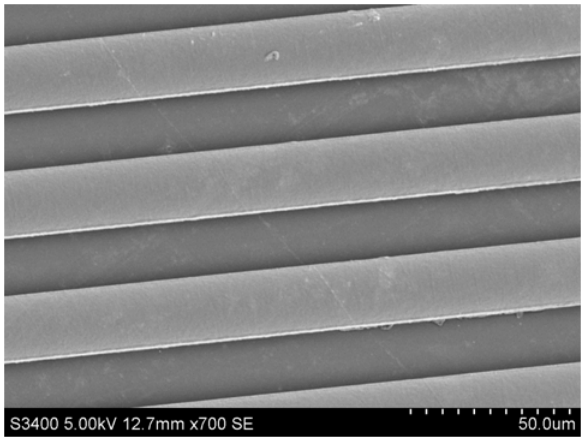

Figure 61 SEM of PEEK film embossed at 260°C/300 psi/35s with the 20µm Si stamp

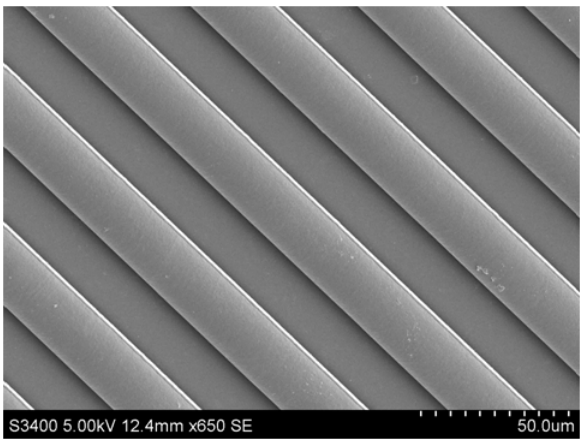

Figure 62 SEM of PEEK film embossed at 260°C/300 psi/7s with the 10 µm Si stamp

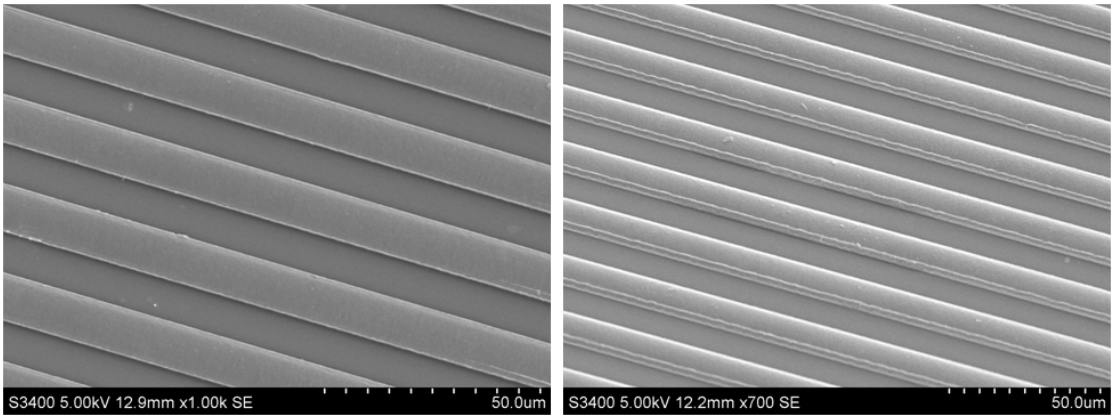

Figure 63 SEM of PEEK film embossed at 260°C/300 psi/35s with the 10 µm Si stamp

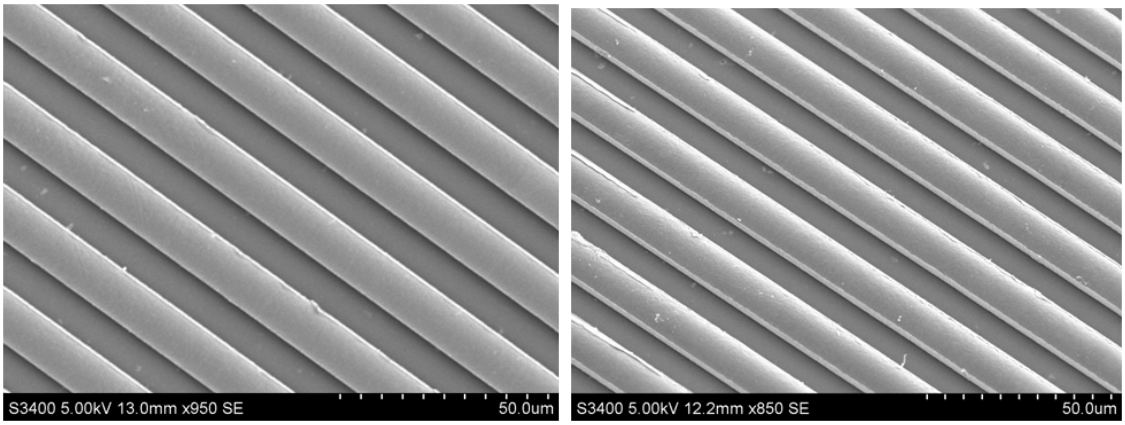

Figure 64 SEM of PEEK film embossed at 260°C/300 psi/35s with the 10 µm Si stamp

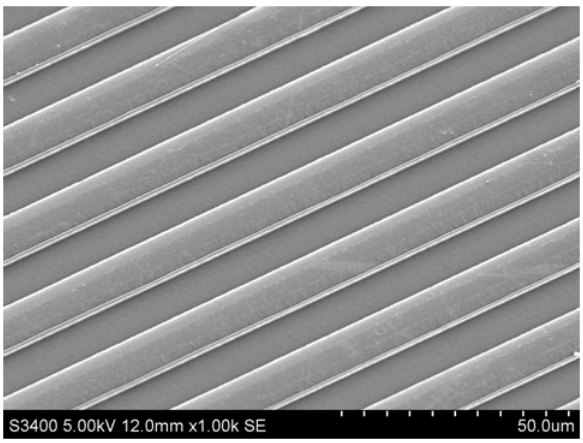

Figure 65 SEM of the PEEK film embossed at 260°C/1000 psi/35s with the 10 µm Si stamp

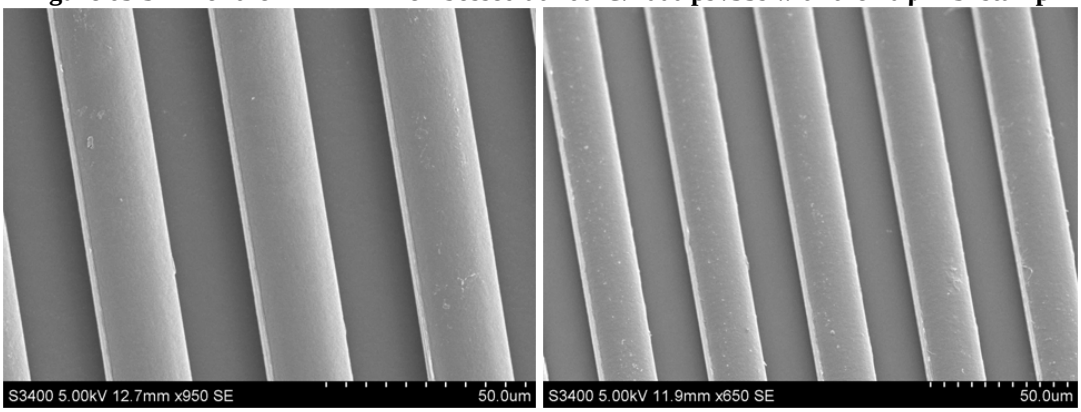

Figure 66 SEM of the PEEK film embossed at 260°C/1000 psi/35s with the 20 µm Si stamp

As seen in the above SEM pictures, the embossing of amorphous PEEK was not similar to that of amorphous PET films in terms of the replication achieved. The amorphous PEEK samples have rounded edges and very little filling. The profilometry picture shown in Figure 67 for the amorphous PEEK embossed at 260°C with very high pressure showed near complete fill. The significant observation in the samples is that of the broken edge in the right side. This might be due to the damage sustained during the demolding stage which also shows that the sample has crystallized completely when the demolding was done. Also, the features were sharp in nature even after the damage sustained which again demonstrates the applicability of the CTE process to amorphous PEEK if suitable amorphous PEEK film is used for the experiments.

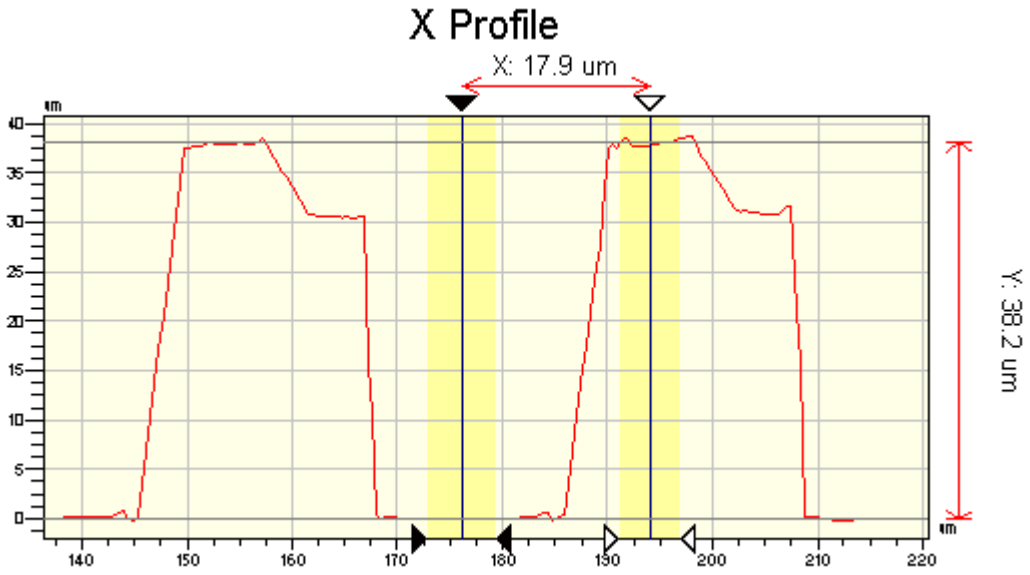

Figure 67 2D profilometer image of the PEEK film embossed at 260°C/1000 psi/35s with the 20 µm Si stamp

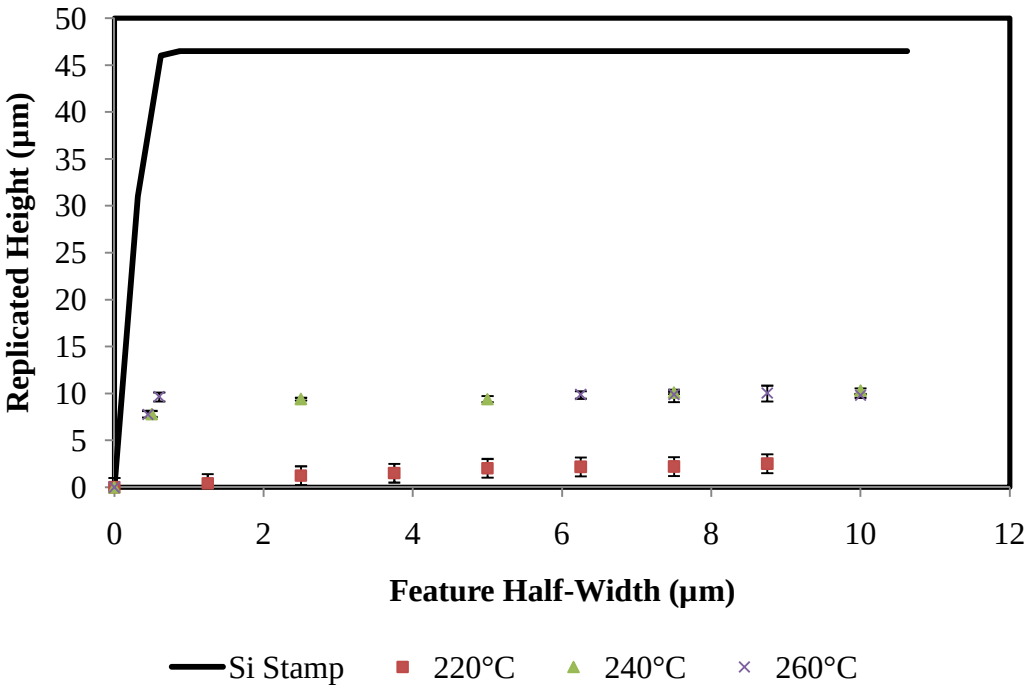

Figure 68 Replicated height of the PEEK film embossed at 300 psi/7s with the 20 µm Si stamp

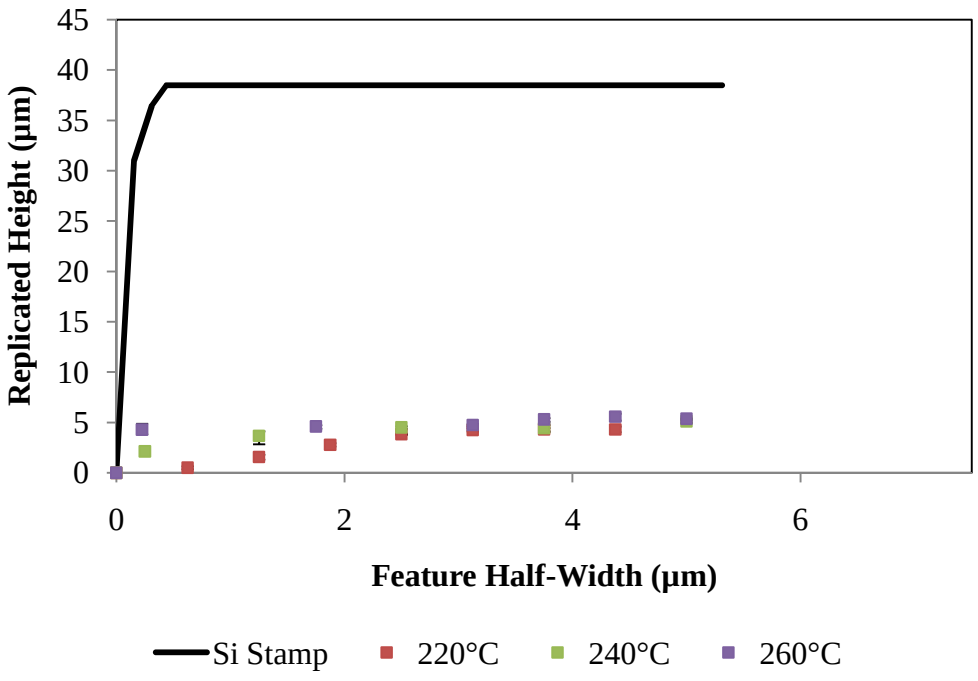

Figure 69 SEM of the PEEK film embossed at 300 psi/7s with the 10 µm Si stamp

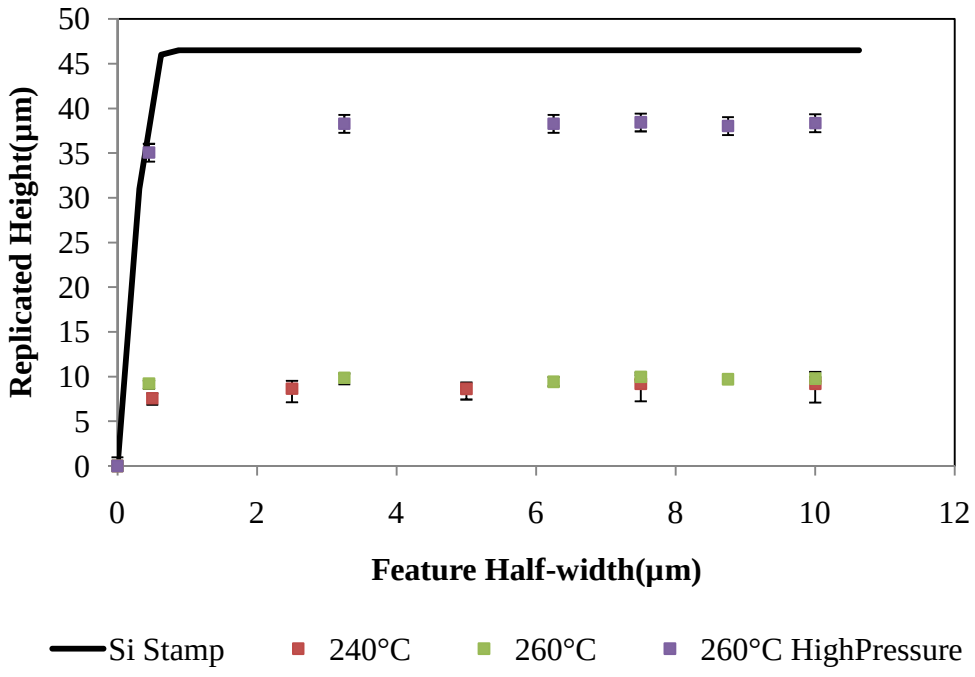

Figure 70 SEM of the PEEK film embossed at 300 psi/35s and 1000 psi/35s with the 10 µm Si stamp

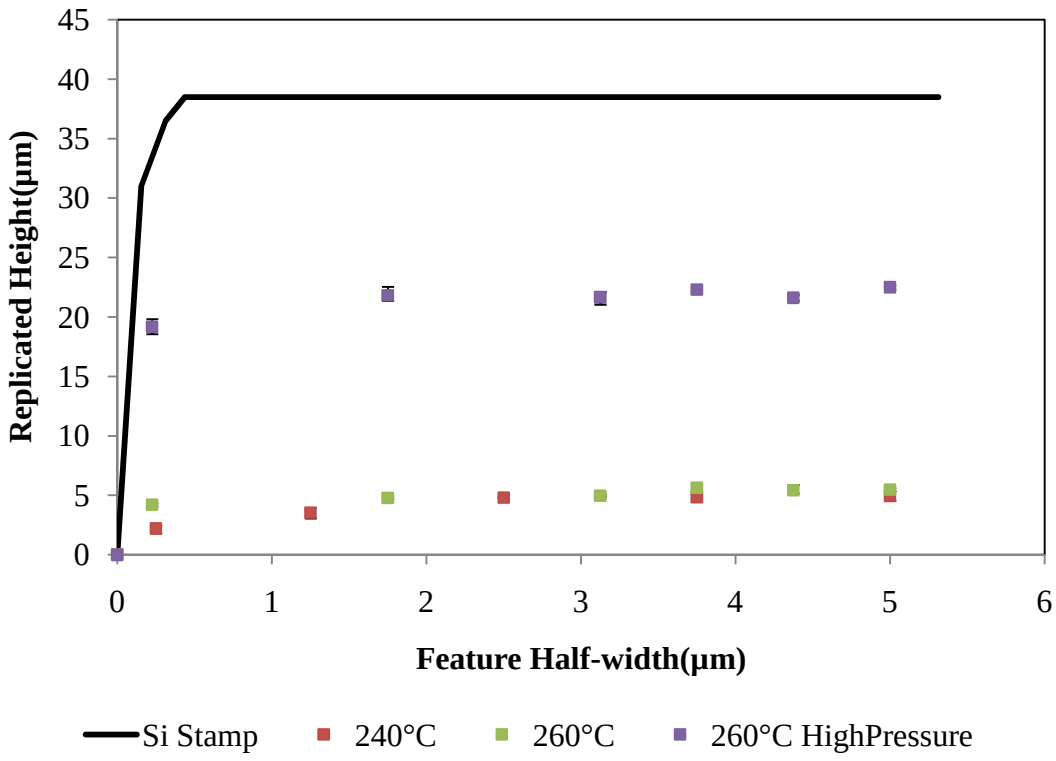

Figure 71 SEM of the PEEK film embossed at 300 psi/35s and 1000 psi/35s with the 20 µm Si stamp

Amorphous PEEK films crystallize at a faster rate than the amorphous PET films. At the embossing temperatures in the range of 240 - 260°C, the films have half time of crystallization in the range of 4-6 s. The polymer filling inside the cavity has to be completed before the advent of crystallization. The crystallization initiation occurs within 2-3 s in the case of the amorphous PEEK film and hence the film loses its fluidity before complete filling of the cavity. The crystallized film due to its high modulus is unable to fill the cavity. The sharp nature of the cold crystallization peak in the DSC thermogram as shown in Figure 72 of the amorphous PEEK film demonstrates the fast crystallizing nature of the film while heated above its T_g. The primary reason for the inability to produce fully replicated films from the amorphous PEEK material is the high viscosity of the films at the embossing conditions compared to the case of amorphous PET in which

the film behaves almost liquid like. The high crystallinity of the starting film and the rapid crystallization rate of the film resulted in difficulty in achieving complete replication of the features.

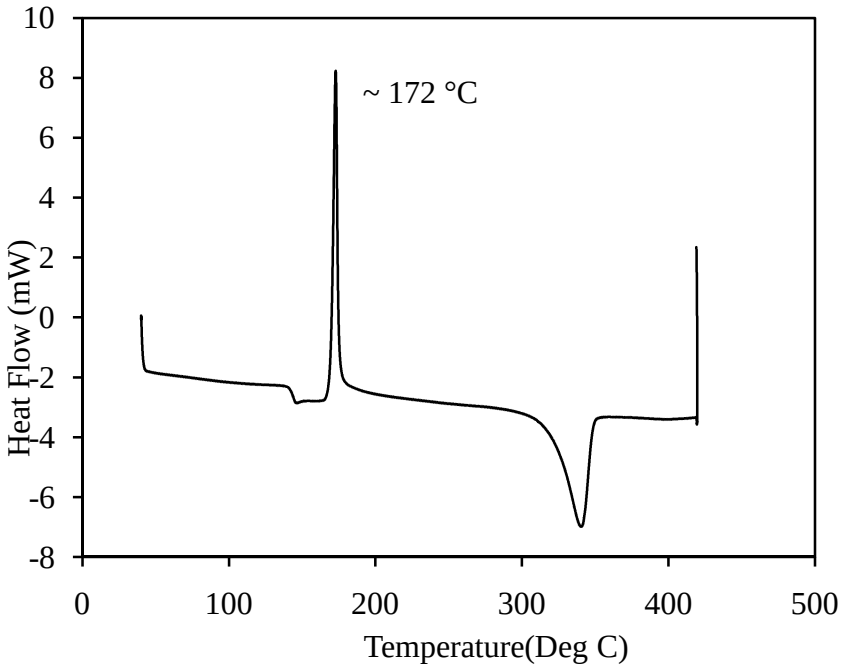

Figure 72 DSC temperature sweep of amorphous PEEK showing sharp cold-crystallization peak

4.5 Conclusions

The CTE process was demonstrated by embossing amorphous PET and PEEK films with a silicon stamp with parallel rectangular trenches. The study of different process parameters showed that the embossing temperature is the most significant factor which affects the replication accuracy and also the versatility of the process. A slightly modified embossing setup was utilized in order to maintain constant pressure during the process by employing a vinyl rubber sheet as shrinkage compensator. In the case of PEEK embossing, the embossing setup was modified to include a collapsible support which prevents any premature crystallization in the film before the holding stage.

The embossing conducted at 160 - 180° C for PET exhibited good replication accuracy in terms of the features embossed. The total time required for embossing at these temperatures was also less due to its high rate of crystallization. The PET films embossed at low temperatures in the range of 100-120°C did not show complete fill of cavities even for low aspect ratio materials at the embossing pressures of less than 100 psi used in the process . This is attributed to the stiffness of the material at these temperature ranges. Allowing the material sufficient time to crystallize improved the replication as the recovery was limited, but in any case the complete replication was not achieved.

The fluidity of the amorphous PEEK films at the processing temperatures were less compared to the complete liquid nature of the amorphous PET. This was attributed to the high crystallinity of the starting films and hence the high viscosity at the processing temperatures. These factors accounted to the less than 5% filling of the cavities at temperatures in the range of 240 - 260°C. The direct comparison of the embossing results of PET and PEEK films could not be made due to the difference in the property of the initial films. While the PET films were nearly amorphous, the PEEK films contained substantial crystalline content in the range of 10-12%. Moreover, the PET films can reach maximum crystallinity in the range of 50-55% whereas the PEEK films generally reach about 30% crystallinity. This narrow gap between the starting crystallinity and the maximum crystallinity it can achieve also compounded the difficulty in embossing PEEK using CTE by increasing the embossing pressure required. The observations lead to the fact that the CTE process can be utilized for polymers which can be obtained in nearly amorphous form. Secondly, as PEEK exhibits very high rate of crystallization,

crystallization initiates in the material once the stamp comes in contact with the film even before the required embossing pressure is achieved. Though the presence of collapsible support eliminated the premature crystallization, the replication was poor. Increasing the pressure to very high values improved the replication to about 60-70% of the total feature height when embossed at 260°C. The high crystallization rate can be countered by using suitable tool modifications. The significant criteria affecting the CTE process is the initial crystallinity of the films and hence its flow behavior during the process. In this study two materials with different starting crystallinity were embossed to determine its effect on the final replication capability.

CHAPTER 5

SEMI-EMPIRICAL MODEL FOR PREDICTING RHEOLOGICAL PROPERTIES DURING CONSTANT TEMPERATURE EMBOSSING

5.1 Abstract

This chapter reports a method to correlate the crystallization phenomena occurring during the CTE process and the resultant change in rheological properties. The principle adopted is to predict the rheological properties of the material from the basic crystallization kinetics parameters such as rate constant and crystallization index. A non-isothermal Nakamura equation is utilized to describe the crystallization kinetics. The polymer crystallization behavior is considered to be analogous to the rheological behavior of a polymer with suspended particles. The increase in viscosity with increase in particle concentration is directly modeled as the increase in viscosity with increase in crystallinity.

5.2 Literature Review

5.2.1 Modeling of Hot Embossing Process

The hot embossing process has been studied extensively to understand the polymer flow behavior and develop numerical models. Conventionally hot embossing process simulation was to predict the flow behavior of different polymers. A quasi-steady process[22] was modeled using the deformation of thermorheologically simple material. Friction and contact conditions are considered in the simulation during the demolding stage. Simulation and numerical analysis of the demolding stage of the embossing process has increased as most of the product failures occur during that stage.

As most of the hot embossing processes are carried out in the entropic-elastic region of the polymer films, viscoplastic[20, 128] and hyper-elastic models have been used to simulate filling behavior. The study[128] used a hyperelastic-viscoplastic model as shown in Figure 73 which consists of springs and dampers arranged in two branches in parallel. The left side intermolecular resistance represents the hyperelastic element (non linear elastic element) and the right side molecular network resistance represents the viscoplastic element (non linear flow element)

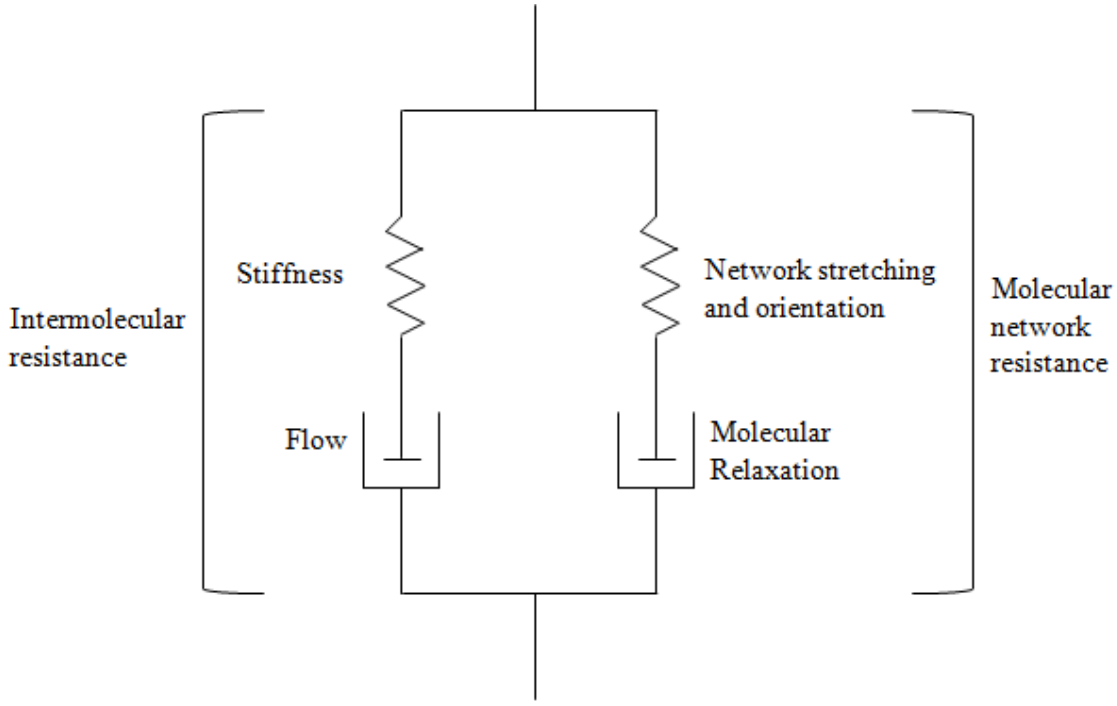

Figure 73[128] Schematic of the hyperelastic-viscoplastic constitutive model redrawn from Ref 128

The nonlinear model predicts the behavior of material subject to very high strains with intermolecular interaction between the polymer segments and molecular network resistance represented in the two branches. The study explored the effect of the post process relaxation on the replication quality and also the nonlinear behavior of materials like PET at high strains.

The rubbery-elastic behavior of PP above the T_g has been studied[129] by using phenomenological models with appropriate modifications. The model proposed by Ogden was used to predict the large deformation behavior. The basic constitutive relations are given as:

$$\sigma_{ij} = \int_0^t g_{ijkl}(t-\tau)\frac{\partial \varepsilon_{kl}}{\partial \tau} d\tau \tag{20}$$

$$S_{ij} = \int_0^t G_{ijkl}(t-\tau)\frac{\partial E_{kl}}{\partial \tau} d\tau \tag{21}$$

$$\sigma(t) = \varepsilon\left(\sum_{j=1}^{3}\frac{G_j}{\beta_j}\left(1-e^{-\beta_j t}\right)\right) \tag{22}$$

$$\beta_j = \frac{\upsilon_j}{(1-2\upsilon_j)} \tag{23}$$

where S_{ij} is second Piola-Kirchhoff stress tensor, E_{ij} is Green Lagrange deformation tensor, $g_{ijkl}(t\text{-}\tau)$ and $G_{ijkl}(t\text{-}\tau)$ are relaxation functions, and $\sigma(t)$ is Cauchy stress.

A linear viscoelastic model[130] has been used to predict the filling behavior of PMMA, PC and cyclic olefin co-polymer Zeonor. The model is able to predict the behavior well with a much reduced computation times as compared to that required for nonlinear viscoelastic models. The study uses a simple Kelvin-Voigt linear viscoelastic model that explains the rubbery behavior of the polymers above T_g. The model tracks the surface response with deformation limited by the elastic modulus E and viscosity η. The model representation is given in Figure 74. The response of the surface position is given as[130]

$$g_{Voigt}(x,y,t) = \frac{-\left(1-\upsilon^2\right)\exp\left(\frac{-Et}{\eta}\right)}{\pi\eta\sqrt{x^2+y^2}} \quad (24)$$

where v is the Poisson's ratio and negative sign indicates the direction of the displacement is downward. The study was limited to low aspect ratio features which reduces the chances of experiencing large deformations which are predominantly nonlinear.

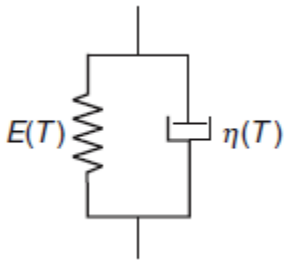

Figure 74[130] Kelvin-Voigt model

Besides these semi-solid constitutive models, simple viscous models have also been used for analyzing and simulating the hot embossing process. The resulting creep flow model is considered satisfactory in some cases especially when a long embossing stage is involved.

Most of current work[131] deals with simulating the cooling and demolding stage of the embossing process as multiple factors such as friction, relaxation has to be taken into account.

5.2.2 Modeling of Polymer Crystallization Kinetics

Polymer crystallization kinetics both with and without shear has been studied by various authors. The morphology of polypropylene during crystallization has been

discussed with respect to the layer growth[77]. Crystallization in PET was studied isothermally and non-isothermally under shear to understand the relaxation phenomena. The effect of isothermal crystallization time was related to the shear history and a double crystallization process was observed[132]. Kinetic analysis was conducted using modified Avrami equations to predict the kinetic rate constants. Kinetics of crystallization in the case of previously oriented PET has shown that the crystallization is rapid to be followed by conventional techniques and also the temperature dependence of crystallinity decreases with the increase in degree of orientation[133].

A variant of the Avrami equation, Nakamura equation, was used to predict the non-isothermal kinetics[71]. The isothermal data and the non-isothermal kinetic data were compared[71] to validate the method for obtaining reliable kinetic model parameters.

The Nakamura equation used is given by Equation 25:

$$\theta = 1 - \exp\left[-\left(\int_0^t K(T)dt \right)^n \right] \tag{25}$$

$$K(T) = [k(T)]^{1/n} = (\ln 2)^{1/n} \left(\frac{1}{t_{1/2}} \right) \tag{26}$$

where θ is relative crystallinity; $K(T)$ is non-isothermal crystallization constant; $k(T)$ is Avrami isothermal rate constant; and n is Avrami index (Isothermal crystallization). The differential form of the Nakamura equation is given by:

$$\frac{d\theta}{dt} = nK(T)(1-\theta)[-\ln(1-\theta)]^{(n-1)/n} \tag{27}$$

The Nakamura equation was used to predict the relative crystallinity development in the material at different cooling/heating rates. A master curve was fitted to the non-isothermal crystallization data for various heating rates which was compared with the

model parameters obtained from the Nakamura equation for quiescent crystallization[70, 72]. The shift factor was determined for the constant degree of crystallinity as:

$$\frac{(d\theta/dt)_{ij}}{(d\theta/dt)_{rj}} = \frac{K(T_{ij})f(\theta_j)}{K(T_{rj})f(\theta_j)} = \frac{K(T_{ij})}{K(T_{rj})} = a_T(T_{ij}) \tag{28}$$

where $a_T(T_{ij})$ is shift factor at temperature T_{ij}; T_{rj} is reference temperature; i=1,2,3,4,..r is i-th cooling rate; and j=1,2,3,4,..r is j-th degree of crystallinity. The reduced time for non-isothermal crystallization kinetics for any reference temperature T_r is given by:

$$\xi = \int_0^t a_T(T(t'))dt'. \tag{29}$$

The non-isothermal melt and cold crystallization kinetics was studied for PET[81] and variants of the high-performance polymer poly (aryl ether ether ketone)[79, 80]. The Ozawa theory for non-isothermal crystallization was used to derive appropriate equations. The Ozawa theory is given as:

$$1 - X_t = \exp\left[-\frac{K(T)}{\phi^m}\right] \tag{30}$$

where X_t is degree of crystallinity; $K(T)$ is a heating/cooling constant; m is the Ozawa exponent. The Mo equation derived by the authors[79] is given as:

$$\log Z_t + n\log t = \log K(T) - m\log\phi \tag{31}$$

$$\log\phi = \log F(T) - a\log t \tag{32}$$

where Z_t is a composite rate constant; $F(T)$ is heating/cooling rate; and a is equal to n (Avrami) / m (Ozawa const.)

5.2.3 Rheology based Molecular and Macroscopic Models

Models from crystallization of polymers under different deformation behavior has been studied extensively by using molecular to macroscopic theories[134]. The study considered the upper convected Maxwell model and the POM-POM molecular model. The general framework was developed for both quiescent and flow-induced crystallization and has the ability to predict behavior for both shear and elongation. The effect of shear on crystallization was studied by correlating the morphology development and crystallization along with the measured rheological properties during transition[94, 96, 98, 135, 136]. The studied developed simple correlation between the crystallinity development from thermal studies such as DSC and changes in the rheological properties as a function of time, temperature and deformation rate.

The crystallization of different polymers during melt spinning[137, 138] or injection molding[139] has been studied extensively. A non-linear viscoelastic model was developed to predict the behavior of polymer crystallization during injection molding. An extended POM-POM model was used for representing the amorphous phase and the crystalline phase was modeled as a rigid rod.

Models were developed using the single mode Geisekus model for the initial melt/amorphous phase and then the crystalline entities are introduced as statistical segments transforming during crystallization[140]. Molecular based models were developed using the free energy principle to predict the molecular relaxation phenomena occurring during crystallization. Studies utilized Leonov, Geisekus, POM-POM models to understand the phase change dynamics and its manifestation in the thermomechanical properties of the polymers[93, 97, 141, 142]. These models are able to quantitatively determine

the effect of ordering of the molecular chains occurring at various stages of crystallization.

5.2.4 Models based on Suspension Rheology

For cases involving slow shear rates, a suspension based model has been proposed to represent polymer crystallization behavior. The suspension theory predicts the change in the viscosity and other material properties as a function of filler concentration. The work has its roots from the work done on the Einstein's formula for dilute suspensions[143-146]. An elementary viscous model is proposed for the polymer before crystallization and suspension theory is used to model the addition of crystalline fractions[147-150]. The equation has been modified to represent the suspension behavior more accurately and for concentrated suspensions. The equations used in the study to model the crystallization are given. From crystallization kinetics and the work of Avrami and Kolmogrov[67-69], the relative crystallinity as a function of time at a particular temperature can be represented by:

$$\alpha(t) = 1 - \exp\left[-\left(\frac{t}{\lambda_c}\right)^n\right] \tag{33}$$

where λ_c is a time constant and λ_c^{-n} is equal to k. Nucleus generation as a function of shear rate is given by:

$$\dot{N} = \left(\frac{\dot{\gamma}}{\dot{\gamma}_n}\right)^2 g_n - \frac{N}{\tau_n} \tag{34}$$

where N is the number of nuclei per unit volume, $\dot{\gamma}_n$ the characteristic shear rate, and g_n and τ_n are functions of temperature. The stress relation is taken as additive – sum of contributions from the amorphous phase and crystalline phase. The equations used for the

change in viscosity as a function of concentration of the suspended particles for concentrated suspensions are

Frankel and Acrivos Model[151]:

$$\frac{\eta}{\eta_a} = \frac{9(\phi/\phi_m)^{1/3}}{8\left(1-(\phi/\phi_m)^{1/3}\right)} \tag{35}$$

and Krieger and Dougherty Model:

$$\frac{\eta}{\eta_a} = \left(1-\frac{\phi}{\phi_m}\right)^{-2.5\phi_m} \tag{36}$$

where η_a is Newtonion fluid viscosity; ϕ is volume concentration of spheres; and ϕ_m is the maximum volume concentration of spheres.

A more general equation taking into account the different shape of particles is proposed as[152]:

$$\frac{\eta}{\eta_a} = \left[1-\frac{\phi}{A}\right]^{-2} \tag{37}$$

where *A* is an empirical parameter dependent on the particle shape. An empirical formula for *A* is $A = 0.55 - 0.013(L/D)$. A data fit using Equation 41 and 43 to the shear viscosity data from isothermal crystallization of PP resulted in the following equation:

$$\alpha = 1-\exp\left[-f(|\dot{\gamma}|)\left(\frac{t}{14200}\right)\right]^{3.1}. \tag{38}$$

Furthermore, considering a crystal growth function, the relation between the crystallinity and rheological parameters is obtained[147]:

$$\frac{\tau}{\eta_0\dot{\gamma}} = \left[\frac{2aC}{A}(q+0.5)(t_c-t)\right]^{-1/(q+0.5)} \tag{39}$$

with $C = n(1-A)[-\ln(1-A)]^{n-1/n}$ where t_c is the asymptotic time at $\boldsymbol{\tau} \to \infty$.

The storage or loss moduli of the polymers were related to the relative crystallinity as a function of time to fit data obtained from the rheological testing and DSC. The relation which is obtained from data fitting is given by:

$$f(\alpha) \sim 1 + 0.54\alpha + 4.0\alpha^2 \quad (\alpha \le 0.4) \tag{40}$$

where $f(\alpha)$ corresponds to the polymer property during phase transfer reaction.

At high concentrations, an model relating the rheological properties of the suspension to the concentration is given by Shinsaku and Motowo[153]:

$$\frac{G^*}{G_c^*} = 1 - \frac{15(1-\upsilon_c)(1-\phi)}{7-5\upsilon_c} \tag{41}$$

$$\frac{\upsilon}{\upsilon_c} = 1 + \frac{3(1-5\upsilon_c)\left(1-\upsilon_c^2\right)(1-\phi)}{2\upsilon_c(7-5\upsilon_c)} \tag{42}$$

where G^* is shear modulus of matrix; ν is Poisson ratio of matrix; ν_c is Poisson ratio of crystalline phase; and G_c^* is shear modulus of crystalline phase.

At low concentrations, the properties of the amorphous phase are dominant and hence the following relations hold:

$$\frac{G^*}{G_a^*} = 1 + \frac{15(1-\upsilon_a)\phi}{8-10\upsilon_a} \tag{43}$$

$$\frac{\upsilon}{\upsilon_c} = 1 + \frac{3(1-5\upsilon_a)(1-2\upsilon_a)(1-\upsilon_a)\phi}{\upsilon_a(8-10\upsilon_a)} \tag{44}$$

where G^* is shear modulus of matrix; ν is Poisson ratio of matrix; ν_a is Poisson ratio of amorphous phase; and G_a^* is shear modulus of amorphous phase.

A power-law type semi-empirical equation has been derived from the Frankel-Acrivos equation to represent the suspension behavior at high concentration by using energy principles[154]. The equation which exhibits a power-law dependence of viscosity is given by:

$$\frac{m^*}{m} = \frac{9}{8}\left(\frac{(\phi/\phi_m)^{1/3}}{1-(\phi/\phi_m)^{1/3}}\right)^n \tag{45}$$

where m and m^* are the coefficients of the solution and suspension, respectively, and ϕ_m is the maximum concentration. More work[155-157] focused on finding the change in viscosity based on an empirical relation derived from the theoretical equation of Maron and Pierce[146], yielding the following relative viscosity:

$$\eta_r = (1-\phi/\phi_0)^{-2} \tag{46}$$

where ϕ_0 is shape-dependent maximum packing concentration. The equation predicts the behavior at concentrations lower than the maximum packing beyond which the viscosity starts to decrease.

Power series expressions were fitted to different data and useful expressions for the high concentration regime for suspensions were proposed[158, 159]. The equation extended from the basic Einstein equation is given as:

$$\eta_r = 1 + 2.5\phi + 10.05\phi^2 + A\exp(B\phi) \tag{47}$$

where A, B are coefficients determined from experiments. The equation fitted the data well as any higher order power series. Different versions[160, 161] of the above given power series relationship or equations extended from dilute solutions theory have been proposed.

Crystallization and dynamic mechanical studies were conducted for two different starting materials: one representing a colloidal system with some amount of nucleation and the other representing a suspension system where crystal formation starts during the measurement[90, 162, 163]. The approach was adopted to understand the relation between morphology and crystallization and create a link to percolation theory. The transformed fraction was related to the measured storage moduli as:

$$\alpha(t) = \frac{G_t - G_0}{G_\infty - G_0} \tag{48}$$

where G_0 , G_t , G_∞ are storage moduli at time 0, t and infinity. A percolation threshold[164, 165] was defined at which macroscopic interconnected clusters are formed. Beyond this concentration, the clusters determine the properties of the suspension.

5.3 Semi-empirical Process Model for Constant Temperature Embossing

The purpose of using a process model in the current study is to establish a generalized relation between the crystallinity developed during the constant temperature embossing process and hence the evolution of mechanical properties of the polymer. The current model used to determine the rheological behavior of the polymer during the embossing process utilizes experimental data along with the theoretical work on suspension based systems. While the experimental data is collected by using conventional and customized techniques, the theories behind suspension based systems are used to correlate the data, examine the validity of the data and derive conclusions. The semi-empirical model hence utilizes the underlying theory of suspension based systems to

explain the rheological behavior of the crystallizing polymer with support from experimental data collected at conditions mimicking the actual embossing process.

The crystallinity developed in the polymer can be described by using the isothermal or non-isothermal kinetics. In the current study, the non-isothermal Nakamura model will be used to predict the crystallinity increase during the process. The increase in crystallinity manifests itself into a resulting increase in viscosity or moduli of the polymer. The rheological properties of the polymer are significant to determine the response of the polymer to various stress fields. The properties are transient and it is pertinent to track the change in properties in real time. The objective for implementing a process model for the current study is to:

- Develop a simple physical model to represent the polymer during the phase transfer step of CTE process.
- Construct a mathematical representation based on the physical model to understand the underlying physical phenomena of the CTE process.

5.3.1 Simple Physical Model for Polymer Structure Representation

The polymer undergoes isothermal phase transition during constant temperature embossing resulting in a semi-crystalline form. The change in material properties is very significant to optimize the process parameters to get good quality parts. The data can then be used to simulate the process and understand better about its versatility. The model can be used to predict data at processing conditions where measuring data accurately is a big challenge. In the current study, the material characterization methods and results adopted were explained in Chapter 3. Attempts were made to characterize the rheological properties of the material during the process. More precisely, the change in properties

during crystallization was characterized. As mentioned in Chapter 3, to overcome the limitations in conventional rheological instruments, an oil-based tensile testing setup was designed and used to characterize the tensile properties of the material. But the tensile testing setup gave unstable results at slightly higher testing speeds and producing transient results was also difficult. The difficulties experienced in rapidly measuring the transition properties during crystallization lead to the implementation of constructing a model for the process. In the model, easily measurable crystallization kinetic parameters are measured using standard instruments and then converted suitably to represent mechanical properties. As mentioned in the literature review of the current chapter, crystallization in polymers can be represented as suspension systems wherein the formation of crystallites can be represented as increase in suspended particles in polymer melt. The physical model for the representation of the crystallization stage is shown in Figure 75.

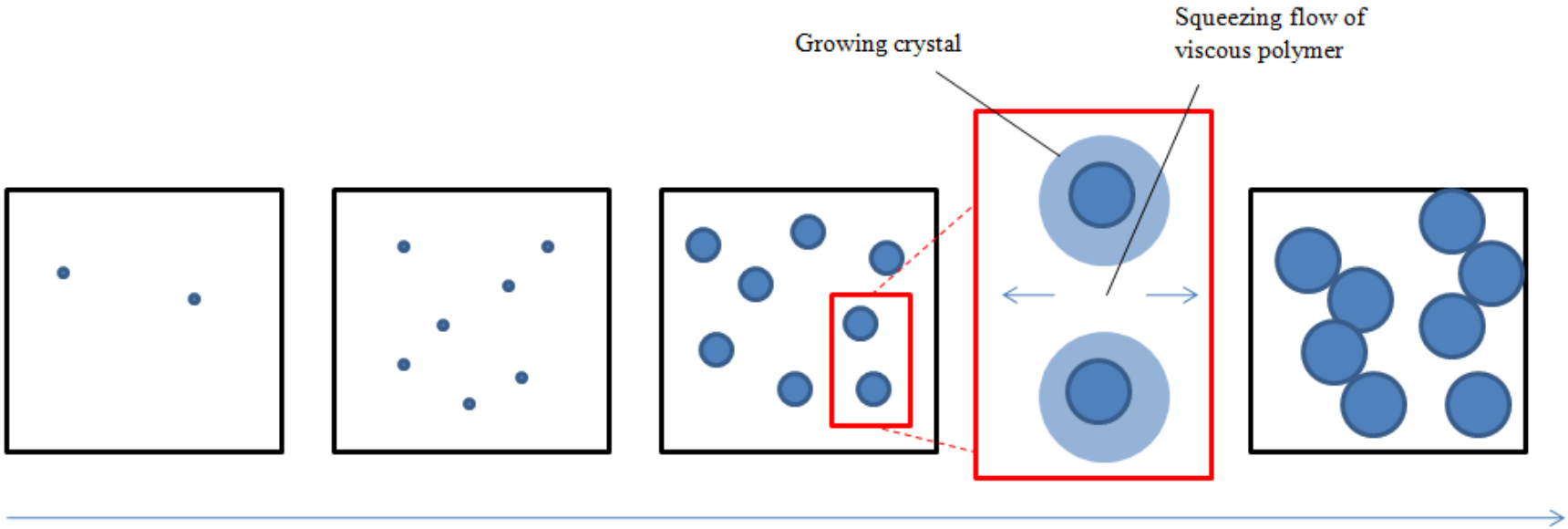

Figure 75 Evolution of crystallites during CTE

As shown in Figure 75, the polymer is assumed to be devoid of crystallites initially. Once the induction time based on the temperature of crystallization is reached crystals start to be populated. The induction time is very crucial as it represents the time available for the embossing stage. Ideally, the embossing stage would have to be completed before the start of induction time. This is partly due to the reason that once crystallization sets in, it is very rapid at the desired processing temperatures so that the modulus of the polymer increases rapidly. This leads to the under-filling of the cavities or very high amount of pressure required to push the polymer into the cavities. This pressure requirement is magnified by the aspect ratio requirement in the process. Secondly, the any solidification of the polymer before the embossing stage is completed can lead to increase in the viscoelastic recovery of the embossed film after the pressure is released. In the current study, since the demolding stage is carried out at high temperature, the viscoelastic recovery would be particularly high if sufficient crystallinity were not yet developed. To simply the problem, only the viscous behavior of the polymer is considered.

During stage 2 as shown in the Figure 75, the crystallites are formed- new nuclei are formed and already existing nuclei grow. This can be correlated to the increase in the concentration of suspended particles in the polymer melt. During this stage since the volume of the crystallites are assumed to be very low, the polymer can be still assumed to be viscous and obey a suitable generalized Newtonian model. This stage only undergoes marginal increase in concentration of the suspended particles wherein the particles do not significantly affect the deformation behavior of the polymer. Such a stage is assumed to be the transfer state from the embossing step to the holding step in an ideal process. This

stage can also act as a buffer state during which the final stage of embossing can be possible. Since the amount of crystals present in the polymer during this stage is very minimal, their effect on the embossing capability should be minimized.

Stage 3 represents the phase where the crystallites have grown substantially such that they start affecting the mechanical properties of the polymer. The polymer in this stage is analogous to the suspension system wherein the concentration of suspended particles has reached a certain level so that the mechanical properties of the system have contribution from both the melt and particle phases. During this stage, additional viscous dissipation happens due to the squeeze flow of the polymer melt between adjacently suspended particles along with the classical shear rate dependency. Similarly, it can be assumed that the amount of crystallites have increased to a certain extent that the response to deformation of the polymer is dependent on both the amorphous and crystalline phases. In the current study, for the sake of simplicity, during this stage the polymer is assumed to show property changes due to the increase in crystallite concentration. The shear-rate dependent behavior is ignored as it complicates the system to also include multiple interconnected effects if both strain rate dependency and crystallization are considered. This assumption is valid because this stage occurs during the holding stage of the embossing process and the deformation experienced by the polymer during the holding stage is very small.

Stage 4 represents the state wherein the crystallite concentration has started to reach the saturation limits. The concentration reaches the maximum possible limit where the crystals are closely packed in the selective regions and the percolation threshold is reached. The polymer melt between the crystals is completely squeezed out in such zones

and the material overall exhibits a solid-like behavior. This stage can be analogous to the presence of very high concentration of the suspended particles in the polymer melt. The suspended particles are located in contact with each other in certain zones where the percolation threshold is reached and slippage and friction between the particles leads to complex behavior of the polymer which can rarely be described sufficiently by the available equations. This stage marks the start of the demolding process or the end of holding stage in the constant temperature embossing process.

5.3.2 Key Assumptions

The key assumptions considered for establishing a process model for the constant temperature embossing process are listed as follows.

- Filling Stage:
  - Filling completed before induction of crystallization, i.e., Total filling time (T_f) < Crystallization induction time (T_i), where $T_i = f(T)$.
  - Flow field consists of viscous dissipation from simple shearing motion.
- Holding Stage:
  - Holding time (T_h) > Crystallization induction time (T_i).
  - The change in viscosity of the medium depends only on the actual percentage of crystallites formed.
  - Shear rate less than the critical shear rate is needed to effect changes in the crystallization phenomena.
  - The rate of crystallization and hence the change in viscosity depends only on the isothermal temperature (T) and time (t).
  - Homogenous crystallization is assumed and effects arising from collisions and

aggregation are ignored.

- Wall effects on the growing crystallite are ignored by considering a cell model with a representative particle at the center of a rigid spherical enclosure.
- The effective viscosity of the crystallizing polymer is primarily from the flow within the narrow gaps between the different growing crystallites.
- The rheological model assumes that the crystallizing polymer is a continuous medium as the macroscopic deformation scales are much larger than the average size or average separation of the particles.
- Bulk stress and bulk velocity gradient is assumed to explain the deformation of the crystallizing polymer well which is also known as the continuum hypothesis.

The model is utilized as a method to determine the mechanical properties of the polymer during the embossing stage under the most ideal conditions. The model considers that the addition of crystallites as the increase in spherical particle concentration in the fluid medium. Studies on the crystal growth nature of PET show that the spherrulites are formed in the polymer under quiescent conditions rather than any other shapes. The model's assumption that spherical particles[59,60] are formed during the embossing process is able to predict the rheological properties of the polymer with reasonable accuracy. Any more accurate prediction of the crystal structures require extensive crystallization morphology studies on the polymer under exactly similar conditions and subsequently accounting for the different crystal structures in the model with a correction factor. Since the objective of the current study is to develop a reliable technique to predict the effect of the change in bulk rheological properties of the material

on the final part quality and replication accuracy, such an extensive investigation on the crystal morphology of the polymer is beyond the scope of the current work.

5.3.3 Salient Features of the Model

5.3.3.1 Non-Isothermal crystallization model

The Nakamura model is used to describe the crystallization kinetics of the polymer. The advantage of the Nakamura model is the more accurate prediction of the non-isothermal crystallization kinetics than Mo's or Ozawa's theory for reasons explained in Chapter 3.

Shift factor can be predicted from data directly or from the model by using the basic relation described earlier. Reduced time (ξ) can be calculated from the shift factor and its dependence on temperature to verify if the model is able to represent the kinetics accurately.

5.3.3.2 Suspension models to correlate change in viscosity to crystallinity

In the current study the viscosity of the polymer is tracked during the crystallization and the relation required for calculating the viscosity when the crystalline content increase is utilized from one of the relations explained in the literature review of the current chapter. The suspension model is chosen based on its suitability for the current system taking all the pertinent assumptions into consideration. The two models considered and their salient features are given as follows.

Frankel and Acrivos (Equation 41, also shown below): This model considers the maximum packing effect resulting in infinite viscosity. It is most efficient to predict the

change in property when particles are considered rigid spheres with hydrodynamic interactions while in motion

$$\frac{\eta}{\eta_a} = \frac{9(\phi/\phi_m)^{1/3}}{8\left(1-(\phi/\phi_m)^{1/3}\right)} \tag{49}$$

where η and η_a are the solution and suspension viscosity respectively, and ϕ_m is the maximum volume concentration of spheres.

Simha model: Simha model is a direct extension of the Einstein theory to accommodate particle- particle interactions in very concentrated suspensions. It assumes that all the contributions from neighboring particles vanish at the boundary of the shell cage. This model predicts the following relation:

$$\frac{\eta}{\eta_0} = 1 + \frac{5}{2}\lambda(\gamma)\phi \tag{50}$$

where η_0 and η are the solution and suspension viscosity respectively, ϕ is the volume concentration of spheres, and $\lambda(\gamma)$ is a complex steeply increasing function of $\gamma = a/b$ where a is the size of the rigid sphere and b is size of spherical shell cage.

5.3.4 Model for the Constant Temperature Embossing Process

The Nakamura model for crystallization kinetics and the Frankel and Acrivos model for the suspension behavior are integrated into one single model to represent the change in viscosity of the polymer with increase in crystallinity. The model is constructed such that knowing the kinetic parameters $K(T)$ and n, the viscosity can be determined without resorting to any experimental characterization techniques. The model can be represented by the following mathematical model as:

$$\frac{\eta}{\eta_0} = \frac{9}{8}\left[\frac{\left(\left(1-\exp\left[-\left(\int_0^t K(T)dt\right)^n\right]\right)\Big/\theta_m\right)^{1/3}}{1-\left(\left(1-\exp\left[-\left(\int_0^t K(T)dt\right)^n\right]\right)\Big/\theta_m\right)^{1/3}}\right] \tag{51}$$

$$\frac{\eta}{\eta_0} = \frac{9}{8}\left[\frac{\left(\left(1-\exp\left[-\left(\int_0^t K(T_r)a_T dt\right)^n\right]\right)\Big/\theta_m\right)^{1/3}}{1-\left(\left(1-\exp\left[-\left(\int_0^t K(T_r)a_T dt\right)^n\right]\right)\Big/\theta_m\right)^{1/3}}\right] \tag{52}$$

where η_0 is the initial viscosity of the polymer melt before the crystallization starts, $K(T_r)$ is the rate constant for the reference temperature, a_T is the shift factor as a function of temperature to predict $K(T)$ at different temperatures and θ_m is the maximum possible packing of the crystallites in the polymer which is taken as 0.64.

The model as given by Equation 52 integrates both the kinetics and suspension models to give a unified approach to predict the viscosity at any time during the process. The experimental determination of crystallization kinetics is sufficient to predict the changes in viscosity for the polymer. The parameters $K(T)$, $K(T_r)$ and n are obtained from the non-isothermal crystallization kinetics and included in the Nakamura model. The Nakamura model is then included into the Frankel and Acrivos model for suspension as shown in Equation 52. The Equation shows the expression wherein $K(T)$ is expressed in terms of the shift factor and reference rate constant $K(T_r)$. Hence, to use the model to determine the viscosity as a function of time, the shift factor for the temperature of interest, $K(T_r)$, and the Avrami index n are the only required parameters.

5.3.5 Experimental Procedure

The above viscosity model was compared with the experimental data collected from the rheometer and DSC. The relative crystallinity data was collected from samples subjected to similar thermal history separately in the rheometer and DSC. The data was collected with semi-crystalline PET as the model system. The steps involved in the collection of data are:

- Sample preparation
  - The semi-crystalline PET pellets were dried under vacuum overnight at 120°C.
  - Sheets were compression molded from the pellets and quenched into ice water to minimize the crystalline content of the polymer.
- Rheometer experiments
  - Circular disks were cut from the sheets prepared by compression molding and tested in the rotational rheometer. The sample was subjected to different thermal history and then quenched in ice water immediately to preserve the structure.
  - The different testing conditions are:
    1. Samples were heated at 300°C for 5 min till the polymer completely melts and then cooled down to the crystallization temperatures such as 200, 210, 220 and 230°C under a cooling rate of 5°C/min the maximum possible in the rheometer. These temperatures were used as the crystallization rate is relatively slower compared to the processing temperatures and allows more accurate data to be collected from the rheometer and DSC experiments. The samples were then held at the respective isothermal crystallization temperatures for a long time under very minute shear field to record the oscillation time data. The samples were

collected after different time intervals and quenched in ice water. New samples were used for each time interval and for each temperature. The samples were then tested in DSC for their relative crystallinity at the end of the thermal history.

2. Samples were initially compression molded at 300°C and quenched immediately in ice water. The samples were then directly exposed to the different isothermal crystallization temperatures and the oscillation time tests were conducted for different time intervals. This condition was followed parallel to the earlier condition as in the case of condition 1 as samples tend to crystallize to a certain extent when bringing down the temperature from their melt state to the desired crystallization temperature in the rheometer itself. Hence the samples were quench-cooled during the compression molding itself to avoid the first step of melting in the rheometer and consequent crystallization during cooling. In both conditions the normal force was set to a constant value to adjust for the shrinkage occurring during the crystallization step. The samples collected after the oscillation time step was quenched and tested for relative crystallinity in the DSC.
3. To determine the shear conditions at which the samples are subjected to near-quiescent state as in the DSC, the samples were subjected to different rotational and oscillatory strains and then tested for their relative crystallinity.

- DSC experiments
  - Samples were directly prepared from the compression molded samples and subjected to the same thermal history as in the rheometer.
  - The different testing conditions are:
    1. The samples were melted at 300°C for 5 min and then brought down to the

desired isothermal temperature at 5°C/min and allowed to crystallize for the same time intervals as in the rheometer and then quenched in ice-water from the DSC cell. The different isothermal temperatures were 200, 210, 220 and 230°C. The quenched samples were subjected to temperature ramp to obtain the relative crystallinity values.

2. The samples were melted at 300°C and then quenched to the desired isothermal temperatures at the maximum available cooling rate and then allowed to crystallize. This condition was used to mimic condition 2 in the rheometry experiments. The samples after the time interval were quenched in ice-water to preserve the structure. The samples were then subjected to temperature ramp to obtain the values of relative crystallinity.

5.3.6 Comparison of Model and Experimental Data

The experimental data obtained in the above section were compared with the predicted values from the model. Figure 76 to Figure 78 shows the comparison between the relative crystallinity values collected at 200°C and 220°C and their overlays with that predicted by the model. The relative crystallinity values plotted in the curves are obtained by normalizing the absolute values of the relative crystallinity by the maximum possible relative crystallinity for both rheometer and DSC samples. The experimental data appears to follow the trend shown by the model though the absolute values are higher.

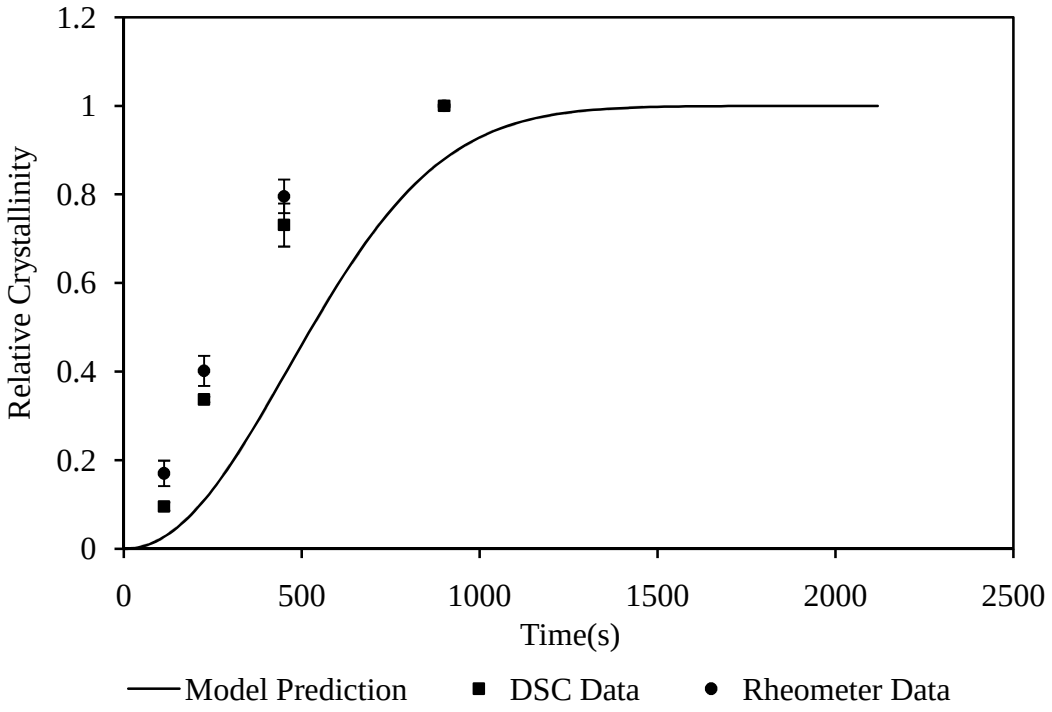

Figure 76 Relative Crystallinity Data at 200°C

The DSC data more closely fits the model data as it is collected in completely quiescent conditions. The relative crystallinity of the samples collected from the rheometer shows higher value than that of the model and DSC data as there are external factors such as exposure to moisture and presence of dirt particles on the parallel plates might aid the crystallization. Both the relative crystallinity obtained from the DSC and the rheometer still follow the trend predicted by the model albeit with some difference in absolute values.

The overlay of the 200°C and 200°C data shows the difference in crystallization rates in these two temperatures as shown in Figure 78. There is some overlap in the data in the initial zone for the two temperatures which can be attributed to the limitations in data measurement, particularly in the rheometer experiments.

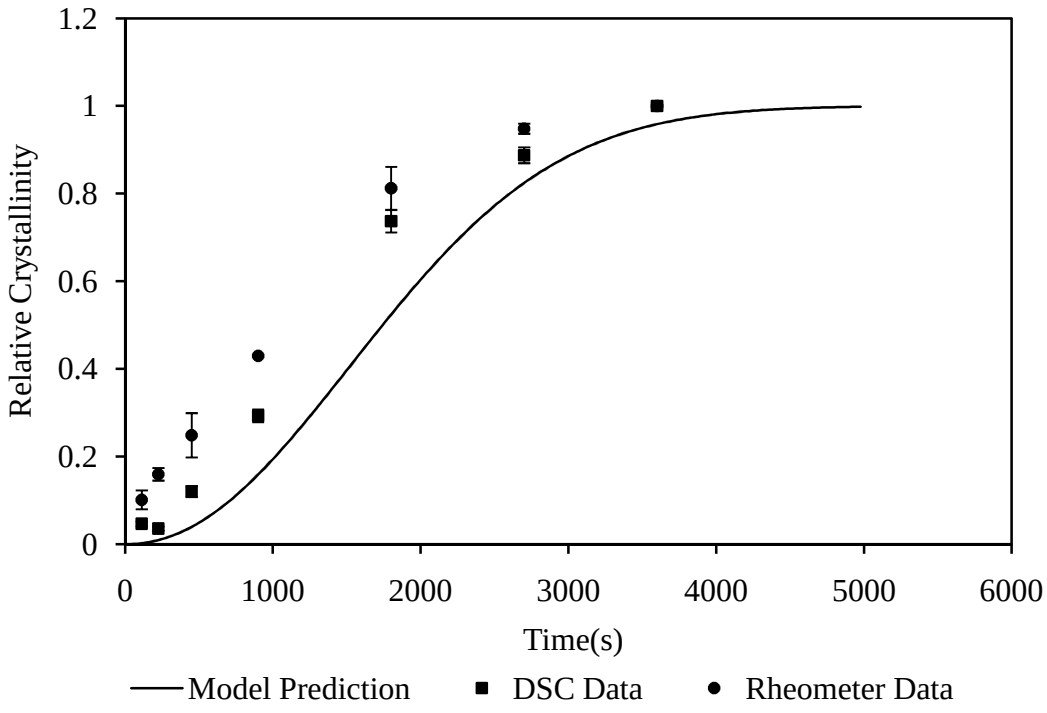

Figure 77 Relative Crystallinity Data at 220°C

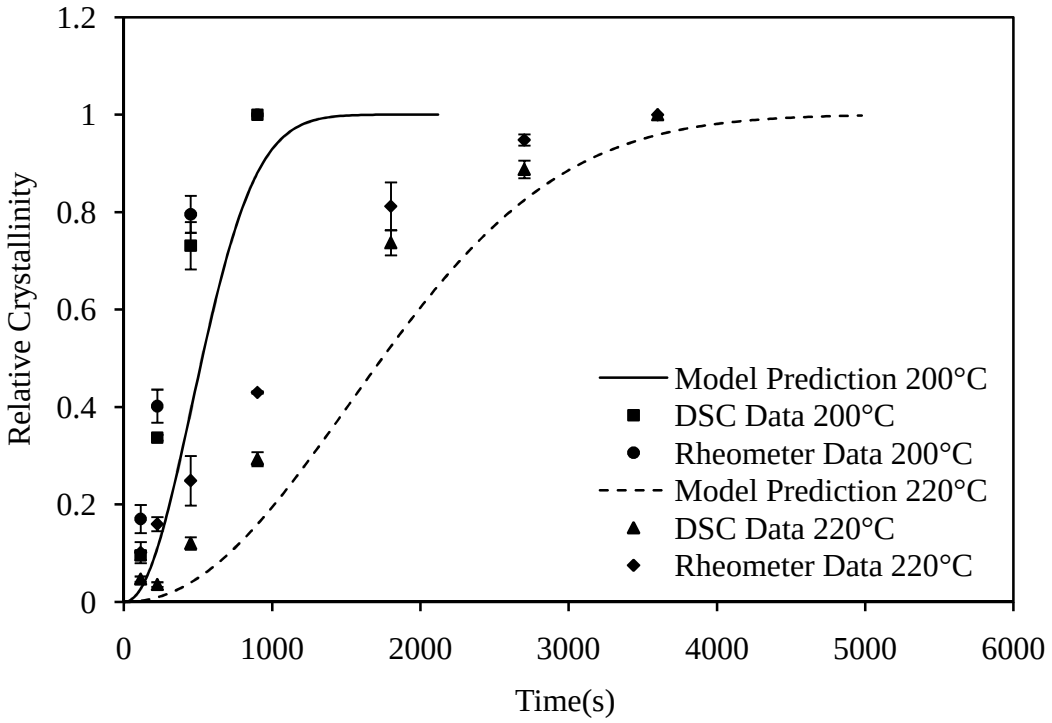

Figure 78 Relative Crystallinity Data at 200°C and 220°C

Figure 79 to Figure 81 show the comparison between the relative viscosity values predicted from the model and those obtained from the rheometer experiments for the same time intervals as in the earlier experiments. The relative viscosity values are obtained by normalizing the absolute viscosity obtained during experiments with the initial melt viscosity. The relative viscosity is thus a ratio of the time-dependent viscosity and a constant initial viscosity when crystals are not present in the melt.

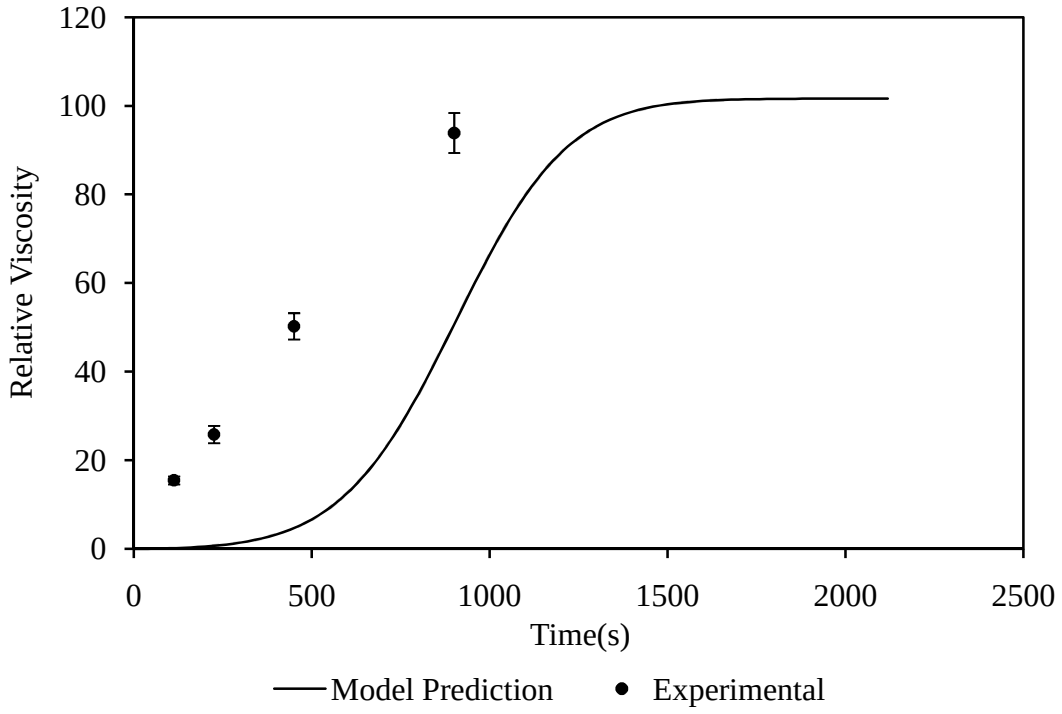

Figure 79 Relative Viscosity Data at 200°C

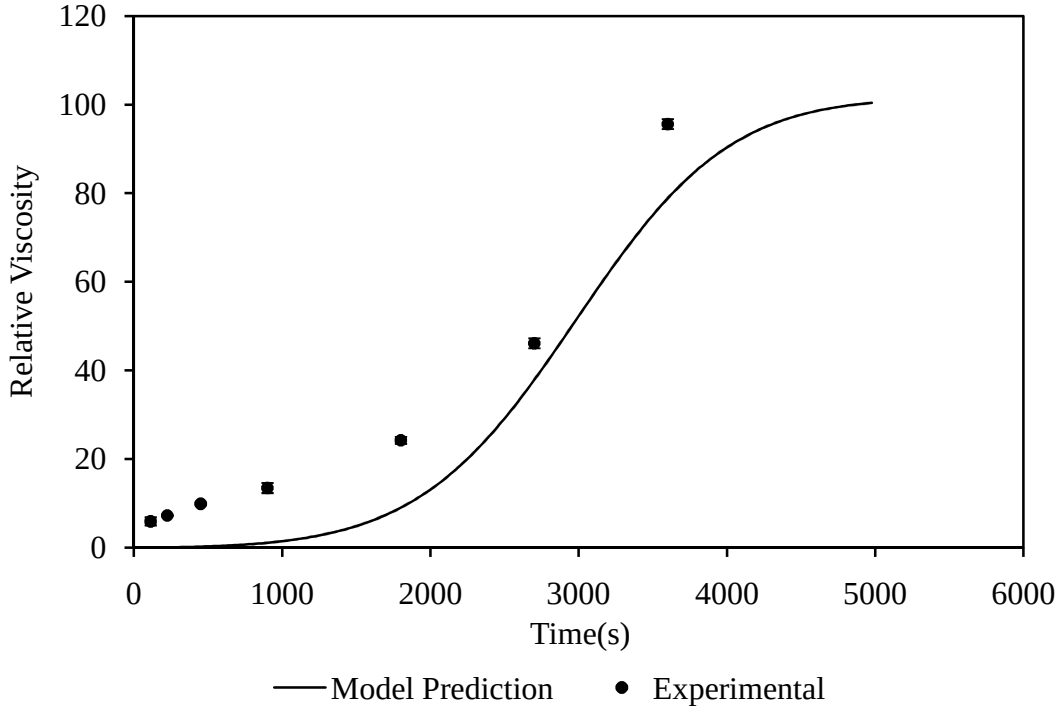

Figure 80 Relative Viscosity Data at 220°C

The temperatures shown here are 200°C and 220°C and the plots show that the experimental data follows the trend exhibited by the predicted data. There is some difference between the experimental and model data for the 200°C, particularly for the shorted time intervals. As the model takes into account the most ideal state where secondary crystallization and other synergistic effects are completely ignored, the data follows the ideal S-shaped curve. But in the real case, the samples collected at different time interval are subject to various secondary effects and hence the difference in the absolute values. The data collected at higher temperature of 220°C correlates well with the predicted data as the rate of crystallization temperature is low and any secondary effect are realized after a long time interval.

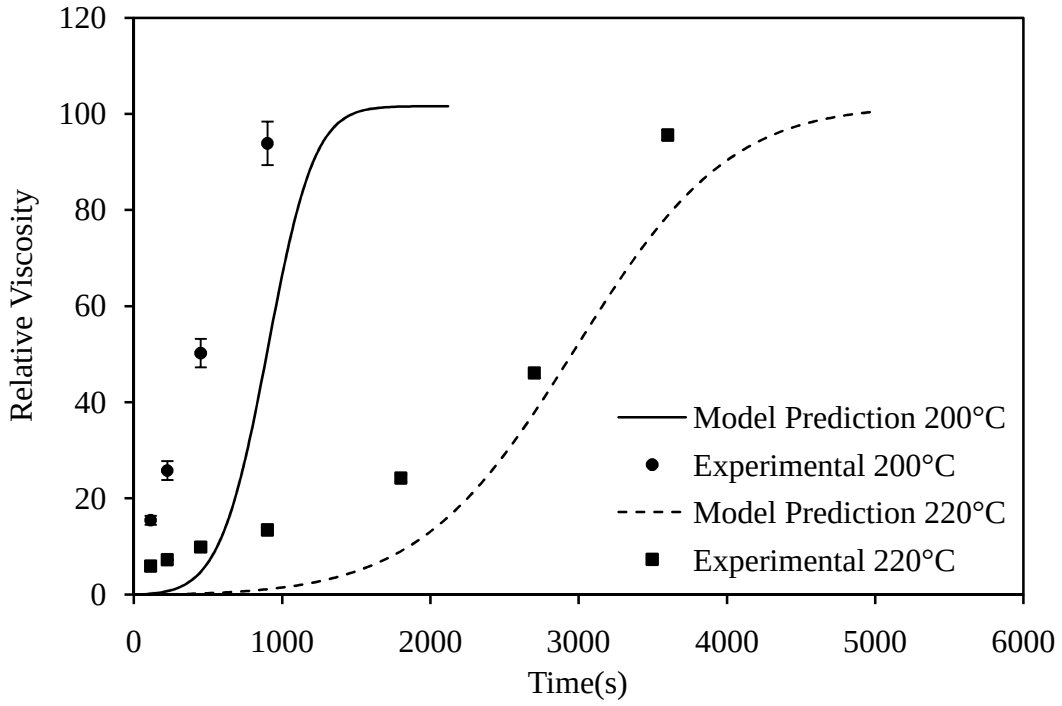

Figure 81 Relative Viscosity Data at 200°C and 220°C

Since the model predictions represent the crystallization behavior in the temperatures where the data is measurable, the model can be used to predict the data at the exact process temperatures where the crystallization kinetics is hard to measure in conventional techniques. The model can thus be used to predict the change in relative crystallinity and relative viscosity as shown in Figure 82- Figure 83. The plots show that the predicted values at low temperatures represent the behavior of the polymer well. The rates of crystallization at these temperatures are quite high which is well represented in the plots obtained. The model once verified to give credible representation of system behavior can be used to predict the data at any processing temperature.

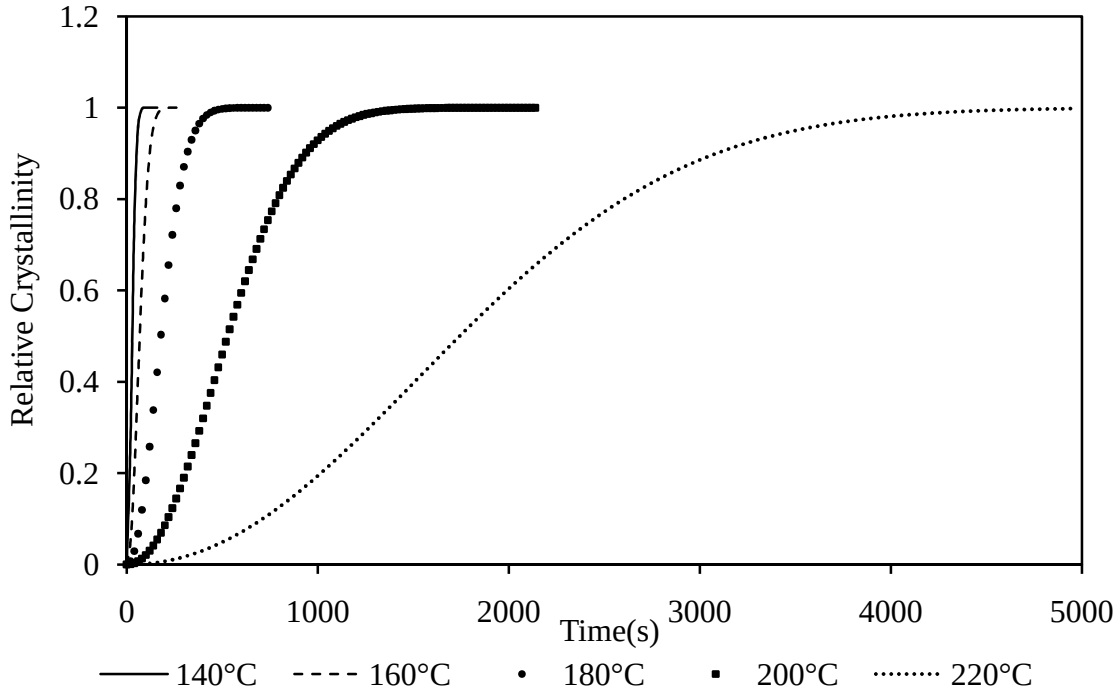

Figure 82 Relative Crystallinity Data Prediction

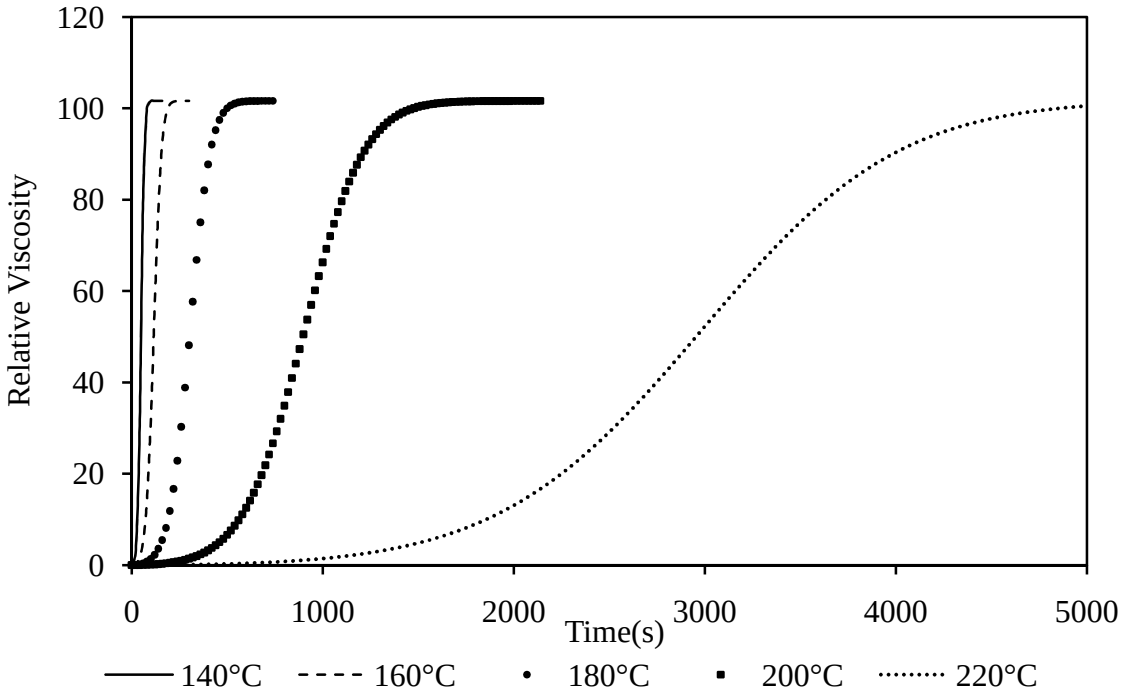

Figure 83 Relative Viscosity Data Prediction

5.3.7 Process window dependence on crystallization, diffusion and crystal size effects

The semi-empirical model though is able to predict the change in rheological properties of the polymer during the embossing process, has limitations in terms of the assumptions used in establishing the semi-empirical model. The model assumes that the crystallites grow in the polymer as spherical particles which are the most ideal case considered in suspension based models. DSC analysis was mainly used to determine the crystallinity of the polymers for the experimental data as it was difficult to use a time resolved x-ray for all the process conditions necessary. As explained in the literature review in Section 2.3.4, for amorphous PET films crystallized under no strain from their glassy state at temperatures between T_g and T_m, spherrulites are formed. This might be the reason behind the model predicting the behavior of the polymer with reasonable

accuracy. The spherrulites are deformed when the samples are subjected to higher stretch ratios more than 3 or 4. This is the region at which the stress induced crystallization is effective in enhancing the crystallization by ordering the chains along the stretch direction. The strain levels experienced in a hot embossing process is very low, and hence it is expected that the stress induced crystallization does not significantly affect the final molecular structure of the polymer. It has been also observed from the literature cited in the Section 2.3.4 that larger crystals are formed if crystallized in an unconstrained mode leading to brittle samples. But the samples collected after embossing did not show a highly brittle nature and were flexible. The non-brittle nature of the crystallized sample may have been due to the thinner cross-sections of the sample as well the rectangular trench configurations running parallel to the sample. The features in the sample may act as ribs structures with a thin back film offering flexibility to the embossed films.

The ductile nature of the embossed film can also be attributed to a certain level of orientation of the samples during embossing resulting in crystallization with smaller crystallites. The embossing process though experiences low strain levels undergoes a faster filling based on the time scale of deformation. This smaller deformation mechanism results in moderate orientation in the chains in the lower temperature ranges near to the Tg. At higher crystallization temperature ranges, the orientation effects might have lesser effect on the final crystal structures[166,52]. It is well known that there is a strong mutual effect between the crystallization and mass transport of the chains as diffusion through the crystals. In isothermal crystallization schemes, the crystallization rate is affected by nucleation and the diffusion rate of the polymer chains.. The ordering of the chains, can have an effect on the diffusion properties as the chains can slide easily

through the crystals and reach various populated nuclei. As explained above, since the embossing process does not involve high strain levels, the mechanism assisting any diffusion enhancement can be safely overlooked. In order to accurately determine the effects of diffusion during crystallization dedicated studies are required to observe the crystal structure variation under different process conditions.

It is well known that at higher temperatures near the melting point the diffusion is assisted by the higher thermal energy available for the chains to easily move around. The effect leads to perfect crystals to be formed in samples crystallized at higher temperature. But the orientation effect which are predominant at relatively lower temperatures at half way between Tg and Tm become less significant when the sample is crystallized at higher temperature[56,57]. There is complex interplay between all these effects as at higher temperatures though the diffusion process is effective, the higher thermal energy in the system decreases the overall crystallization rate producing smaller crystals. At temperatures mid way between Tg and Tm, the diffusion is restricted but the samples have sufficient nucleation rate to crystallize at higher rates. It is also well known that depending on the amount of strains experienced by the sample, the crystal structure contains large to smaller crystals. In the current study, samples were opaque after crystallization indicating that large spherrulites were formed during the crystallization, but small enough to retain the ductility.

5.4 Conclusions

A semi-empirical model was demonstrated by combining the non-isothermal crystallization kinetics model by Nakamura and a suspension viscosity model. The model provided an alternate way of predicting the rheological data of the films used for the CTE process. The increase in crystallite concentration was held analogous to the increase in particle concentration in a suspension. The available equations for predicting the suspension viscosity is combined with the Nakamura model to demonstrate a general model for this study.

Amorphous PET was used as the material for data collection for verification of the model. The rheological experiments were conducted at high temperatures 200 and 220°C where the materials exhibited low rate of crystallization and also had the required material properties suitable for use in the rheometers. The material property probed was the viscosity and its change with increase in crystalline content. The viscosity was calculated from the semi-empirical model and compared with the data.

The data followed the trend exhibited by the model with some noticeable differences in the initial time zone and with reasonable accuracy. The major limitation in the model was the simplification in terms of the size of the crystals formed. In the current study, an ideal case of spherical particles are considered. In the current study, the reasonable fit to the experimental data may be attributed to the observation in various studies that spherrulites are predominantly formed in similar process conditions. The purpose of establishing a simple procedure to correlate the change in crystallinity to viscosity only from the crystallization kinetics parameters was achieved with reasonable accuracy. Based on the predictions for higher temperatures 200°C and 220°C, the change

in viscosity was predicted for the processing temperatures of 140°C, 160°C and 180°C. The model was simplified through assumptions which were valid for the current case considered and can be refined for different scenarios.

CHAPTER 6

CONSTANT TEMPERATURE EMBOSSING PROCESS ANALYSIS

6.1 Abstract

This chapter reports the methods used to analyze the CTE process and develop a suitable process strategy to ensure good quality parts. The process is simulated as a 2D problem using POLYFLOW®. Two cases with different rates of crystallization are compared with a conventional embossing simulation. The mold translational velocities are maintained constant and the pressure field is calculated. The increase in pressure due to crystallization occurring at various stages of the embossing process is compared. The analysis is useful to predict the increase in the pressure required when pre-crystallization sets in during the embossing stage itself.

6.2 Introduction

The CTE process can be analyzed by utilizing the model parameters obtained and a process strategy can be developed. Simulation of the process helps to understand the process better and compare some of the findings from the experiments. The process simulation is used as a tool to understand the effect of crystallization on the filling behavior of the polymer. The filling behavior of the polymer occurring at various process conditions is simulated using the relative viscosity values obtained from the model predictions.

6.2 Hot Embossing Simulation

The conventional hot embossing process can be simulated based on isothermal conditions and has been well studied. In the current study the embossing process was simulated for a classical system to compare with the case where crystallization occurs. The conventional method of simulating the hot embossing process considers the polymer exhibiting viscoelastic behavior during the embossing and holding stage. For the sake of simplicity, in the current study the polymer is assumed to be a generalized Newtonian fluid, and crystallization effects are included during the embossing.

6.2.1 Geometry and Boundary Conditions

The geometry and the boundary conditions used for the simulation are shown in Figure 84.

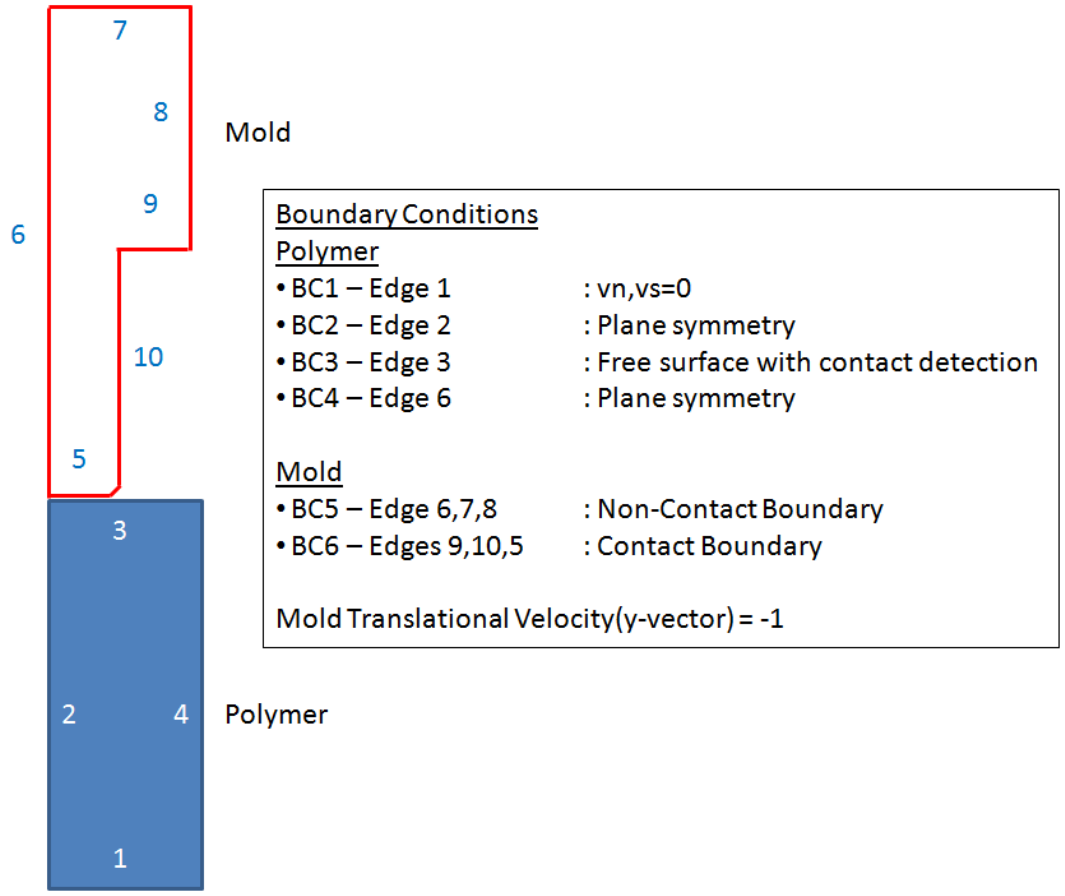

Figure 84 Geometry and boundary conditions

As shown in Figure 84, the mold with a translational velocity was pressed against a polymer blank which is modeled by the modified Cross law. The modified Cross law is given in Equation 53.

$$\eta = \frac{\eta_0}{1+(\lambda\dot{\gamma})^m} \tag{53}$$

where η_0 is the zero-shear rate viscosity, λ is the inverse of shear-rate at which the fluid changes from Newtonian to power-law behavior and m is the Cross law index

The modified Cross law parameters were determined from the experiments and subsequent model fitting. The parameters found are given as: λ = 53.98 and m = 0.376

The dimensions of the cavity to be filled are 40 µm depth and 10 µm half-width after considering plane symmetry on both sides. The parameters were determined and inputted in the data file. The embossing stage can be simulated with this condition as during the filling the crystallization is considered to be not initiated as explained earlier. The filling of the polymer follows only the classical shear-thinning behavior. The translational velocity can be varied to -10 or -0.1 to study the filling behavior and optimize the process parameters. For a translational velocity of -1 µm/s, complete fill is achieved at around 20 s.

6.2.2 Simulation results and discussion

6.2.2.1 Case 1: Embossing Stage without Crystallization

Figure 85 and Figure 86 show the embossing stage where the polymer fills into the cavity at a mold velocity of 1µm/s. The polymer is modeled only by the modified Cross law and no crystallization is considered. This also represents a conventional hot embossing simulation where the fluid fills inside the cavity showing only shear thinning behavior. Figure 85 and Figure 86 show the pressure experienced by the polymer at various stages of fill. Since the polymer exhibits shear thinning behavior, any decrease in viscosity manifests itself as a slight decrease in pressure. Moreover, the shear rates experienced during hot embossing is small, so the reduction in viscosity is not as high as in other polymer processing operations. The complete filling of the cavity is attainable in this case and the pressure values reached are similar to the pressure applied during the embossing experiments.

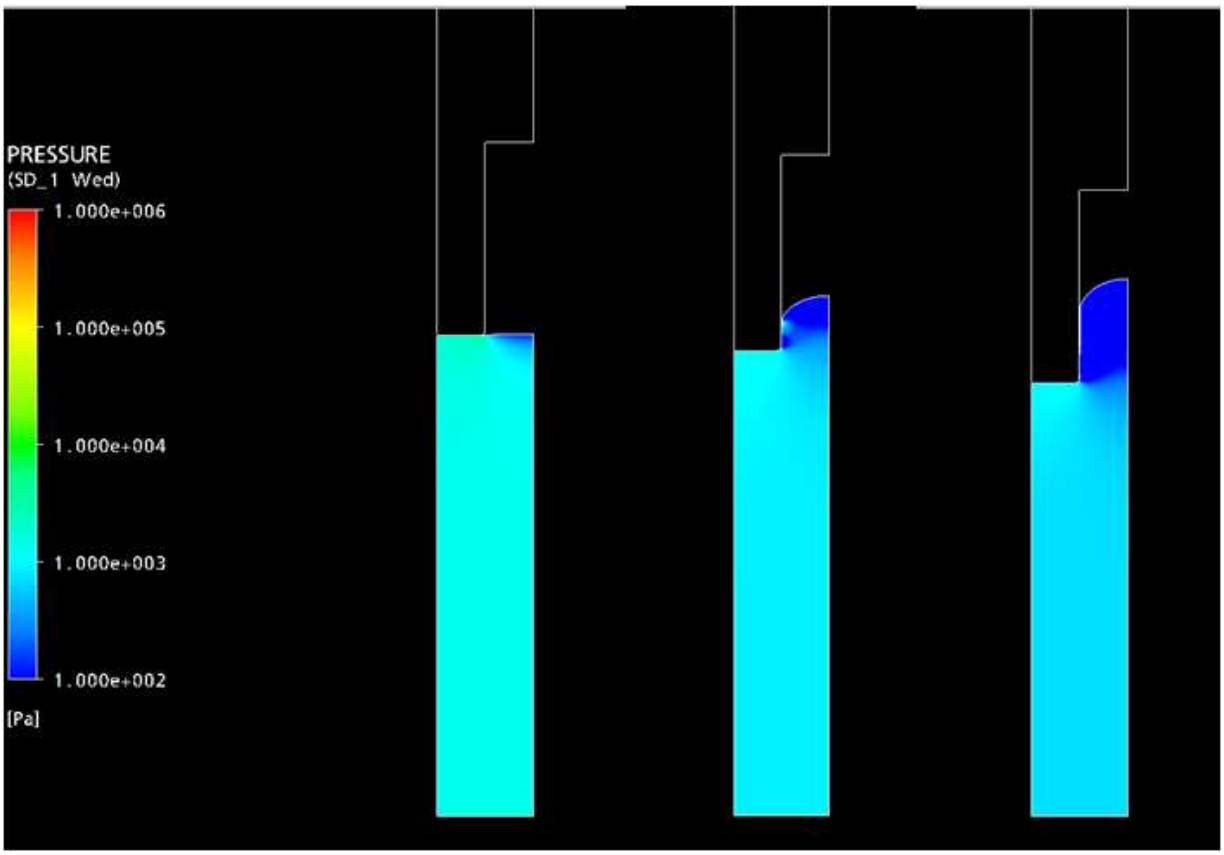

Figure 85 Case 1(No crystallization): Pressure profile during filling (a)

It can be observed from the final stage of the embossing stage the pressure does not exceed a cut-off value of 10^5 Pa. The simulation is based on the embossing at a temperature of 210°C where the viscosity values are obviously less than at the processing temperatures of 140-180°C. In a real case, since the viscosity is higher, the pressure values tend to reach higher values which are offset by the higher shear rates experienced. Hence the cut-off values though varying for different temperatures are a valuable tool to predict if the complete fill is achieved at the applied pressure during the embossing.

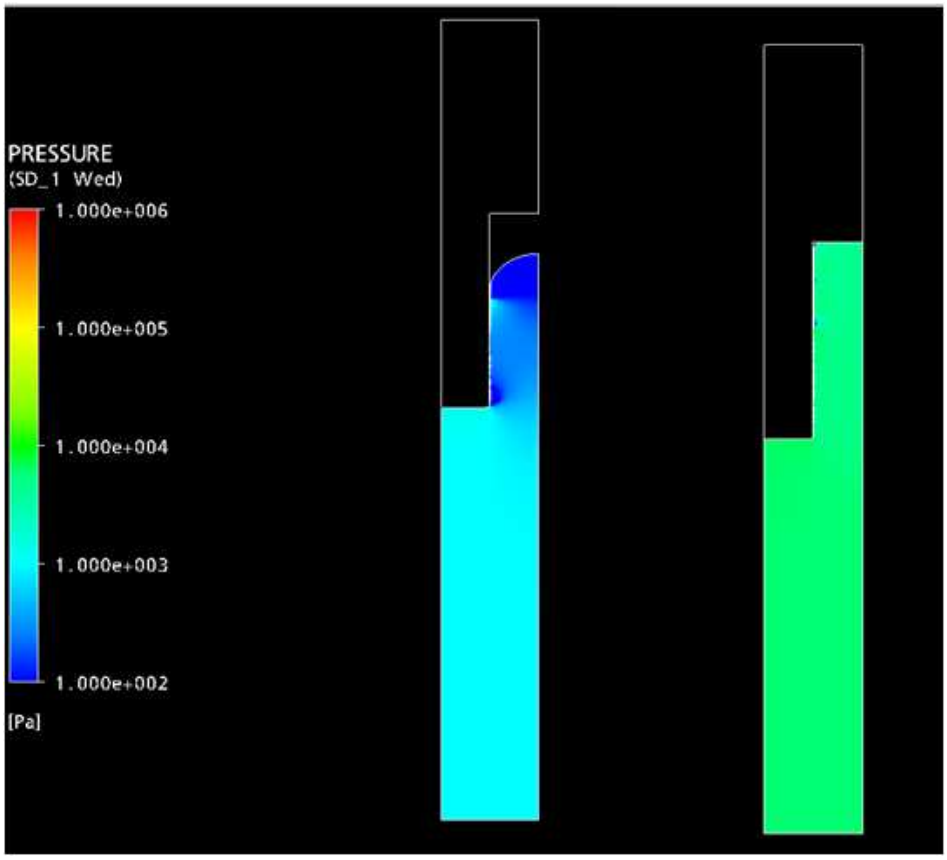

Figure 86 Case 1(No crystallization): Pressure profile during filling (b)

6.2.2.2 Case 2: Embossing Stage with Crystallization

Figure 87 – Figure 88 show the case where the material starts to crystallize during the embossing stage. The relative viscosity values predicted from the model is inputted into the data file. The study represents the case wherein the viscosity starts to increase even before the complete fill resulting in increase in pressure required for the fill. In the current case, the crystallization is given to start after 10s and follows a linear increase thereafter till the polymer fills the cavity completely. The rate of viscosity is similar to the crystallization rate at higher temperature 200°C.

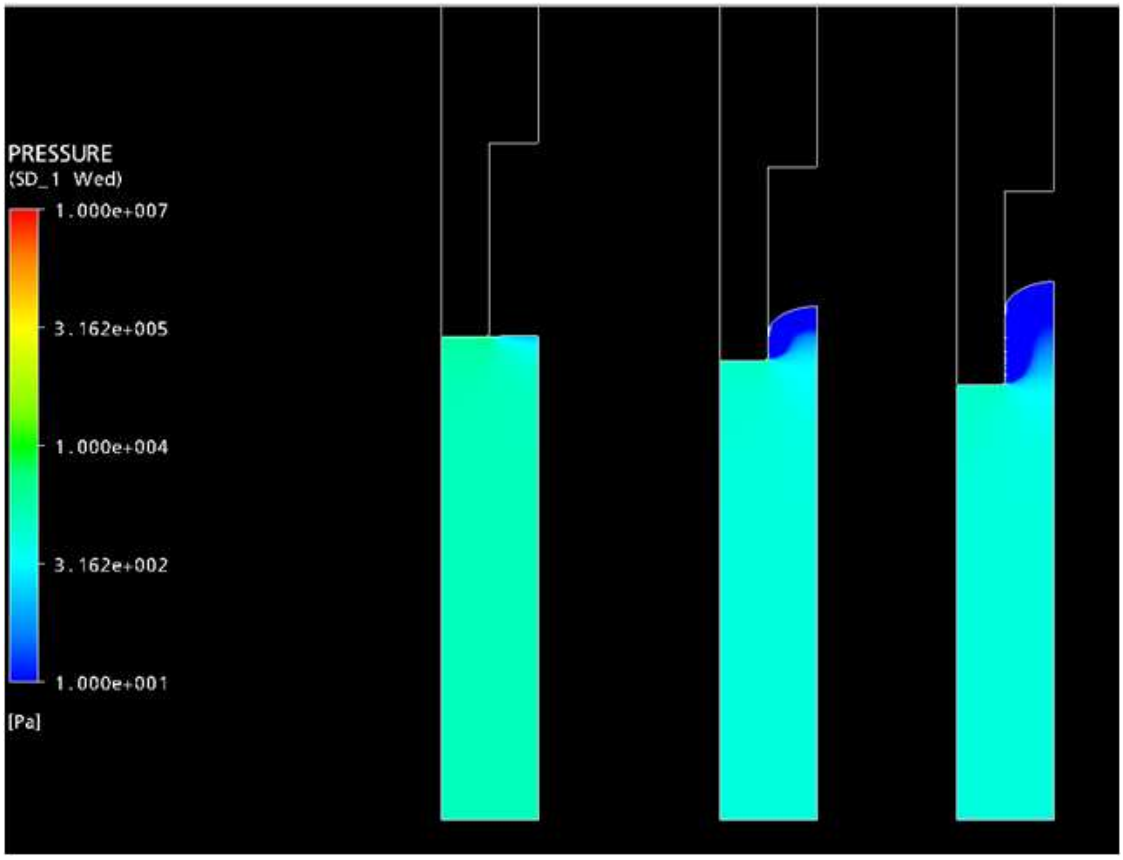

Figure 87 Case 2 (Slow rate of crystallization): Pressure profile during filling (a)

As observed from the figures, the pressure required for the fill increases after the crystallization sets in after 10s and then the pressure reaches values of about 10^6 – 10^7 Pa. This represents a situation where the polymer starts crystallizing in the embossing stage and the complete fill is not possible for a given pressure limit. In the simulation results shown in Figure 87 and Figure 88, complete fill is achieved as the simulation is speed controlled. But in the actual embossing experiments a uniform pressure is applied on the embossing setup and the filling is observed. Thus when a uniform embossing pressure of 10^5 is applied on the embossing setup in this case, complete fill would not be achieved. A high amount of pressure is required to push the solidifying polymer into the cavity. If the required pressure of 10^6 Pa is applied and the cavity is filled, the polymer tends to

recover more compared to the earlier case. This may due to the fact that in the end stages of embossing, a solid polymer is deformed.

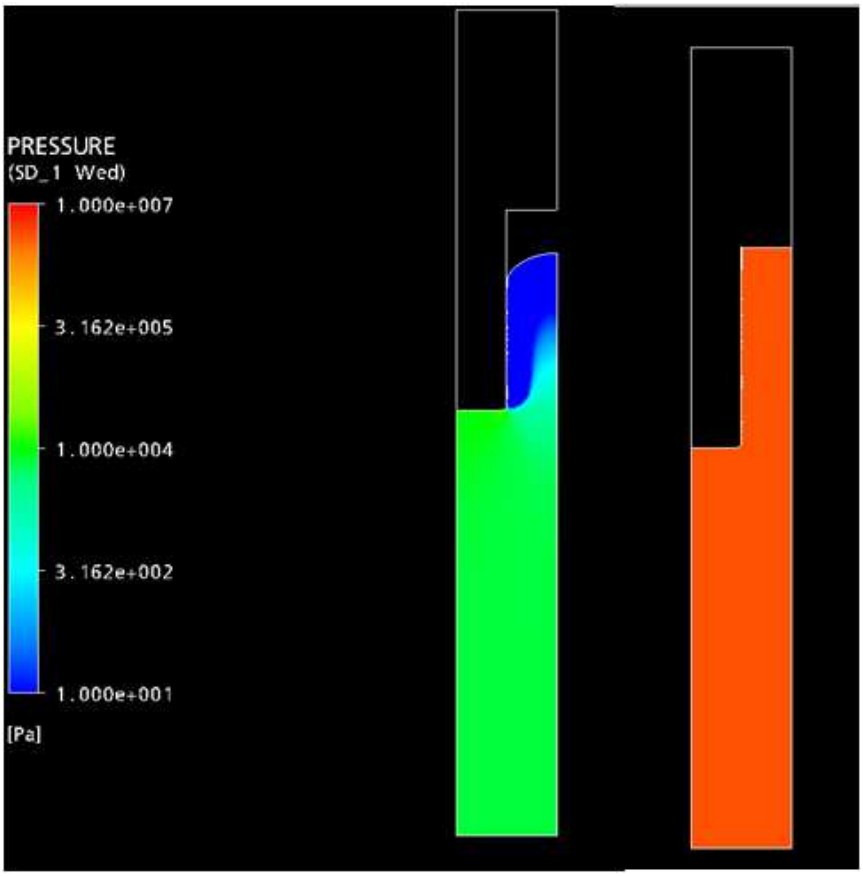

Figure 88 Case 2(Slow rate of crystallization): Pressure profile during filling (b)

6.2.2.3 Case 3: Embossing Stage with Faster Crystallization at Lower Temperature

Case 3 is similar to Case 2 but the crystallization induction time is earlier with the viscosity starts to increase linearly after 5s. This case represents the embossing stage when the polymer crystallization is rapid at low temperature of 160°C. The initial viscosity is maintained the same as in case 2, to facilitate better comparison. In real situation, the starting viscosity at 160°C will be quite high which can be calculated from the temperature-dependence law such as the Arrhenius or WLF equation. The cut-off pressure is maintained the same at 10^5 Pa. As seen in Figure 89 and Figure 90, the

pressure increases to about 10^6 even for 50% filling and the pressure required for a complete fill reaches 10^7– 10^8 Pa.

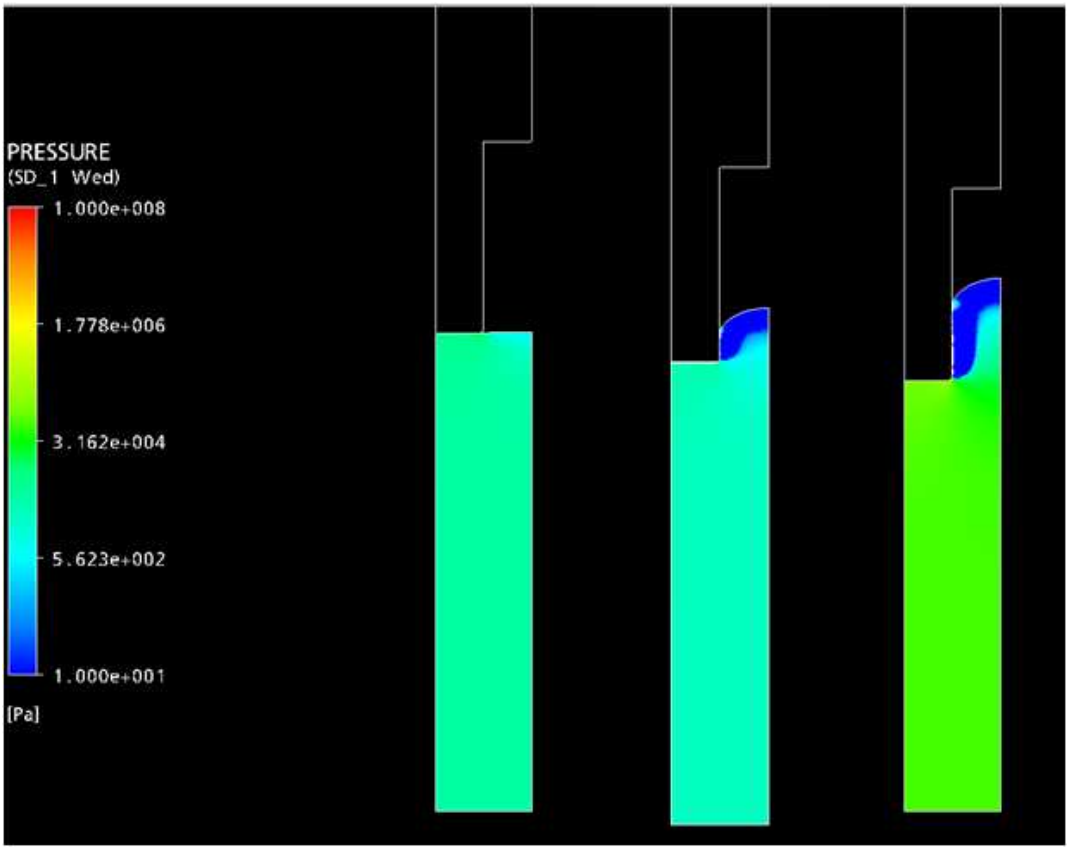

Figure 89 Case 3(Fast rate of crystallization): Pressure profile during filling (a)

The filling of the polymer is more difficult for an applied pressure of 10^5 Pa, as extremely high values of viscosity is obtained. The pressure needed to completely fill the cavity is quite high and also leads to a large amount of rebound when filled in that way.

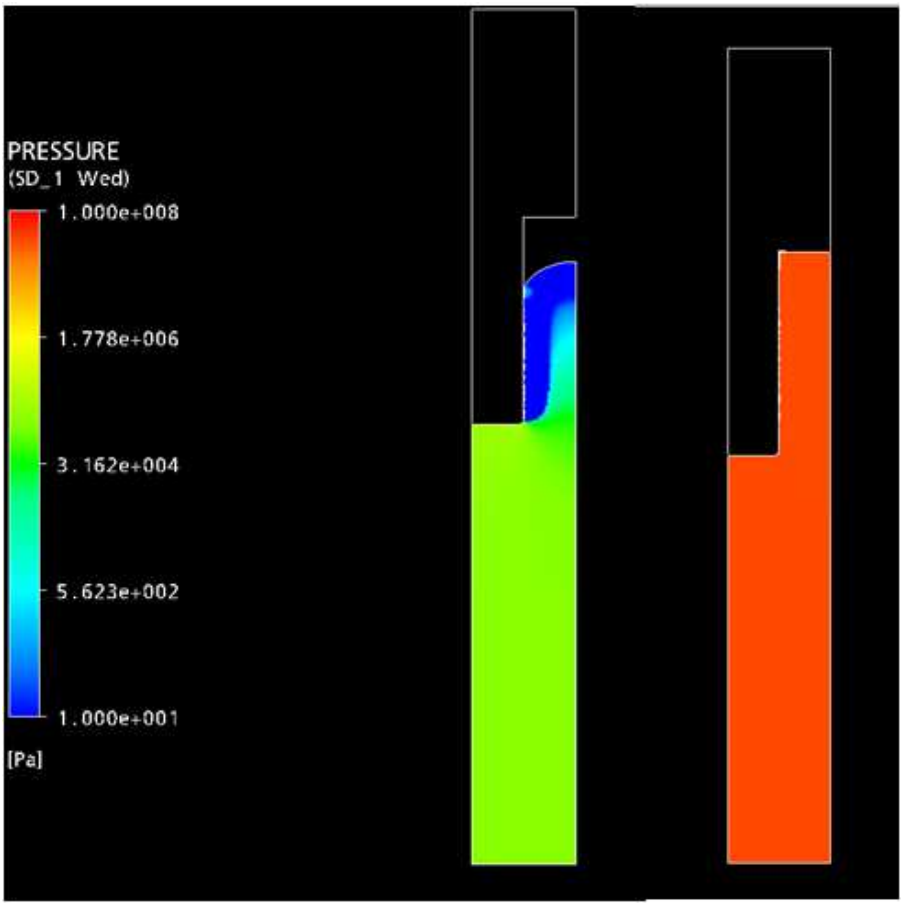

Figure 90 Case 3(Fast rate of crystallization): Pressure profile during filling (b)

Figure 91 plots the increase in pressure for the three cases described above. From the plot it can be observed that for case 2, for a constant pressure of 10^5 Pa, only about 80% fill can be achieved. For case 3, less than 50% filling can be achieved for a constant pressure of 10^5 Pa. These simulation studies establish a process strategy for the CTE process to achieve complete fill. The simulation studies also enable the understanding of the underlying filling pattern and the pressure and shear rate during the process. This understanding is vital to optimize the process to get good shaped parts. The simulation enables to analyze the process for its effect of crystallization on the final outcome of the process.

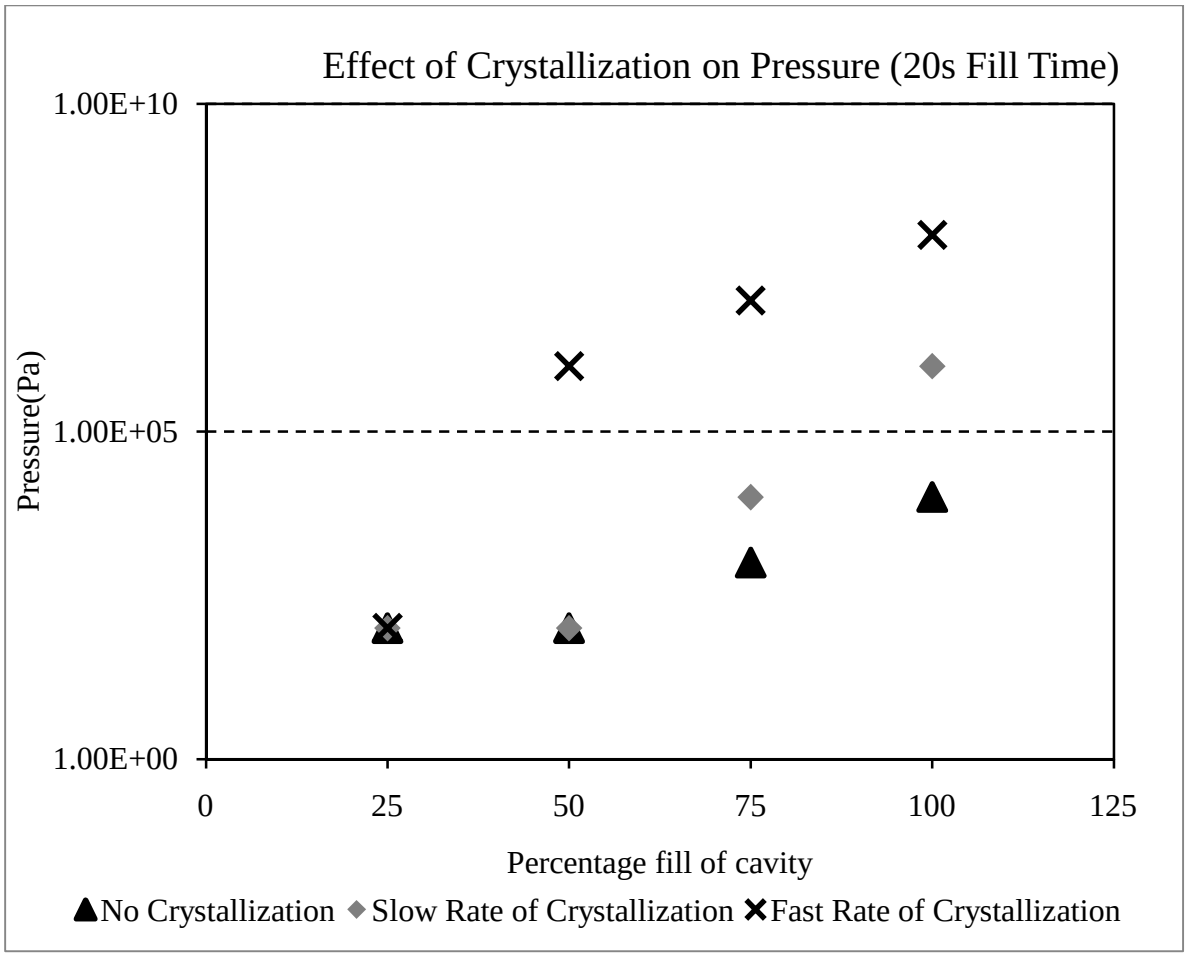

Figure 91 Pressure profile during embossing for Case 1(No crystallization), Case 2(Slow rate of crystallization) and Case 3(Fast rate of crystallization)

6.3 Conclusions

The CTE process was simulated as a 2D problem by using a planar geometry. The simulation results help in devising a process strategy. The change in pressure in the film when the mold velocity is held constant is determined and compared qualitatively with the experimental findings. The simulation predicted complete filling of the polymer for conventional embossing process with low pressure requirements.

For a constant pressure of less than 10^5 Pa, only less than 80-85% filling of the cavity is achieved when the rate of crystallization is low and the viscosity levels reach a range of $10^5 – 10^6$ Pa.s even during the embossing stage. This illustrated a case where the crystallization sets in during the embossing stage itself and hence resulting in high amount of pressure required to push the material inside the cavities.

In the case where the rate of crystallization is high, only less than 50% of the final feature height is achieved as the crystallization initiates even before the embossing stage has started. This rapid crystallization results in a material with viscosity range of 10^7-10^8 during the embossing stage. This result shows that when the polymer is embossed at optimum processing temperatures 160-180°C, any premature crystallization during the embossing stage would completely hinder the filling and result in very poor replication.

CONCLUSIONS AND RECOMMENDATIONS

Conclusions

The current thesis reports an attempt to develop a new type of isothermal hot embossing process called Constant Temperature Embossing (CTE). The CTE process can be defined as a hot embossing process where the substrate can be embossed and demolded at high isothermal temperatures without the need for cooling. The premise of enabling a new method is to utilize the crystallizing nature of certain polymers in amorphous forms. The process is material-based, rather than the usual tool-based variations attempted in the literature. Amorphous PET and PEEK films that can crystallize when heated above their T_g were used for demonstrating the feasibility and versatility of the process.

The films were embossed using silicon stamps with parallel rectangular trenches in a hydraulic press. The embossed films were characterized to understand the replication accuracy and surface morphology. The raw PET films were characterized for their thermal, rheological and tensile properties with focus on understanding the property changes during the phase transfer in the material in the embossing stage. The mechanical properties of the polymer before and after embossing were not studied in detail to the scope of the project being confined to relative property changes during the processing. The material properties in the actual processing range were predicted with reasonable accuracy using a semi-empirical rheological model established by combining the crystallization kinetics and suspension rheology. The predicted material properties when used in a 2D simulation reasonably described the filling behavior observed on the actual embossing process. The key findings and conclusions of the current study are:

- The CTE process utilizes the unique crystallization kinetics of slowly crystallizing polymers to enable the embossing, holding and demolding stages at an isothermal temperature.
- The amorphous PET film was characterized by DSC, rheometry and tensile testing mainly to understand the crystallization kinetics and its effect on the rheological/mechanical properties during the holding stage. The rate and nature of change of the mechanical properties as well as the crystallization kinetics of the polymer film can be used to determine a feasible process window and optimize the processing parameters.
- The CTE process has been used to successfully emboss rectangular trenches with aspect ratios of 2 and 3.5 with amorphous PET and PEEK as raw materials. The replication quality measured by SEM and optical profilometry showed that the features were fully replicated when the optimized process conditions were employed.
- Amorphous PET film showed good replication when embossed with CTE in the temperature range 160-180°C. The embossing time and holding time had a direct correlation with the crystallization induction time and the rate of crystallization which in turn is dependent on the embossing temperature.
- At the same level of embossing pressure and embossing time as used for the PET films, amorphous PEEK film showed reduced replication quality due to higher initial crystallinity of the raw film, the high viscosity of the material even at temperatures in the range of 240-260°C and also due to the faster rate of crystallization. However, complete replication of grooves can be achieved by using a material with lower initial

crystallinity, robust tool embossing set-up to avoid time lags and better control of the process parameters.

- A semi-empirical model based on the analogy of the change in particle concentration in suspensions to the change in crystalline content during the process was demonstrated. The Nakamura equation for the non-isothermal crystallization kinetics was used to predict the increase in crystalline content when the kinetic parameters are determined. A suspension based model was chosen based on its applicability to the current system and the Nakamura model was incorporated into the suspension model. The data predicted from the semi-empirical model was compared with the data collected independently from experiments and a reasonable fit was observed based on the assumptions considered.
- The process was simulated as a 2D planar problem using POLYFLOW. The simulation was used as a tool to qualitatively understand the effect of crystallization on the final replication fidelity.
- The simulation studies show that for a constant embossing pressure of 10^5 Pa and a quiescent zero-shear viscosity of 11000 Pa.s, any crystallization occurring during the embossing stage reduces the total fill to less than 85% if the rate of crystallization is low and less than 50% if the rate of crystallization is high.
- The process analysis was conducted to understand the determination of an acceptable processing window which can produce parts with good replication fidelity and with better control over the processing parameters.

Future Recommendations

This study has been successful in establishing a new process variant of the conventional hot embossing process and demonstrating its capability in constant temperature processing of PET and PEEK. Additional studies can be followed to apply this process to other slowly crystallizing polymers (with a relatively slow crystallization rate compared with the normal processing speed during embossing) such as PEN and poly (L-lactic acid) (PLLA) and to consider other aspects of the process not within the scope of the current study. The key recommendations for future considerations include:

- The study can be improved foremost by better prediction of material properties during the process. This can be achieved by designing systems to capture the change in material properties without time lag and with good accuracy.
- A preliminary method was proposed to measure the tensile properties of the material. The system can be improved by imparting better stability in the system by devising an alternate way of transferring the heating medium to the testing bath.
- The embossing process can be tested for its versatility by using a vacuum assisted embossing setup that can eliminate some of the problems with moisture and bubbles.
- The CTE process can be tested for its capability to emboss very high aspect ratio features.
- The model can be further improved by considering other facets of crystallization such as secondary crystallization and percolation thresholds observed in high crystalline content, as well as viscoelastic behaviors of the polymer

REFERENCES

1. Heckele, M.; Schomburg, W. K., Review on micro molding of thermoplastic polymers. *Journal of Micromechanics and Microengineering* **2004,** 14, (3), R1.
2. Becker, H.; Heim, U., Hot embossing as a method for the fabrication of polymer high aspect ratio structures. *Sensors and Actuators A: Physical* **2000,** 83, (1-3), 130-135.
3. Holger, B.; Claudia, G., Polymer microfabrication methods for microfluidic analytical applications. *Electrophoresis* **2000,** 21, (1), 12-26.
4. Gerner, M.; Paatzsch, T.; Weber, L.; Schift, H.; Smaglinski, I.; Bauer, H. D.; Abraham, N.; Ehrfeld, W. In *Micro-optical components for fiber and integrated optics realized by the LIGA technique*, Amsterdam, Neth, 1995; IEEE: Amsterdam, Neth, 1995; pp 328-333.
5. Olsson, A.; Larsson, O.; Holm, J.; Lundbladh, L.; Ohman, O.; Stemme, G., Valve-less diffuser micropumps fabricated using thermoplastic replication. *Sensors and Actuators, A: Physical* **1998,** 64, (1), 63-68.
6. Kempen, L. U.; Kunz, R. E.; Gale, M. T. In *Micromolded structures for integrated optical sensors*, Austin, TX, United states, 1995; SPIE: Austin, TX, United states, 1995; pp 278-285.
7. Nagarajan, P.; Yao, D.; Ellis, T. S.; Azadegan, R., Through-thickness embossing process for fabrication of three-dimensional thermoplastic parts. *Polymer Engineering and Science* **2007,** 47, (12), 2075-2084.
8. Pemg, B.-Y.; Wu, C.-W.; Shen, Y.-K.; Lin, Y., Microfluidic chip fabrication using hot embossing and thermal bonding of cop. *Polymers for Advanced Technologies* 21, (7), 457-466.
9. Lee, G.-B.; Chen, S.-H.; Huang, G.-R.; Sung, W.-C.; Lin, Y.-H., Microfabricated plastic chips by hot embossing methods and their applications for DNA separation and detection. *Sensors and Actuators, B: Chemical* **2001,** 75, (1-2), 142-148.
10. Shan, X. C.; Ikehara, T.; Murakoshi, Y.; Maeda, R., Applications of micro hot embossing for optical switch formation. *Sensors and Actuators, A: Physical* **2005,** 119, (2), 433-440.
11. Trautmann, A.; Heuck, F.; Mueller, C.; Ruther, P.; Paul, O. In *Replication of microneedle arrays using vacuum casting and hot embossing*, Seoul, Korea, Republic of, 2005; Institute of Electrical and Electronics Engineers Computer Society: Seoul, Korea, Republic of, 2005; pp 1420-1423.
12. Cai, Y.; Sammoura, F.; Chi, C.-Y.; Lin, L.; Chiao, J. C. In *Micro hot embossed plastic millimeter-wave systems*, Brisbane, Australia, 2006; SPIE: Brisbane, Australia, 2006; pp Queensland University of Technology, Australia; Air Force Office of Scientific Research, AOARD, Japan; Defence Science and Technology Organisation, Australia; Bandwidth Foundry, Australia.
13. Escarre, J.; Bertomeu, J.; Asensi, J. M.; Andreu, J.; Terrazzoni-Daudrix, V.; Haug, F. J.; Niquille, X. In *Hot embossing of polymer substrates for thin silicon cell applications*, Waikoloa, HI, United states, 2007; Inst. of Elec. and Elec. Eng. Computer Society: Waikoloa, HI, United states, 2007; pp 1556-1559.
14. Heckele, M.; Worgull, M.; Mappes, T.; Tosello, G.; Metz, T.; Gavillet, J.; Fugier, P.; Koltay, P.; Hansen, H. N. In *Hot embossing of high aspect ratio sub-m structured*

surfaces for micro fluidic applications, Milwaukee, WI, United states, 2008; Society of Plastics Engineers: Milwaukee, WI, United states, 2008; pp 2497-2501.
15. Kim, J.; Hong, S.; Kang, J.; Hwang, C. J. In *Fabrication of partition wall for solar cell by hot embossing*, Gyeonggi-do, Korea, Republic of, 2008; Inst. of Elec. and Elec. Eng. Computer Society: Gyeonggi-do, Korea, Republic of, 2008; pp 387-388.
16. Pan, C. T.; Wu, T. T.; Chen, M. F.; Chang, Y. C.; Lee, C. J.; Huang, J. C., Hot embossing of micro-lens array on bulk metallic glass. *Sensors and Actuators, A: Physical* **2008,** 141, (2), 422-431.
17. Schneider, P.; Steitz, C.; Schafer, K. H.; Ziegler, C., Hot embossing of pyramidal micro-structures in PMMA for cell culture. *Physica Status Solidi (A) Applications and Materials* **2009,** 206, (3), 501-507.
18. Wang, Y.; Liu, Z.; Han, B.; Huang, Y.; Zhang, J.; Sun, D.; Du, J., Compressed-Co2-assisted patterning of polymers. *Journal of Physical Chemistry B* **2005,** 109, (25), 12376-12379.
19. Juang, Y.-J.; Lee James, L.; Koelling, K. W., Hot embossing in microfabrication. Part II: Rheological characterization and process analysis. *Polymer Engineering and Science* **2002,** 42, (3), 551-566.
20. Liu, C.; Li, J. M.; Liu, J. S.; Wang, L. D., Deformation behavior of solid polymer during hot embossing process. *Microelectronic Engineering* **2010,** 87, (2), 200-207.
21. Shen, X. J.; Pan, L.-W.; Lin, L. In *Microplastic embossing process: Experimental and theoretical characterizations*, Munich, Germany, 2002; Elsevier: Munich, Germany, 2002; pp 428-433.
22. Worgull, M.; Heckele, M.; Hetu, J. F.; Kabanemi, K. K., Modeling and optimization of the hot embossing process for micro- And nanocomponent fabrication. *Journal of Microlithography, Microfabrication and Microsystems* **2006,** 5, (1).
23. Yao, D.; Kuduva-Raman-Thanumoorthy, R., An enlarged process window for hot embossing. *Journal of Micromechanics and Microengineering* **2008,** 18, (4).
24. Eusner, T.; Hale, M.; Hardt, D. E., Process robustness of hot embossing microfluidic devices. *Journal of Manufacturing Science and Engineering, Transactions of the ASME* 132, (3), 0309201-0309208.
25. Sahli, M.; Barriere, T.; Gelin, J. C. In *Experimental Analysis and Numerical Simulation of the Flow Behaviour of Thin Polymer Films during Hot Embossing*, USA, American Institute of Physics: USA, pp 651-8.
26. He, Y.; Fu, J.-Z.; Chen, Z.-C., Research on optimization of the hot embossing process. *Journal of Micromechanics and Microengineering* **2007,** 17, (12), 2420-2425.
27. Yong, H.; Jian-Zhong, F.; Zi-Chen, C., Optimization of control parameters in micro hot embossing. *Microsystem Technologies* **2008,** 14, (3), 325-9.
28. Jeong, J.-H.; Choi, Y.-S.; Shin, Y.-J.; Lee, J.-J.; Park, K.-T.; Lee, E.-S.; Lee, S.-R., Flow behavior at the embossing stage of nanoimprint lithography. *Fibers and Polymers* **2002,** 3, (3), 113-119.
29. Juang, Y.-J.; Lee James, L.; Koelling, K. W., Hot embossing in microfabrication. Part I: Experimental. *Polymer Engineering and Science* **2002,** 42, (3), 539-550.
30. Haber, A.; Kamal, M. R., Experimental analysis of the thermoplastic film embossing process. *Advances in Polymer Technology* **1992,** 11, (3), 159-180.
31. Kimerling, T.; Liu, W.; Kim, B.; Yao, D., Rapid hot embossing of polymer microfeatures. *Microsystem Technologies* **2006,** 12, (8), 730-735.

32. Chen, C.-H.; Liu, C.-P.; Lee, Y.-C.; Hsiao, F.-B.; Chiu, C.-Y.; Chung, M.-H.; Chiang, M.-H., IR laser-assisted micro/nano-imprinting. *Journal of Micromechanics and Microengineering* **2006,** 16, (8), 1463-1467.
33. Lu, C.; Juang, Y.-J.; Lee, L. J.; Grewell, D.; Benatar, A., Analysis of laser/IR-assisted microembossing. *Polymer Engineering and Science* **2005,** 45, (5), 661-668.
34. Grewell, D.; Mokhtarzadeh, A.; Benatar, A.; Lu, C.; James Lee, L. In *Feasibility of selected methods for embossing micro-features in thermoplastics*, Nashville, TN, United states, 2003; Society of Plastics Engineers: Nashville, TN, United states, 2003; pp 1094-1098.
35. Lin, C.-H.; Chen, R., Ultrasonic nanoimprint lithography: A new approach to nanopatterning. *Journal of Microlithography, Microfabrication and Microsystems* **2006,** 5, (1).
36. Khuntontong, P.; Blaser, T.; Schomburg, W. K., Fabrication of molded interconnection devices by ultrasonic hot embossing on thin polymer films. *IEEE Transactions on Electronics Packaging Manufacturing* **2009,** 32, (3), 152-156.
37. Chang, J. H.; Yang, S. Y., Development of fluid-based heating and pressing systems for micro hot embossing. *Microsystem Technologies* **2005,** 11, (6), 396-403.
38. Shih-Jung, L.; Yu-Tsai, D., Hot embossing precise structure onto plastic plates by ultrasonic vibration. *Polymer Engineering & Science* **2005,** 45, (7), 915-925.
39. Khang, D.-Y.; Lee, H. H., Room-temperature imprint lithography by solvent vapor treatment. *Applied Physics Letters* **2000,** 76, (7), 870-872.
40. Cecchini, M.; Signori, F.; Pingue, P.; Bronco, S.; Ciardelli, F.; Beltram, F., High-resolution polyethylene terephthalate (PET) hot embossing at low temperature: Thermal, mechanical, and optical analysis of nanopatterned films. *Langmuir* **2008,** 24, (21), 12581-12586.
41. Lu, C.; Cheng, M. M.-C.; Benatar, A.; Lee, L. J., Embossing of high-aspect-ratio-microstructures using sacrificial templates and fast surface heating. *Polymer Engineering and Science* **2007,** 47, (6), 830-840.
42. W. H. Cobbs, J.; Burton, R. L., Crystallization of polyethylene terephthalate. *Journal of Polymer Science* **1953,** 10, (3), 275-290.
43. Mayhan, K. G.; James, W. J.; Wouter, B., Poly(ethylene terephthalate). I. Study of crystallization kinetics. *Journal of Applied Polymer Science* **1965,** 9, (11), 3605-3616.
44. Groeninckx, G.; Reynaers, H.; Berghmans, H.; Smets, G., MORPHOLOGY AND MELTING BEHAVIOR OF SEMICRYSTALLINE POLY(ETHYLENE TEREPHTHALATE) - 1. ISOTHERMAL CRYSTALLIZED PET. *Journal of polymer science. Part A-2, Polymer physics* **1980,** 18, (6), 1311-1324.
45. Heffelfinger, C. J.; E. L. Lippert, J., X-ray low-angle scattering from oriented poly(ethylene terephthalate) films. *Journal of Applied Polymer Science* **1971,** 15, (11), 2699-2731.
46. Imai, M.; Mori, K.; Mizukami, T.; Kaji, K.; Kanaya, T., Structural formation of poly (ethylene terephthalate) during the induction period of crystallization: 1. Ordered structure appearing before crystal nucleation. *Polymer* **1992,** 33, (21), 4451-4456.
47. Radhakrishnan, J.; Kaito, A., Structure formation during the isothermal crystallization of oriented amorphous poly(ethylene terephthalate) films. *Polymer* **2001,** 42, (8), 3859-3866.

48. Robertson, R. E., Polymer Order and Polymer Density. *The Journal of Physical Chemistry* **1965,** 69, (5), 1575-1578.
49. Chen, W.; Lofgren, E. A.; Jabarin, S. A., Microstructure of amorphous and crystalline poly(ethylene terephthalate). *Journal of Applied Polymer Science* **1998,** 70, (10), 1965-1976.
50. Taniguchi, A.; Cakmak, M., The suppression of strain induced crystallization in PET through sub micron TiO2 particle incorporation. *Polymer* **2004,** 45, (19), 6647-6654.
51. Harget, P. J.; Siegmann, A., SMALL-ANGLE X-RAY SCATTERING FROM AMORPHOUS POLYETHYLENE TEREPHTHALATE. *Journal of Applied Physics* **1972,** 43, (11), 4357-4362.
52. Asano, T.; Baltá Calleja, F. J.; Flores, A.; Tanigaki, M.; Mina, M. F.; Sawatari, C.; Itagaki, H.; Takahashi, H.; Hatta, I., Crystallization of oriented amorphous poly(ethylene terephthalate) as revealed by X-ray diffraction and microhardness. *Polymer* **1999,** 40, (23), 6475-6484.
53. Renninger, A. L.; Uhlmann, D. R., On the structure of glassy polymers. III. Small-angle x-ray scattering from amorphous polyethylene terephthalate. *Journal of Polymer Science: Polymer Physics Edition* **1976,** 14, (3), 415-425.
54. Samuels, R. J., QUANTITATIVE STRUCTURAL CHARACTERIZATION OF THE MECHANICAL PROPERTIES OF POLY(ETHYLENE TEREPHTHALATE). **1972,** 10, (5), 781-810.
55. Gupta, V. B.; Radhakrishnan, J.; Sett, S. K., Interaction between thermal shrinkage and crystallization in axially oriented poly(ethylene terephthalate) fibres and films. *Polymer* **1993,** 34, (18), 3814-3822.
56. Dulmage, W. J.; Geddes, A. L., Structure of drawn polyethylene terephthalate. *Journal of Polymer Science* **1958,** 31, (123), 499-512.
57. Gorlier, E.; Haudin, J. M.; Billon, N., Strain-induced crystallisation in bulk amorphous PET under uni-axial loading. *Polymer* **2001,** 42, (23), 9541-9549.
58. Daubeny, R. d. P.; Bunn, C. W., The Crystal Structure of Polyethylene Terephthalate. *Proceedings of the Royal Society of London. Series A, Mathematical and Physical Sciences* **1954,** 226, (1167), 531-542.
59. Keller, A., The spherulitic structure of crystalline polymers. Part I. Investigations with the polarizing microscope. *Journal of Polymer Science* **1955,** 17, (84), 291-308.
60. Yamashita, Y., Single crystals of poly(ethylene terephthalate). *Journal of Polymer Science Part A: General Papers* **1965,** 3, (1), 81-92.
61. Meissner, J.; Hostettler, J., A new elongational rheometer for polymer melts and other highly viscoelastic liquids. *Rheologica Acta* **1994,** 33, (1), 1-21.
62. Muller, R.; Froelich, D., NEW EXTENSIONAL RHEOMETER FOR ELONGATIONAL VISCOSITY AND FLOW BIREFRINGENCE MEASUREMENTS: SOME RESULTS ON POLYSTYRENE MELTS. *Polymer* **1985,** 26, (10), 1477-1482.
63. Sentmanat, M. L. A., OH) Dual windup extensional rheometer. 2003.
64. Sentmanat, M. L., Miniature universal testing platform: from extensional melt rheology to solid-state deformation behavior. *Rheologica Acta* **2004,** 43, (6), 657-669.
65. Muenstedt, H., NEW UNIVERSAL EXTENSIONAL RHEOMETER FOR POLYMER MELTS. MEASUREMENTS ON A POLYSTYRENE SAMPLE. *Journal of Rheology* **1979,** 23, (4), 421-436.

66. Lorenzo, A. T.; Arnal, M. L.; Albuerne, J.; Müller, A. J., DSC isothermal polymer crystallization kinetics measurements and the use of the Avrami equation to fit the data: Guidelines to avoid common problems. *Polymer Testing* **2007,** 26, (2), 222-231.
67. Melvin, A., Kinetics of Phase Change. I General Theory. *The Journal of Chemical Physics* **1939,** 7, (12), 1103-1112.
68. Melvin, A., Kinetics of Phase Change. II Transformation-Time Relations for Random Distribution of Nuclei. *The Journal of Chemical Physics* **1940,** 8, (2), 212-224.
69. Melvin, A., Granulation, Phase Change, and Microstructure Kinetics of Phase Change. III. *The Journal of Chemical Physics* **1941,** 9, (2), 177-184.
70. Chan, T. V.; Shyu, G. D.; Isayev, A. I., Master curve approach to polymer crystallization kinetics. *Polymer Engineering & Science* **1995,** 35, (9), 733-740.
71. Chan, T. W.; Isayev, A. I., Quiescent polymer crystallization: Modelling and measurements. *Polymer Engineering & Science* **1994,** 34, (6), 461-471.
72. Kim, K. H.; Isayev, A. I.; Kwon, K., Crystallization kinetics for simulation of processing of various polyesters. *Journal of Applied Polymer Science* **2006,** 102, (3), 2847-2855.
73. Nakamura, K.; Katayama, K.; Amano, T., Some aspects of nonisothermal crystallization of polymers. II. Consideration of the isokinetic condition. *Journal of Applied Polymer Science* **1973,** 17, (4), 1031-1041.
74. Nakamura, K.; Watanabe, T.; Amano, T.; Katayama, K., Some aspects of nonisothermal crystallization of polymers. III. Crystallization during melt spinning. *Journal of Applied Polymer Science* **1974,** 18, (2), 615-623.
75. Nakamura, K.; Watanabe, T.; Katayama, K.; Amano, T., Some aspects of nonisothermal crystallization of polymers. I. Relationship between crystallization temperature, crystallinity, and cooling conditions. *Journal of Applied Polymer Science* **1972,** 16, (5), 1077-1091.
76. Patel, R. M.; Spruiell, J. E., Crystallization kinetics during polymer processing—Analysis of available approaches for process modeling. *Polymer Engineering & Science* **1991,** 31, (10), 730-738.
77. Janeschitz-Kriegl, H.; Krobath, G.; Roth, W.; Schausberger, A., On the kinetics of polymer crystallization under shear. *European Polymer Journal* **1983,** 19, (10-11), 893-898.
78. Hammami, A.; Spruiell, J. E.; Mehrotra, A. K., Quiescent nonisothermal crystallization kinetics of isotactic polypropylenes. *Polymer Engineering & Science* **1995,** 35, (10), 797-804.
79. Liu, T.; Mo, Z.; Wang, S.; Zhang, H., Nonisothermal melt and cold crystallization kinetics of poly(aryl ether ether ketone ketone). *Polymer Engineering and Science* **1997,** 37, (3), 568-575.
80. Qiu, Z.; Mo, Z.; Yu, Y.; Zhang, H.; Sheng, S.; Song, C., Nonisothermal melt and cold crystallization kinetics of poly(aryl ether ketone ether ketone ketone). *Journal of Applied Polymer Science* **2000,** 77, (13), 2865-2871.
81. Renate, M. R. W.; Marcelo, S. R., Non-isothermal cold crystallization kinetics and morphology of PET + SAN blends. *Journal of Applied Polymer Science* **2010,** 116, (2), 1077-1087.

82. Tianxi, L.; Zhishen, M.; Hongfang, Z., Nonisothermal crystallization behavior of a novel poly(aryl ether ketone): PEDEKmK. *Journal of Applied Polymer Science* **1998,** 67, (5), 815-821.
83. Tianxi, L.; Zhishen, M.; Shanger, W.; Hongfang, Z., Nonisothermal melt and cold crystallization kinetics of poly(aryl ether ether ketone ketone). *Polymer Engineering & Science* **1997,** 37, (3), 568-575.
84. Wellen, R. M. R.; Rabello, M. S., Non-Isothermal cold crystallization kinetics and morphology of PET + SAN blends. *Journal of Applied Polymer Science* **2010,** 116, (2), 1077-1087.
85. Zhaobin, Q.; Zhishen, M.; Yingning, Y.; Hongfang, Z.; Shouri, S.; Caisheng, S., Nonisothermal melt and cold crystallization kinetics of poly(aryl ether ketone ether ketone ketone). *Journal of Applied Polymer Science* **2000,** 77, (13), 2865-2871.
86. Khanna, Y. P.; Taylor, T. J., Comments and recommendations on the use of the Avrami equation for physico-chemical kinetics. *Polymer Engineering and Science* **1988,** 28, (16), 1042-1045.
87. Kamal, M. R.; Chu, E., Isothermal and nonisothermal crystallization of polyethylene. *Polymer Engineering & Science* **1983,** 23, (1), 27-31.
88. Dietz, W., Spherulitic Growth in Polymers
SPHAEROLITHWACHSTUM IN POLYMEREN. *Colloid and Polymer Science* **1981,** 259, (4), 413-429.
89. Hatzikiriakos, S. G.; Heffner, G.; Vlassopoulos, D.; Christodoulou, K., Rheological characterization of polyethylene terephthalate resins using a multimode Phan-Tien-Tanner constitutive relation. *Rheologica Acta* **1997,** 36, (5), 568-578.
90. Boutahar, K.; Carrot, C.; Guillet, J., Crystallization of Polyolefins from Rheological MeasurementsRelation between the Transformed Fraction and the Dynamic Moduli. *Macromolecules* **1998,** 31, (6), 1921-1929.
91. Carrot, C.; Guillet, J.; Boutahar, K., RHEOLOGICAL BEHAVIOR OF A SEMICRYSTALLINE POLYMER DURING ISOTHERMAL CRYSTALLIZATION. *Rheologica Acta* **1993,** 32, (6), 566-574.
92. Coppola, S.; Acierno, S.; Grizzuti, N.; Vlassopoulos, D., Viscoelastic Behavior of Semicrystalline Thermoplastic Polymers during the Early Stages of Crystallization. *Macromolecules* **2006,** 39, (4), 1507-1514.
93. Dairanieh, I. S.; McHugh, A. J.; Doufas, A. K., A phenomenological model for flow-induced crystallization. *Journal of Reinforced Plastics and Composites* **1999,** 18, (5), 464-71.
94. Dumazet, P.; Douillard, A.; Chabert, B.; Guillet, J., A comparative study of rheological evolution and crystallization kinetics of poly(ethylene terephthalate). *Polymer* **1994,** 35, (13), 2828-2833.
95. Khanna, Y. P., Rheological mechanism and overview of nucleated crystallization kinetics. *Macromolecules* **1993,** 26, (14), 3639-3643.
96. Koscher, E.; Fulchiron, R., Influence of shear on polypropylene crystallization: Morphology development and kinetics. *Polymer* **2002,** 43, (25), 6931-6942.
97. van Meerveld, J.; Peters, G. W. M.; Hutter, M., Towards a rheological classification of flow induced crystallization experiments of polymer melts. *Rheologica Acta* **2004,** 44, (2), 119-34.

98. Vleeshouwers, S.; Meijer, H. E. H., A rheological study of shear induced crystallization. *Rheologica Acta* **1996,** 35, (5), 391-9.
99. Janeschitz-Kriegl, H.; Wippel, H.; Paulik, C.; Eder, G., Polymer crystallization dynamics, as reflected by differential scanning calorimetry. Part 1: On the calibration of the apparatus. *Colloid & Polymer Science* **1993,** 271, (12), 1107-1115.
100. Wu, C. H.; Eder, G.; Janeschitz-Kriegl, H., Polymer crystallization dynamics, as reflected by differential scanning calorimetry. Part 2: Numerical simulations. *Colloid & Polymer Science* **1993,** 271, (12), 1116-1128.
101. Meissner, J.; Raible, T.; Stephenson, S. E., ROTARY CLAMP IN UNIAXIAL AND BIAXIAL EXTENSIONAL RHEOMETRY OF POLYMER MELTS. *Journal of Rheology* **1981,** 25, (1), 1-28.
102. Meissner, J. In *Development of a universal extensional rheometer for the uniaxial extension of polymer melts*, USA, 1972; USA, 1972; pp 405-20.
103. Petrie, C. J. S., Extensional viscosity: A critical discussion. *Journal of Non-Newtonian Fluid Mechanics* **2006,** 137, (1-3), 15-23.
104. Cogswell, F. N., MEASURING THE EXTENSIONAL RHEOLOGY OF POLYMER MELTS. *Transactions of the Society of Rheology* **1972,** 16, (3), 383-403.
105. Meissner, J., RHEOMETRY OF POLYMER MELTS. In Annual Reviews Inc: Palo Alto, CA, USA, 1985; Vol. 17, pp 45-64.
106. Tirtaatmadja, V.; Sridhar, T., A filament stretching device for measurement of extensional viscosity. *Journal of Rheology* **1993,** 37, (6), 1081-102.
107. Laun, H. M.; Munstedt, H., Elongational behaviour of a low density polyethylene melt. I. Strain rate and stress dependence of viscosity and recoverable strain in the steady-state. Comparison with shear data. Influence of interfacial tension. *Rheologica Acta* **1978,** 17, (4), 415-25.
108. Ishizuka, O.; Koyama, K., ELONGATIONAL VISCOSITY AT A CONSTANT ELONGATIONAL STRAIN RATE OF POLYPROPYLENE MELT. *Polymer* **1980,** 21, (2), 164-170.
109. Everage, A. E.; Ballman, R. L., Extensional viscosity of amorphous polystyrene. *Journal of Applied Polymer Science* **1976,** 20, (4), 1137-1141.
110. Ide, Y.; White, J. L., EXPERIMENTAL STUDY OF ELONGATIONAL FLOW AND FAILURE OF POLYMER MELTS. *Journal of Applied Polymer Science* **1978,** 22, (4), 1061-1079.
111. Axtell, F. H.; Haworth, B., Elongational rheometry of thermoplastic PET in the rubbery region. *Polymer Testing* **1990,** 9, (1), 53-70.
112. Vinogradov, G. V.; Fikhman, V. D.; Radushkevich, B. V.; Malkin, A. Y. A., Viscoelastic and relaxation properties of a polystyrene melt in axial extension. **1970,** 8, (5), 657-678.
113. White, J. L.; Ide, Y., RHEOLOGY AND DYNAMICS OF FIBER FORMATION FROM POLYMER MELTS. *Applied Polymer Symposia* **1975**, (27), 61-102.
114. Münstedt, H., Viscoelasticity of polystyrene melts in tensile creep experiments. *Rheologica Acta* **1975,** 14, (12), 1077-1088.
115. C.W. Macosko, J. M. L., *S.P.E Tech. Papers* **1973,** 19, 7.
116. Connelly, R. W.; Garfield, L. J.; Pearson, G. H., LOCAL STRETCH HISTORY OF A FIXED-END-CONSTANT-LENGTH-POLYMER-MELT STRETCHING EXPERIMENT. *Journal of Rheology* **1979,** 23, (5), 651-662.

117. Padmanabhan, M.; Kasehagen, L. J.; Macosko, C., Transient extensional viscosity from a rotational shear rheometer using fiber-windup technique. *Journal of Rheology* **1996,** 40, (4), 473-481.
118. Maia, J. M.; Covas, J. A.; Nobrega, J. M.; Dias, T. F.; Alves, F. E., Measuring uniaxial extensional viscosity using a modified rotational rheometer. *Journal of Non-Newtonian Fluid Mechanics* **1999,** 80, (2-3), 183-197.
119. Sentmanat, M. L. A., OH) Dual windup drum extensional rheometer. 2004.
120. Sridhar, T.; Tirtaatmadja, V.; Nguyen, D. A.; Gupta, R. K., Measurement of extensional viscosity of polymer solutions. *Journal of Non-Newtonian Fluid Mechanics* **1991,** 40, (3), 271-280.
121. Spiegelberg, S. H.; Ables, D. C.; McKinley, G. H., The role of end-effects on measurements of extensional viscosity in filament stretching rheometers. *Journal of Non-Newtonian Fluid Mechanics* **1996,** 64, (2-3), 229-267.
122. Ooi, Y. W.; Sridhar, T., Extensional rheometry of fluid S1. *Journal of Non-Newtonian Fluid Mechanics* **1994,** 52, (2), 153-162.
123. David, F. J.; Tam, S., Molecular conformation during steady-state measurements of extensional viscosity. *Journal of Rheology* **1995,** 39, (4), 713-724.
124. Tadao Kotaka, A. K., Masami Okamoto, Elongational flow opto-rheometry for polymer melts – 1. Construction of an elongational flow opto-rheometer and some preliminary results. *Rheologica Acta* **1997,** 36, (6), 646-656.
125. Katayama, K.; Amano, T.; Nakamura, K., SOME PROBLEMS IN STRUCTURAL FORMATION DURING MELT SPINNING. *Applied Polymer Symposia* **1973**, (20), 237-246.
126. Koyama, K.; Ishizuka, O., Birefringence of polyethylene melt in transient elongational flow at constant strain rate. *Journal of Polymer Science, Part B: Polymer Physics* **1989,** 27, (2), 297-306.
127. Stelter, M.; Brenn, G., Elongational Rheometry for the Characterization of Viscoelastic Liquids. *Chemical Engineering & Technology* **2002,** 25, (1), 30-35.
128. Dupaix, R. B.; Cash, W., Finite element modeling of polymer hot embossing using a glass-rubber finite strain constitutiwe model. *Polymer Engineering and Science* **2009,** 49, (3), 531-543.
129. Sahli, M.; Millot, C.; Roques-Carmes, C.; Khan Malek, C., Experimental analysis and numerical modelling of the forming process of polypropylene replicas of micro-cavities using hot embossing. *Microsystem Technologies* **2009,** 15, (6), 827-835.
130. Taylor, H.; Lam, Y. C.; Boning, D., A computationally simple method for simulating the micro-embossing of thermoplastic layers. *Journal of Micromechanics and Microengineering* **2009,** 19, (7).
131. Kabanemi.K.K., M. J. P., Hétu.J.F.,Worgull.M,Heckele.M, Numerical Simulation of a Thermoviscoelastic Frictional Problem with Application to the Hot-Embossing Process for Manufacturing of Microcomponents. *International Polymer Processing* **2009,** 24, (2), 11.
132. Kim, S. P.; Kim, S. C., Crystallization kinetics of poly(ethylene terephthalate): Memory effect of shear history. *Polymer Engineering and Science* **1993,** 33, (2), 83-91.
133. Pankaj, V.; Lofgren, E. A.; Jabarin, S. A., Properties and kinetics of thermally crystallized oriented poly(ethylene terephthalate) (PET). I: Kinetics of crystallization. *Polymer Engineering & Science* **1998,** 38, (2), 237-244.

134. Poitou, A.; Ammar, A.; Marco, Y.; Chevalier, L.; Chaouche, M., Crystallization of polymers under strain: from molecular properties to macroscopic models. *Computer Methods in Applied Mechanics and Engineering* **2003,** 192, (28-30), 3245-3264.
135. WASSNER ERIK, M. R.-D., SHEAR-INDUCED CRYSTALLIZATION OF POLYPROPYLENE MELTS. *XIII International Congress on Rheology, Cambridge, UK, 2000* **2000,** 1, 3.
136. Peters.W.M.Gerrit, Z. H., Meijer E.H. Han, A viscoelastic based model for flow induced crystallisation. *XIII International Congress on Rheology. Cambridge, UK. 2000* **2000,** 1, 3.
137. Kim, K. H.; Isayev, A. I.; Kwon, K., Simulation and experimental verification of crystallization and birefringence in melt spinning of PET. *International Polymer Processing* **2006,** 21, (1), 49-63.
138. William, H. K.; Anthony, J. M., 2D Modeling of high-speed fiber spinning with flow-enhanced crystallization. *Journal of Rheology* **2007,** 51, (4), 721-733.
139. Kim, K. H.; Isayev, A. I.; Kwon, K., Flow-induced crystallization in the injection molding of polymers: A thermodynamic approach. *Journal of Applied Polymer Science* **2005,** 95, (3), 502-523.
140. Doufas, A. K.; McHugh, A. J.; Miller, C., Simulation of melt spinning including flow-induced crystallization: Part I. Model development and predictions. *Journal of Non-Newtonian Fluid Mechanics* **2000,** 92, (1), 27-66.
141. Antonios, K. D.; Issam, S. D.; Anthony, J. M., A continuum model for flow-induced crystallization of polymer melts. *Journal of Rheology* **1999,** 43, (1), 85-109.
142. Bushman, A. C.; McHugh, A. J., A continuum model for the dynamics of flow-induced crystallization. *Journal of Polymer Science Part B: Polymer Physics* **1996,** 34, (14), 2393-2407.
143. Henry, E., Viscosity, Plasticity, and Diffusion as Examples of Absolute Reaction Rates. *The Journal of Chemical Physics* **1936,** 4, (4), 283-291.
144. Taikyue, R.; Henry, E., Theory of Non-Newtonian Flow. I. Solid Plastic System. *Journal of Applied Physics* **1955,** 26, (7), 793-800.
145. Taikyue, R.; Henry, E., Theory of Non-Newtonian Flow. II. Solution System of High Polymers. *Journal of Applied Physics* **1955,** 26, (7), 800-809.
146. Maron, S. H.; Pierce, P. E., Application of ree-eyring generalized flow theory to suspensions of spherical particles. *Journal of Colloid Science* **1956,** 11, (1), 80-95.
147. Tanner, R. I., A suspension model for low shear rate polymer solidification. *Journal of Non-Newtonian Fluid Mechanics* **2002,** 102, (2), 397-408.
148. Tanner, R. I., On the flow of crystallizing polymers: I. Linear regime. *Journal of Non-Newtonian Fluid Mechanics* **2003,** 112, (2-3), 251-268.
149. Tanner, R. I.; Qi, F., A comparison of some models for describing polymer crystallization at low deformation rates. *Journal of Non-Newtonian Fluid Mechanics* **2005,** 127, (2-3), 131-141.
150. Shao-Cong, D.; Fuzhong, Q.; Roger, I. T., Strain and strain-rate formulation for flow-induced crystallization. *Polymer Engineering & Science* **2006,** 46, (5), 659-669.
151. Frankel, N. A.; Acrivos, A., On the viscosity of a concentrated suspension of solid spheres. *Chemical Engineering Science* **1967,** 22, (6), 847-853.
152. Metzner, A. B., Rheology of Suspensions in Polymeric Liquids. *Journal of Rheology* **1985,** 29, (6), 739-775.

153. Shinsaku, U.; Motowo, T., Application of the theory of elasticity and viscosity of two-phase systems to polymer blends. *Journal of Applied Polymer Science* **1966,** 10, (1), 113-125.
154. Jarzebski, G. J., On the effective viscosity of pseudoplastic suspensions. *Rheologica Acta* **1981,** 20, (3), 280-287.
155. Kataoka, T.; Kitano, T.; Nishimura, T., UTILITY OF PARALLEL-PLATE PLASTOMETER FOR RHEOLOGICAL STUDY OF FILLED POLYMER MELTS. *Rheologica Acta* **1978,** 17, (6), 626-631.
156. Kataoka, T.; Kitano, T.; Sasahara, M.; Nishijima, K., VISCOSITY OF PARTICLE FILLED POLYMER MELTS. *Rheologica Acta* **1978,** 17, (2), 149-155.
157. Kitano, T.; Kataoka, T.; Shirota, T., AN EMPIRICAL-EQUATION OF THE RELATIVE VISCOSITY OF POLYMER MELTS FILLED WITH VARIOUS INORGANIC FILLERS. *Rheologica Acta* **1981,** 20, (2), 207-209.
158. Thomas, D. G., Transport characteristics of suspension: VIII. A note on the viscosity of Newtonian suspensions of uniform spherical particles. *Journal of Colloid Science* **1965,** 20, (3), 267-277.
159. Utracki, L. A.; Fisa, B., Rheology of fiber- or flake-filled plastics. *Polymer Composites* **1982,** 3, (4), 193-211.
160. Quemada, D., Rheology of concentrated disperse systems and minimum energy dissipation principle. *Rheologica Acta* **1977,** 16, (1), 82-94.
161. Quemada, D., Rheology of concentrated disperse systems II. A model for non-newtonian shear viscosity in steady flows. *Rheologica Acta* **1978,** 17, (6), 632-642.
162. Te Nijenhuis, K.; Winter, H. H., Mechanical properties at the gel point of a crystallizing poly(vinyl chloride) solution. *Macromolecules* **1989,** 22, (1), 411-414.
163. Lin, Y. G.; Mallin, D. T.; Chien, J. C. W.; Winter, H. H., Dynamic mechanical measurement of crystallization-induced gelation in thermoplastic elastomeric poly(propylene). *Macromolecules* **1991,** 24, (4), 850-854.
164. Campbell, G. A.; Forgacs, G., Viscosity of concentrated suspensions: An approach based on percolation theory. *Physical Review A* **1990,** 41, (8), 4570.
165. Adam, M.; Delsanti, M.; Durand, D., Mechanical measurements in the reaction bath during the polycondensation reaction, near the gelation threshold. *Macromolecules* **1985,** 18, (11), 2285-2290.
166. Cakmak, M.; Spruiell, J. E.; White, J. L., A basic study of orientation in poly(ethylene terephthalate) stretch-blow molded bottles. *Polymer Engineering & Science* **1984,** 24, (18), 1390-1395.